Kent Academic Repository

Huq, Nafisa Nazmun (2018) *Role of Filamentous Virion Morphology during Influenza Virus Infection.* **Doctor of Philosophy (PhD) thesis, University of Kent,.**

Role of Filamentous Virion Morphology during Influenza Virus Infection

Nafisa Nazmun Huq

A thesis submitted to the University of Kent at Canterbury for the degree of PhD in Microbiology in the Faculty of Sciences

Department of Biosciences

2018

Declaration

No part of the thesis has been submitted in the support of an application for any degree or other qualification of the University of Kent, or any other University or Institution of learning.

Nafisa Nazmun Huq

21st September 2018

Acknowledgements

I would like to thank Dr Jeremy Rossman, my supervisor, for giving me the opportunity to do this PhD. I am really thankful for his support and advice throughout the course of the study. He has always been positive and optimistic, even at hard times, which helped me to overcome all the hardships.

I also want to thank all the members from the Rossman group, both old and current, who were always there whenever I needed them. I want to especially thank Mathew Badham, Dr Basma Bahsoun and Diego Cantoni for their constant help regarding technical issues in the lab. I am also thankful for their advice and friendship.

Ian Brown was always there to help me with Transmission Electron Microscopy and Confocal Microscopy, and I am very thankful to him for that.

Finally, I could not have done this PhD without the help of my family and friends. I am very thankful to my parents and sisters for their continuous support and their relentless patience with me. I am very grateful for the help I have received from my husband, Sadik Hossain. He has been there to assist and motivate me through all the ups and downs of the study.

Contents

Abbreviations

A41V- A/Udorn/301/1972-M1-A41V

A549- Adenocarcinomic Human Alveolar Basal Epithelial Cells

BSA- Bovine Serum Albumin

Cal/09- A/California/04/2009

CLIC- clathrin independent carriers

CPSF30- 30kDa subunit of cleavage protein and polyadenylation specific factor

CPZ- Chlorpromazine

CSF-1 Colony Stimulating Factor-1

DAPI- 4′,6-Diamidine-2′-phenylindole dihydrochloride

DMEM- Dulbecco's Modified Eagle Medium

dsRNA- double stranded Ribonucleic Acid

EGF- Epidermal Growth factor

EIPA- 5-(N-Ethyl-N-isopropyl) amiloride

ER- Endoplasmic reticulum

FBS- Foetal Bovine Serum

GEEC- Glycosylphosphotidylinositol- anchored protein enriched compartments

HA- Hemagglutinin

HEK 293T- Human Embryonic Kidney Cells 293 containing the SV40 T antigen

IAV- Influenza A Virus

IkB- nuclear factor of kappa light polypeptide gene enhancer in B-cells inhibitor

IKK- IkB Kinase

IL-6- Interleukin 6

IRAK 4- Interleukin-1 receptor-associated kinase 4

LC3- MAP1LC3B Gene

M1- Matrix 1 Protein

M2- Matrix 2 Ion Channel Protein

MDCK- Madin-Darby Canine Kidney Cells

MOI- Multiplicity of Infection

NA- Neuraminidase

NEP/NS2- Nuclear Export Protein

NF-kB- Nuclear factor kappa-light-chain-enhancer of activated B cells

NP- Nucleoprotein

NS1- Non-structural Protein

PA- Polymerase Acid

PABPII- poly(A)binding protein II

PAMPs- Pathogen Associated Molecular Patterns

PB1- Polymerase Basic 1

PB2- Polymerase Basic 2

PBS- Phosphate Buffered Saline

PDGF- Platelet Derived Growth factor

PFU- Plaque Forming Units

PMA- Phorbol 12-myristate 13-acetate

PR/8- A/PR/8/1934

PTA- Phosphotungstic Acid

RNA- Ribonucleic Acid

RNP- Ribonucleoprotein

RPMI 1640- Roswell Park Memorial Institute Medium

SEAP- Secreted Embryonic Alkaline Phosphatase

ssRNA- single stranded Ribonucleic Acid

TAK1- Mitogen-activated protein kinase kinase 7

TEM- Transmission Electron Microscopy

TLR- Toll Like Receptor

TNF- α- Tumour Necrosis Factor alpha

Udorn- A/Udorn/301/1972

UV- Ultra Violet Radiation

WSN- A/WSN/1933

Abstract

Influenza A virus is a very important pathogen as it can cause both health and economic burden around the world. It causes annual epidemics and occasional pandemics. IAV is a negative sensed enveloped RNA virus. Influenza is pleomorphic in nature, meaning it can form different morphologies, mainly spherical and filamentous. Filamentous viruses are well documented, but how and why they form is still not known. However, it is known that filamentous viruses enter host cells by macropinocytosis, while spherical viruses mostly enter by clathrin mediated endocytosis (Rossman et al., 2012).

Both host and viral factors can have a role in the formation of the morphology of the virions. It is also believed that host factors can also have an effect on infectivity of the virus. In this study, the focus was on how viral morphology can affect innate immune response at early stages of infection. It was shown that filamentous virions can reduce the activation of the NF-kB thus reducing its signalling. As NF-kB is one of the first responders of the host's immune system, this means filamentous virions can successfully reduce the effects of the innate immune system during early infection. Here, we tried to find the steps that the filaments follow to bring about this reduction in activity.

Influenza virus uses clathrin mediated endocytosis and macropinocytosis to enter host cells. When both the pathways are blocked it was thought that infection should decrease. However, it was noticed that blocking clathrin

mediated endocytosis and micropinocytosis increases infectivity of spherical viruses. We are proposing that IAV can enter cells by a third pathway.

It had been proposed that some non-infectious filamentous virions exist. The main purpose of these viruses is suggested to be to prime host cells, for increasing the cellular entry rate of the infective virions which follow it. It has been shown in this study that this concept is not true and priming of host cells beforehand does not help with consecutive infection.

Understanding the morphology of filaments is a complex process. This study looked at filamentous virion's infectivity through cellular entry and the effects of host's innate immunity.

CHAPTER 1

INTRODUCTION

1.1 Influenza Virus: An Important Pathogen

Influenza Virus is a cause of annual epidemics and occasional pandemics all over the world. It can cause high rate of morbidity and mortality and has large socio-economic cost, causing financial and economic burdens to society. Influenza viruses play a vital role in human health.

Influenza Virus can be one of four types: A, B, C and D. Of the four, A, B and C infect humans, and A predominantly causes most of the infections by influenza viruses. Influenza A Virus (IAV) was the cause of the most severe viral outbreak known in 1918, where more than 50 million people were killed in one year, during the First World War, which is more than the number of people who were killed due to the war itself (Johnson and Mueller, 2002). This is now known as 'Spanish' Flu. IAV has continued to spread pandemics throughout the world, including the 'Asian' Flu in1957 and 'Hong Kong' Flu in 1968, which are each believed to have caused about 1 million deaths (Kilbourne, 2006). A more recent outbreak was the 'Swine' Flu pandemic in 2009, where it affected 60 million people, and caused 12000 deaths in the USA alone (Badham and Rossman, 2016).

In the USA, it has been estimated that the direct costs related to hospitalisation of IAV-infected children younger than 5 years old is $809 million annually, on average. In addition, children (under 5) treated at outpatient visits add another $389 million annually to the cost (Molinari et al., 2007, Wang et al., 2013). However, these figures do not include the indirect costs (e.g. work leave, transport costs etc.) which can increase the

costs even higher. According to WHO/IVB/16.04, the total economic burden needs to include direct medical costs, direct non-medical costs and indirect costs, highlighting the significant economic costs of annual IAV outbreaks. It had been estimated that from 2001/2002 to 2008/2009 the healthcare costs in the US ranged from \$2.0-5.8 billion (Yan et al. 2017).

1.2 Disease and Epidemiology

Influenza infection is very contagious and causes respiratory tract infections in humans and other animals (birds, pigs, horses, seals etc.). The symptoms for mild IAV infection are fever, headache, sore throat, congestion and muscle aches. However, in severe cases the symptoms can progress to severe cough, wheezing, breathing difficulties and respiratory failure (Coates et al. 2016). Although anyone can be infected by influenza viruses, it is believed that children under the age of 5 and people who are 65 and over are more susceptible to severe infection (CDC, 2018).

It is thought that most of the infection is spread through the air by respiratory droplets when an infected individual cough, sneezes or talks. In addition, IAV can also spread by surface contact when someone touches a surface with IAV on it, and then touches their mouth, nose or eyes. During the first 3-4 days of infection, the individual is most contagious, and can spread the virus before they themselves start showing symptoms. It usually takes about 2 days for the onset of infection, but can go up to 4 days (CDC, 2018).

There are vaccines (depending on age groups and seasonal outbreaks) and antiviral medications (Tamiflu) available to treat influenza infections.

IAV is a very successful virus and has survived due to its ability to adapt and evade the human immune system. One of the main ways it can survive is by antigenic variations in the hemagglutinin (HA) and neuraminidase (NA) glycoproteins. IAV can continuously change its antigenic properties, through the introduction of point mutations in the HA and NA genes during error-prone replication, which can amplify in favourable conditions, thus giving rise to annual epidemics. This process is known as 'antigenic drift' (Cox and Subarao, 2000). Sometimes, more than one variant of influenza virus can co-infect a cell, leading to a complete reassortment of the viral genomic segments, and giving rise to a new viral subtype. This is known as 'antigenic shift', and cause pandemic strains to form. As this can result in a completely new strain for which individuals may have no existing immunity, they can often spread rapidly through the human population (Strauss and Strauss, 2008).

Infectivity of IAV varies between different types of cells, and HA determines the cells capable of being infected. During seasonal IAV infection, HA binds to α2-6 sialylated glycans which are found in the upper respiratory tracts of many mammals (Shinya et al., 2006). However, in more pathogenic strains of IAV, HA binds to α2-3 sialyated glycans in the lower respiratory tract, resulting in infection of type 2 pneumocytes of lungs and alveolar macrophages (Fukuyama and Kawaoka, 2011). Furthermore, some strains

of IAV can also infect gastrointestinal cells, though the function of this cell type in IAV infection is not known (Horimoto et al., 1997).

1.3 Structure of Influenza Virus

IAV belongs to the *Orthomyxoviridae* family. This family comprises pleiomorphic (filamentous and spherical) enveloped viruses that have a segmented single-stranded negative-sense RNA genome (Palese, 2007). The virus types (e.g. IAV) can be classified by the antigenic differences in the main virion proteins, the nucleoproteins (NP) and Matrix Protein 1 (M1). IAV is further classified into 16 HA and 9 NA subtypes, again depending on their antigenic and genetic properties (Noda, 2012). These subtypes lead to the naming of different Influenza virus strains, e.g. A/Udorn/1972 (H3N2) is an Influenza A virus, isolated from the Udorn valley in Russia in 1972 and is antigenically classified as HA type 3 and NA type 2 (Noda, 2012).

The IAV genome is formed by eight RNA segments and eleven genes. These express several different proteins, which can be categorised as structural and non-structural proteins. The structural proteins include HA, NA, NP and matrix proteins one and two (M1 and M2), and in addition they have functional roles as well. On the other hand, polymerase subunits [polymerase basic 1 (PB1), polymerase basic 2 (PB2) and polymerase acid (PA)] and non-structural proteins (NS1), are the non-structural proteins, and have functional roles which help in virus replication (Badham and Rossman, 2016). Before transporting and assembling, the NP proteins binds to the

polymerase subunits to package the viral genome. They also interact with different cellular proteins to export the replicated viral genome to the nucleus (Badham and Rossman, 2016).

HA is the most abundant envelope protein. IAV viruses contain at least 500 copies of HA per virion, which function as the receptor for binding and membrane fusion activity. In comparison, NA has fewer copies in the virion and is mainly involved in enzymatic activity, cleaving sialic acid bonds and releasing newly formed virus particles (Badham and Rossman, 2016). HA and NA can be seen as the glycoprotein spikes on the surface of the virion in a ratio of 1:4 approximately (Noda, 2012). The least abundant viral protein is the M2 protein, comprising only of 20-60 copies in each virion. M2 plays a major role in viral entry, assembly and budding (Wilschut et al., 2006, Rossman, 2011). The most abundant structural protein of IAV is M1, and this lies on the inside of the viral envelope. M1 can interact with the ribonucleoprotein complex (RNP) (Watnabe et al., 1996) and with the surface glycoproteins HA and NA (Enami and Enami, 1996) to play a major role in genome nuclear export, assembly and budding. RNPs are comprised of the viral RNA (vRNA) segments, NP and the three polymerase proteins, PB1, PB2 and PA (Palese and Shaw, 2007). An additional protein variant of PB1, PB1-F2 can be seen in some strains, and is thought to have a pro-apoptotic activity (Wilschut et al., 2006). The non-structural protein 1 (NS1) plays an important role in antagonizing the host antiviral response and aiding replication. NS1 can restrict host immunity at different levels, including binding to the 30kDa subunit of polyadenylation specificity factor

(CPSF30) and the poly(A) binding protein II (PABPII) which can inhibit cellular mRNA processing. This in turn can block the host antiviral response (Wing-Yee-Mol et al., 2012). Previously believed to be a non-structural protein, the nuclear export protein (NEP/NS2) helps in the nuclear export of viral RNPs. Later it was found to be incorporated into the virus particle in small quantities (Richardson and Akkina, 1991). The structure of IAV is shown in Figure 1.1.
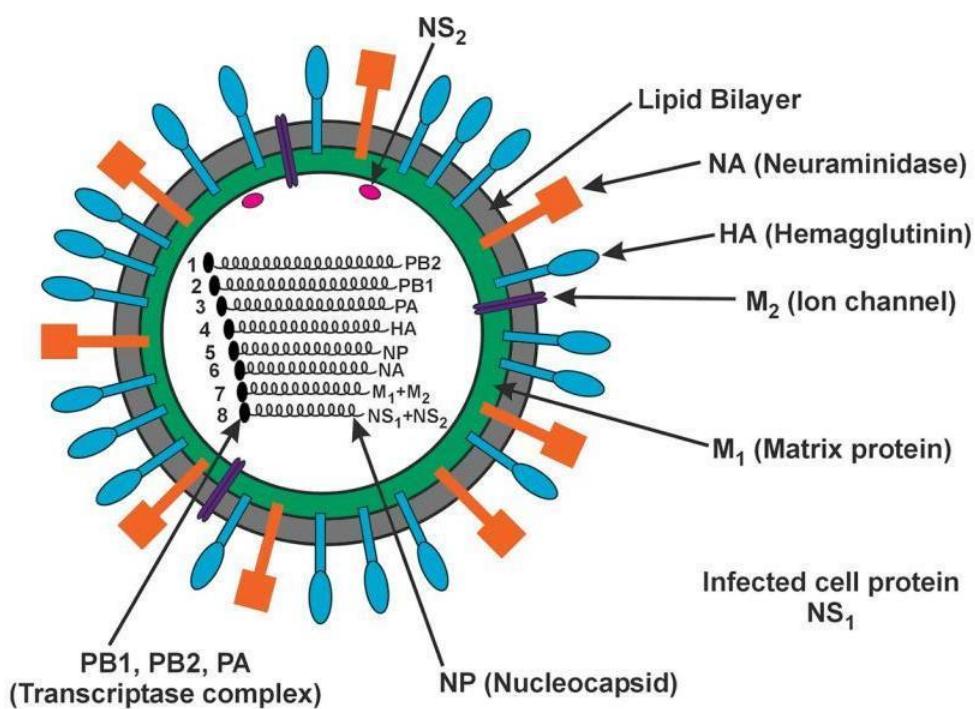
Figure 1.1 Structure of Influenza Virus showing the proteins in the virus. The virus consists of an RNP complex with 8 negative stranded RNA segments, the NP protein and RNA polymerase proteins. There is a layer of M1 protein, just beneath the lipid bilayer, and the membrane contains the M2 ion channel. The HA and NA glycoproteins are embedded in the membrane and seen as the outer layer of the virion. Figure modified from Lambs and Krug, 2004.

1.4 Budding of IAV

The infection of the virus can be spread from cell to cell and from one host to another. Infected cells release infectious particles from specific cellular sites, after the viral components are organised and concentrated through a series of budding events (Schmitt and Lamb, 2005). The process of assembly and budding is very complex and is thought to occur in the lipid raft domains on the surface of the infected cell, with the help of HA, NA, M1 and M2 (Rossman and Lamb, 2011). Figure 1.2 summarises the current model of influenza virus budding.

Influenza budding is a complex process, requiring all the viral proteins at different stages. It is known however that all influenza virions form at lipid raft domains in the plasma membrane of the infected cell (Chen et al. 2007, Leser and Lamb, 2005, Takeda et al., 2003). The lipid rafts concentrate proteins in specific regions and work as functional domains (Lingwood and Simons, 2010). The HA and NA proteins are exclusively found in these domains (Chen et al., 2007) and HA is capable of forming rafts within these domains, resulting in a viral 'budozone' (Schmitt and Lamb, 2005). The HA and NA proteins are thought to initiate the budding process (Wang et al., 2010). Budozone clustering of the HA and NA proteins is thought to alter the membrane curvature which sets off the budding process. The cytoplasmic tails of these proteins then act as anchors for M1 to bind, and this may lead to M1 polymerization. M1 is thought to make further changes to membrane curvature, helping the budding to continue. NP and the RNPs bind to M1 at this point, which also recruits the M2 protein at this site, further

altering membrane curvature and resulting in membrane scission, so that

the virions can be released (Rossman and Lamb, 2011). NA then cleaves

sialic acid off the surface of the cell, so that the release virions can be freed.
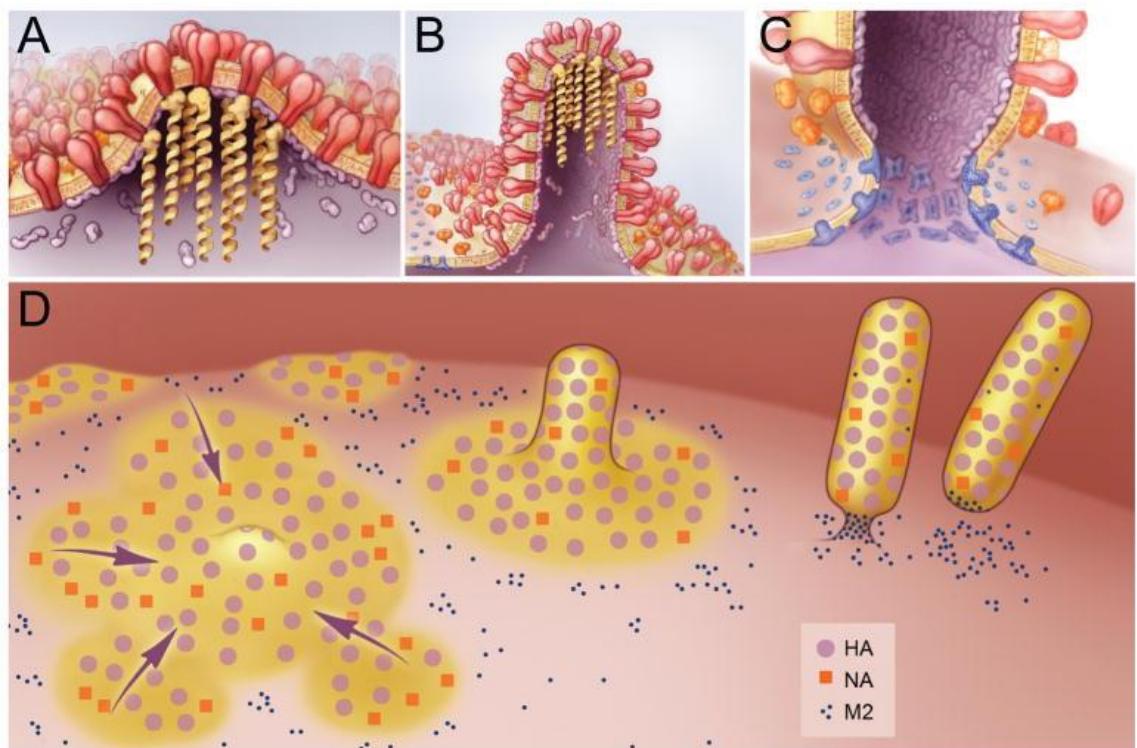
Figure 1.2 Model of Influenza Virus Budding (Rossman and Lamb, 2011). In figure A, it can be seen that HA (red) and NA (orange) cluster in the lipid raft domains to cause initiation of budding of influenza virus. M1 (purple) binds to the cytoplasmic tails of HA and NA. This acts as a docking site for the vRNPs (yellow) to come and attach. In Figure B, it can be seen that the budding virions elongate. The M1 proteins get polymerized which causes the vRNPs to localize, and the M2 (blue) interacts with M1 at the periphery. Figure C shows the occurrence of membrane scission due to the M2 amphipathic helix which leads to the change in membrane curvature and the release of the budding virus. Figure D shows all the above processes- HA and NA come together in the lipid rafts leading to the formation of a filamentous virion, resulting in viral release due to the clustering of M2 at the neck of the virus and its membrane scission activity.

1.5 IAV entry pathways

Entry of spherical influenza virions has been widely studied, and has been determined that the virions enter cells via clathrin-mediated endocytosis. When the virus reaches the host cell, HA binds to the sialic acid moieties of host glycoproteins (Chu and Whittaker, 2004). When the HA binds to these glycoproteins it triggers the virion to enter the cell by clathrin-dependent receptor mediated endocytosis. This occurs through the Epsin-1 adapter protein through a dynamin dependant process (Chen and Zhuang, 2008). Once the virus enters the cell, it passes through the endosomal maturation pathway, which creates a low pH, and this triggers the HA to be activated. Once activated, HA mediates fusion of the virus and host endosomal membranes (Yoshimura and Ohnishi, 1984). The low pH also activates the M2 proton channel protein, so that protons can enter the virus and make it more acidified. This in turn releases the M1 protein from the RNP core, enabling the RNP to be trafficked into the nucleus, which is necessary for viral replication (Rossman et al., 2012). Once viral genome is replicated in the nucleus, it is exported through NS2 and travels through the Endoplasmic Reticulum (ER) to the Golgi Apparatus, and then to the cell membrane where they await to be incorporated in budding virions, as described earlier in Section 1.4. This is shown in Figure 1.3.

However, filamentous virions are much larger in size, and it is not possible for them to enter host cells via clathrin mediated endocytosis. It has been suggested by Rossman, Lesser and Lamb (2012) that influenza viruses can also use macropinocytosis to enter cells. Filamentous influenza uses
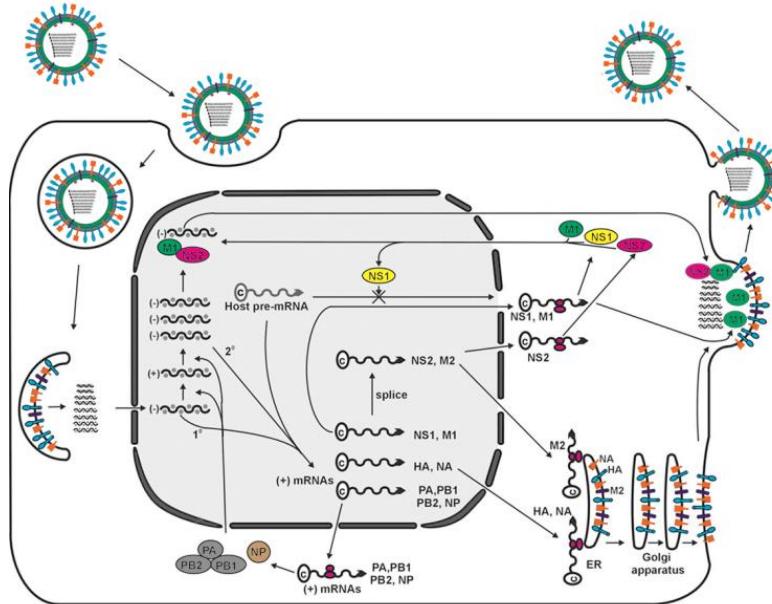
Figure 1.3 Spherical IAV enters host cells via clathrin mediated endocytosis. The IAV binds to host cell sialic acid moieties via the HA protein which induces the virus to be taken up. It passes through the endocytic pathway and is trafficked through the endosomes, experiencing a continuous drop in ph. When the pH is about 5.5 the HA goes through a conformational change which dismantles the virus core, and the vRNPs enter the cytoplasm (Sieczkarski and Whittaker, 2005). The vRNPs then enter the nucleus, where transcription and replication occur, and are then transported via the ER to the Golgi apparatus and then to the cell membrane for virus budding (figure from Lamb and Krug, 2004)

macropinocytosis as a primary entry pathway, while the spherical virions can also utilise it as an alternate pathway. Macropinocytosis is a type of endocytosis to collect solutes in bulk, and thus can take up dissolved molecules, viruses, bacteria, cell fragments etc. along with it (Falcone et al., 2006). Upon activation, membrane ruffles form on the cell surface, which in turn can form large endocytic vacuoles termed macropinosomes (Lim, 2011). This is shown in Figure 1.4. Macropinosomes depend on actin to be activated and need growth factors like Colony Stimulating Factor-1 (CSF-1), Epidermal Growth Factor (EGF) or Platelet Derived Growth Factor (PDGF) for activation (Burry, 1990). During macropinocytosis, the entire filamentous virus is engulfed from the cell surface and trafficked to an acidified compartment. It passes through early and late endosomes, and goes through decreasing ph. When the pH reaches 5.5 the virus goes through a conformational change which us induced by the HA. This causes the viral envelope and the vesicle membrane to fuse (Sieczkarski and Whittaker, 2005). The low pH of the compartment also causes the activation of M2 and causes the amphipathic helix to cause changes in membrane curvature, fragmenting the filaments and helping membrane fusion. This helps the filaments to avoid the size constraint of the clathrin-coated vesicles, and facilitates entry into cells (Rossman et al., 2012).
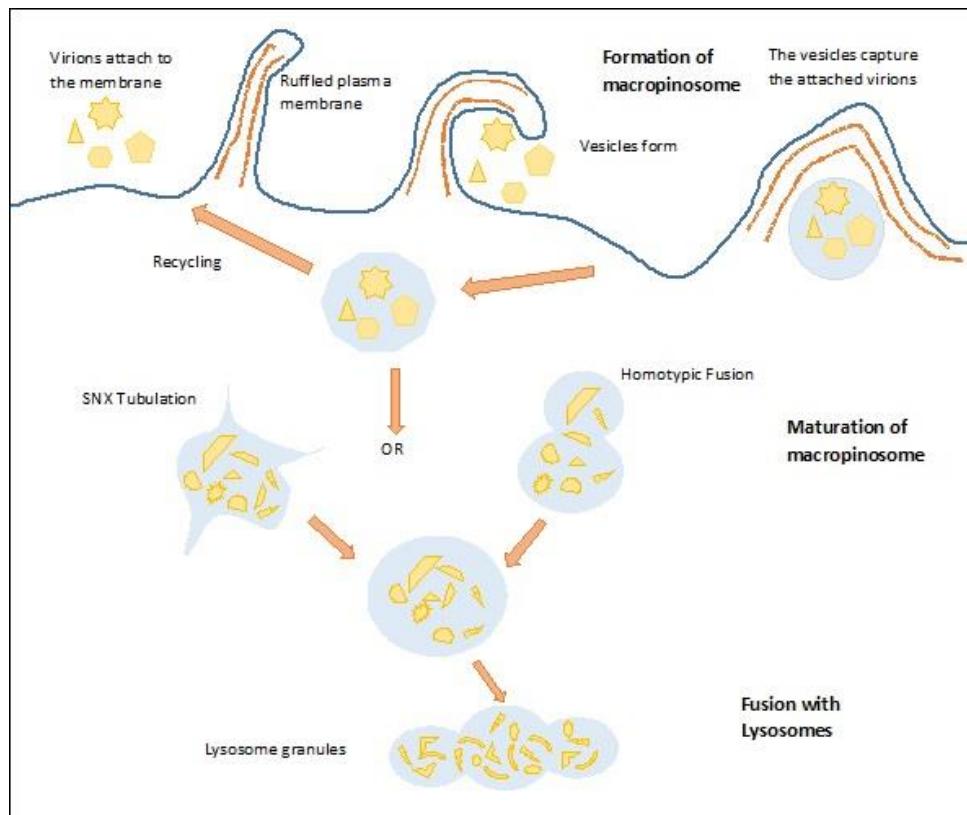
Figure 1.4 Macropinocytosis is a process of engulfing solutes in bulk. Along with the solute, other particles can also be taken up, including viruses. Ruffles form on the surface of the cell, which helps to engulf the particles and form the macropinosomes. These acidify, mature and eventually fuse with lysosomes, which then degrades the contents (Figure adapted from Lim, 2011).
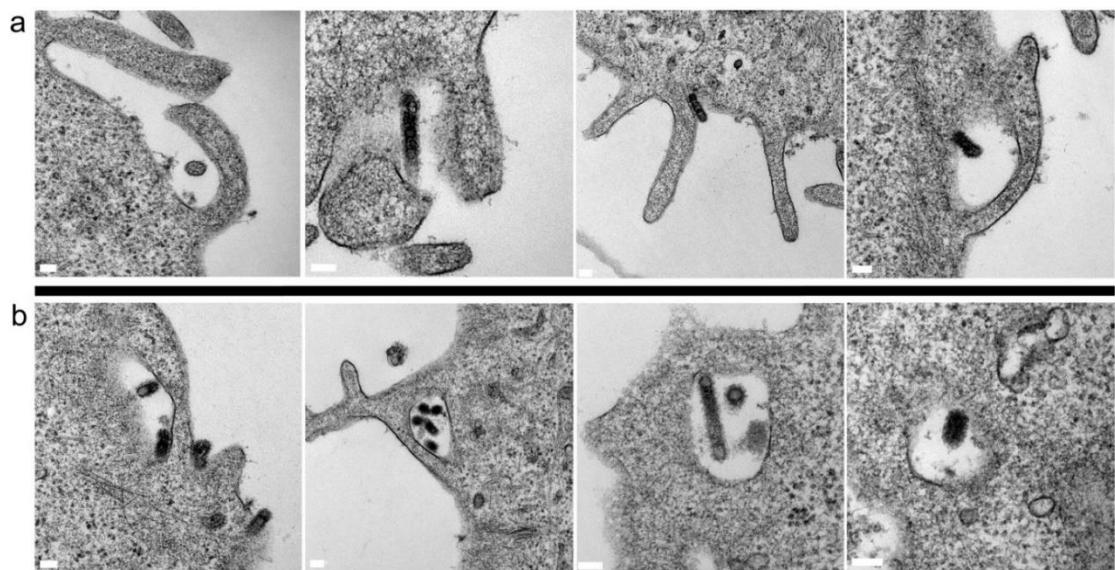
Figure 1.5 Electron Microscopy images showing micropinocytosis occurring engulfing filamentous influenza viruses. Figure a shows the virus being engulfed into the cell after initiating micropinocytosis. Figure b shows the virus after being engulfed, inside the macropinosomes (Rossman et al., 2012).

1.6 Viral Morphology

The influenza virus can display various morphologies and are thus known as pleomorphic. The morphologies can range from spherical to filamentous (which are most commonly seen during human infection), with intermediate structures looking ovoid or ellipsoidal (Noda, 2012), (Cader et al., 2011). Certain IAV strains exist which only forms spherical structures. However, the filamentous strains are always seen as a mixture of spheres and filaments. Despite the length of the virion, it is believed that all the morphologies have one IAV genome, making each virion a single infectious unit. Figure 1.6 shows the spherical and filamentous morphologies of influenza virus.

The spherical viruses, as named, are spherical in shape, and usually have a diameter of 120nm. The filamentous structures are more elongated, and are commonly a few micrometres long, but can go up to 10um in length. The spheres are common in laboratory grown strains, while the filaments are observed more in samples from clinical isolates (Choppin and Murphy, 1960, Chu et al., 1949, Elton et al.,2013, Itoh et al., 2009, Hayase et al.,1995, Kilbourne and Murphy, 1960).

Filamentous structure is conserved across IAV strains and hosts, indicating that it has some advantages in the host which may be lost when grown in a laboratory setting. The changes in morphology has so far not shown any effects on transmissibility and infectivity (Choppin and Murphy, 1960). The ability of certain strains to form filamentous virions depend on their genetical

features (Kilbourne and Murphy, 1960). Irrespective of the HA and NA subtype of the viral strain, filamentous structure is continuously produced naturally, which suggests that they are important in survival of the virus in the nature (Siezkarski and Whittaker, 2005).

Furthermore, it is noticed that continuous passaging of a filamentous strain in a chicken egg causes the strain to go through a morphological adaptation, causing only spherical virions to form. However, when a spherical strain is grown in guinea pigs, adaptation restores the ability to grow filaments (Choppin and Murphy, 1960, Kilbourne, 1959).

Many different viral and host factors can influence the viral structure to be either spherical or filamentous. The virus undergoes different mutations to adapt to the different environments and thus the phenotype changes accordingly. However, despite much research it is not known what the function of influenza virus morphology is.
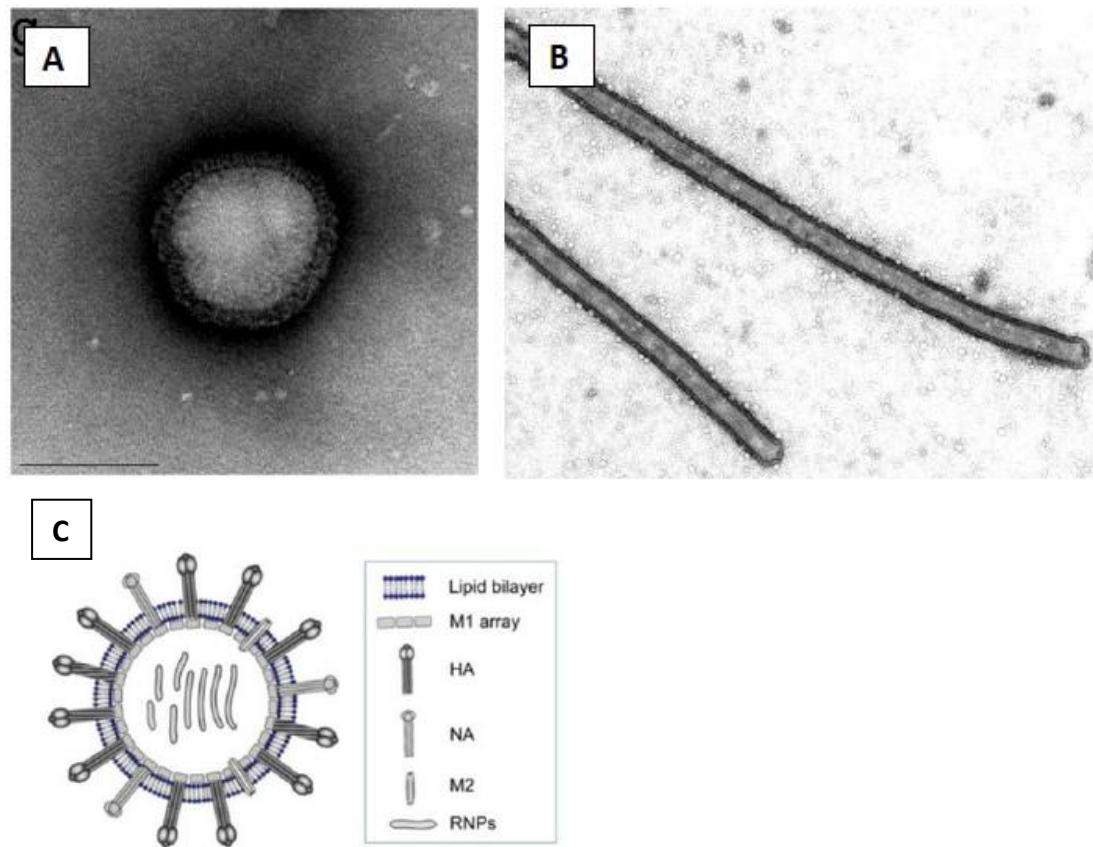
Figure 1.6 TEM images of spherical IAV (A) and filamentous IAV (B). Supernatant from A/Udorn/72 infection was negative stained and imaged by TEM. Scale bar shows 100nm. Figure C is adapted from Choi et al (2014) and shows the viral proteins of influenza, including the M1 and M2 protein.

What determines the viral morphology is a subject that has been investigated by different studies over the years. Most of these studies look at M1 and M2 as the determining the viral factors which affect viral filament formation. M1 protein is not only an important determinant of assembly and budding of both filamentous and spherical virion, but also plays a major role in filament formation (Elleman and Barclay, 2004). The maintenance of the viral morphology predominantly lies at the intersection between the M1 protein the viral envelope and a minimal role of the RNPs. M1 is the most abundant protein, and it resides under the viral envelope and interacts with HA, NA and cytoplasmic tail of the M2 to bring about the specific viral morphology (Elton et al., 2013, Lakdawala, 2011) and oligomerises into a ribbon like structure (Badham and Rossman, 2016, Nayak et al., 2004, Rossman et al., 2010). It has also been noticed that M2 protein plays an important role in viral morphology and changes in the c-terminal amphipathic helix and can have a direct effect on the viral morphology (Badham and Rossman, 2016).

When there are specific mutations in M1, it can lead to changes in the virus morphology. For example, in A/Udorn/72 strain it has been shown that changes in amino acids at position 41, 95 and 218 of M1 (Figure 1.6C) can change the filamentous phenotype. Of these three changes, alteration at position 41 shows the most significant changes in viral morphology. At position 41, the matrix protein encodes a highly conserved alanine residue in human and avian lineages. If the alanine residue is mutated, it has very limited effect on the growth of the virus, but the morphology of the virus

changes significantly. If the alanine is replaced by a valine at this position, the filamentous morphology is lost. In A/Udorn/72 strain, an A41V mutation causes the filamentous morphology to be entirely missing (Campbell et al., 2014, Badham and Rossman, 2016).

It was also shown by Chen et al, 2007, that the M1 protein is not required to form bacilliform (<1um) or spherical virions but is required to form filamentous virions. Furthermore, it was shown that in filaments the M1 protein forms a helical structure that may be different from that seen in spheres. These suggest that structural changes in the M1 protein are important determinants of the morphology of IAV. M1 forms a scaffold like complex under the viral envelope that interacts with NA, HA and M2 proteins. The M2 protein may stabilise this complex to allow the continuous polymerisation of M1 which helps in filament formation (Badham and Rossman, 2016). If there are mutation of the C terminal amphipathic helix of the M2 (which is predicated to interact with M1), then a filamentous virion can turn into a spherical one. If there is a truncation at residue 70 of the C terminal helix, then filaments form in an otherwise spherical virus. Also, it was observed that a single amino acid change (Y76A) in the M2 cytoplasmic tail of a filamentous strain, causes the length and number of filaments produced to be reduced. This suggests that M2 changes filamentous morphology by interacting with M1, while M1 determines the actual structure of the virus. This means that viral morphology is a complex and multistep process, with different determinants involved in forming the structure (Badham and Rossman, 2016).

Not only are the viral factors responsible for the morphological determination of IAV, but host factors can also play a role. It has been observed that the virus adapts in response to different host factors, which implies that the host organism influences morphology-specific functions. As described before, the filamentous virions are seen in human clinical isolates, but when they are continuously passaged in embryonated chicken eggs, they change morphology to become more spherical (Choppin and Murphy, 1960, Kilbourne, 1959). However, if the filamentous virions (especially A/Udorn/72) are passaged on Madin-Darby Canine Kidney (MDCK) cells, they retain their filamentous morphology (Choppin and Murphy, 1960, Seladi-Schulman et al., 2013, Burnet and Lind, 1957). For this reason, the A/Udorn/72 strain was grown in MDCK cells for most of the work which will be described in the later sections.

It has been observed that in polarised MDCK cells, when Udorn is grown it forms highly filamentous virus that bud from the apical plasma membrane (Scheiffele et al, 1999, Zhang et al., 2000). This can explain why the upper respiratory tract is the primary site of IAV infection, as the epithelial cells here are highly polarised (Badham and Rossman, 2016). However, filamentous virions can also form in human embryonic kidney 293T cells, in absence of polarisation and without a defined apical membrane (Bruce et al., 2009), showing that filament formation is a much more complex process than previously thought.

From previous research it has been shown that when the actin cytoskeleton of host cells was disrupted, filament formation was decreased, but there

was no effect on spherical virion budding (Roberts and Compans, 1998). It was also reported that Rab11 and Rab11 family interacting protein 3 (FIP3) are important for filament formation (Bruce et al., 2010). Rab11 is necessary for IAV budding for all morphologies by trafficking the viral RNP to the site of budding, while Rab11-FIP3 is used in filamentous virion formation by regulating the localising and trafficking of unknown target proteins (Bruce et al., 2010, Hales et al., 2001). In a complex process, Rab11 interacts with PB2 of the viral RNP complex (Ying et al., 2013). Rab11 then traffics the RNPs to the site of virus budding through the microtubule network, and interacts with M1 to aid in the budding, potentially affecting filament formation (Martin and Helenius, 1991).

1.7 Host Factors Affecting IAV Infection

Although, the full extent has not been shown of what viral and host factors play a role in viral morphology, it is known that they both have their own individual roles which determines the structure of the virion. Furthermore, it is possible that host immune factors influence influenza infectivity and morphology at both innate and adaptive immunity stages (Fukuyama and Kawaoka, 2011). Innate immunity of the host is very important in the early stages of IAV infections (Cauldwell et al., 2014). For successful infection of IAV, the virus must overcome the host's immune system.

When IAV infects a host, it releases its RNA which traffics through the cytoplasm to the nucleus to be replicated. Toll-like receptor 7 (TLR7) and

retinoic-acid-inducible-gene I (RIG-I) are pattern recognition receptors (PRR) that recognise the RNA of the virus and activate the Interferon (IFN) antiviral response (Koyama et al., 2007, Wu et al., 2007, Lee et al 2013). TLR7 and RIG-I activate the Nuclear factor kappa-light-chain-enhancer of activated B cells (NF-kB) pathway, resulting in the production of inflammatory proteins, including IFN (Kawai and Akira, 2010). Furthermore, during virus infection autophagy can be activated, and autophagosomes contain viral proteins which again can be recognised by endosomal and autophagosomal TLRs (Fukuyama and Kawaoka, 2011, Kawai and Akira, 2010). This is summarised in figure 1.7.
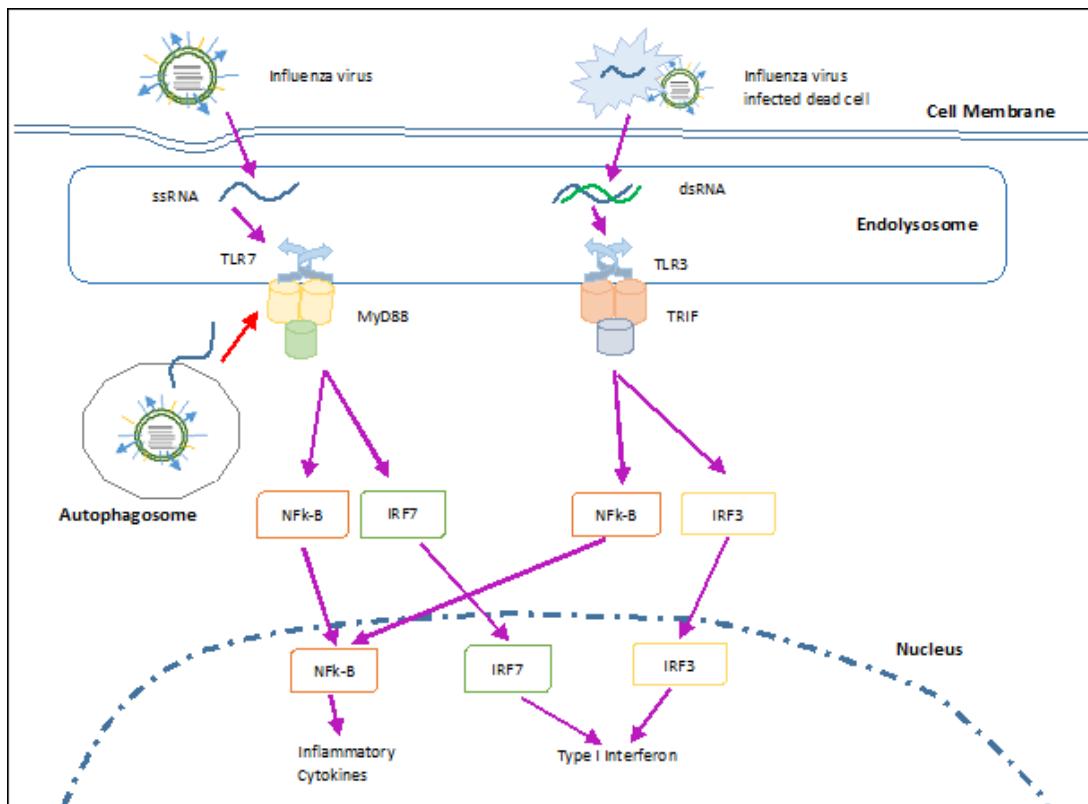
Figure 1.7 TLR7 can recognise the single stranded RNA of IAV. Activated TLRs then activate the NF-kB pathway. THE ssRNA of IAV can be presented to TLR7 during viral genome trafficking or during the process of autophagy (Kawai and Akira, 2010).

1.7.1 NF-kB Activation During IAV Infection

NF-kB is an important protein complex involved in regulating DNA transcription, cytokine production and cell survival. It can be found in almost all animal cells. NF-kB is a key player in the immune response to infections and is one of the central mediators of immune responses (Hiscott et al., 2006). When NF-kB does not function correctly it can lead to different

problems including cancer, autoimmune diseases and viral infections (Meffert et al., 2003).

NF-kB pathway is an attractive target for viral pathogens to evade activating the host immune response. When a host cell is exposed to a pathogen, the activation of NF-kB can be almost immediate, as it does not require de novo protein synthesis, and is trafficked to the nucleus within minutes (Hiscott et al., 2001). This leads to strong transcriptional stimulations of many early cellular anti-viral genes and can regulate both pro- and anti-apoptosis signals. Viruses are very proficient in exploiting the anti-apoptotic properties of NF-kB and influences the host defence mechanism, to reduce the killing of infected of cells or effect apoptosis to increase the release of virions from the infected cells (Hiscott et al., 2001). Furthermore, NF-kB plays important roles in cell growth and proliferation, which makes it a more attractive target for the virus to manipulate, causing more virus growth (Hiscott et al., 2001). It has been suggested that IAV overexpresses HA, NP and M1 to activate the NF-kB pathway.

Inactivated NF-kB stays in the cytoplasm of cell, which still have not received any stress signals. The location of NF-kB I determined by IkB proteins, a family of inhibitory proteins. The IkB proteins directly bind to NF-kB proteins, preventing it from entering the nucleus. When the cell receives a stimulus, it undergoes phosphorylation and ubiquitination, which degrades the IkB. Without the bound IkB, the NF-kB can move to the nucleus and regulate gene transcription (Karin and Ben-Neriah, 2000). During IAV infection, when NF-kB gets activated it in turn activates the host

immune response and the non-structural NS1 protein of IAV acts as an antagonist to suppress the host IFN response (Hiscott et al., 2001, Gaur et, al. 2011, Pahl and Baeuerle, 1995, Nimmeriahn et al., 2004).
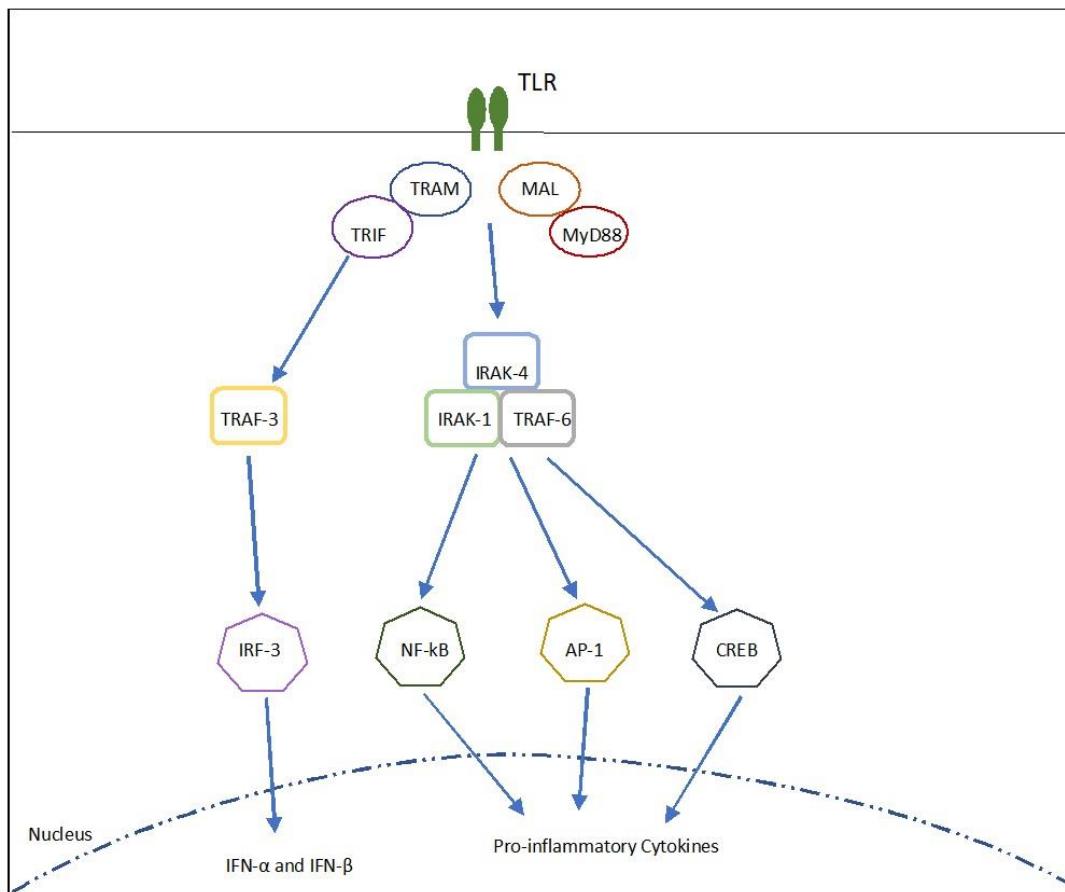
Figure 1.8 Mammalian TLR signalling pathways, including the NF- κB signalling cascade. The NF-kB signalling pathway goes through a cascade of steps before it is activated and enters the nucleus to activate gene transcription to produce pro-inflammatory cytokines. Different TLRs are involved in the activation of this process (Figure modified from L. O'Neill et al 2013).

1.7.2 Pattern Recognition Receptors and NF-kB Activation

Toll-like receptors (TLRs) are an important group of proteins which are vital for the innate immune system. TLRs are single, membrane spanning, non-catalytic receptors which are mainly found in immune cells, including dendritic cells and macrophages. These cells are important for recognizing the structural components of microbes which are conserved in nature and are thus crucial for the innate immune response to pathogens. When the microbes come in contact with the host cell, TLRs are ready to recognise them and activate the immune cells against them (Mahla, 2013).

The host innate immune system mainly recognises microorganisms and respond to it via TLRs and other PRRs. TLRs can identify and respond to pathogen associated molecular patterns (PAMPs), and in turn activate intracellular signalling pathways (e.g. NF-kB) and lead to changes in immune gene expression. In viruses, TLRs can recognise structures like nucleic acids and enveloped glycoproteins. This TLR activation leads to a cascade of signalling pathways which activates Type I interferons, inflammatory cytokines and chemokines, which induce the anti-viral state and can facilitate pathogen clearance (Xagorari and Chlichlia, 2008).

TLRs 3,7,8 and 9 are responsible for recognising viral nucleic acids-dsRNA, ssRNA and CpG oligodeoxynucleotides. In influenza virus infection, TLR 7 activates Type I interferons and NF-kB (to activate pro-inflammatory cytokines, e.g. IL-6, TNF- α), which leads to inflammation and in turn reduces IAV replication and budding, while triggering the activation

of adaptive immunity development (Koyama et al., 2007, Wu et al., 2007).
Lee et al (2013) suggested that there is another cytosolic system of RIG-1
like receptor proteins (RLRs) that can also detect influenza viral RNAs and
aiding in the innate response. The influenza vRNA is a potent activator of
TLR7, which through the MyD88 pathway can induce the production of type
I IFN and NF-kB (Wang, et al., 2006). The cascade of the TLR pathway,
including the activation of IKKB pathway, is shown in Figure 1.8.

When TLR7 gets activated due to influenza infection, MyD88 recruits IL-1
receptor kinases, including IRAK4 which is vital for the activation of NF-kB.
K63 ubiquitin recruits TAK1 to form IKK complex, which causes
phosphorylation of the IkB proteins. This then causes NF-kB to be
activated, enter the nucleus and activate transcription (Kawai and Akira,
2010).

1.7.3 Autophagy and IAV

Autophagy is a regulated mechanism by which cells degrade and recycle
unwanted or toxic cellular components. It takes place in all nucleated cells,
helps to maintain cellular homeostasis (Ryter et al., 2013) and is seen to
increase during stress and viral infections (Kroemer et al., 2010, Perot et
al., 2018). Like apoptosis, autophagy is induced when the cell receives
signals of DNA damage, oxidative stress or cell starvation (Desai et al.,
2015). During the autophagy process, there are a series of rearrangements
of the membrane, which causes the targeted material to be engulfed by

double membraned autophagosomes. These in turn fuse with lysosomes and the content inside is degraded (Desai et al., 2015). Other than protein degradation, autophagy is also suggested to aid in host's immunity. Autophagosomes take up the microbes and degrade them, and they present the microbial proteins to TLR receptors. The receptors in turn can activate the immune responses (Levine et al, 2011).

Viruses have developed ways to overcome the autophagy pathway by finding ways to change autophagy activation or maturation mechanisms. It has been shown that RNA viruses can also use autophagy for their benefit. Some viruses induce autophagy, block autophagosomes from maturing, and uses the immature autophagosomes to replicate themselves (Deretic and Levine, 2009). Replicating inside the autophagosomes causes the viral components to be confined inside the small space to increase their concentration and thus increasing virus replication. Also, if the viral components are inside the autophagosomes, the innate immune responses of the host cannot detect the virus (Perot et al., 2018).

Influenza can alter autophagy activation through a short-linear protein-protein interaction motif in the cytoplasmic tail of the M2 ion channel protein. The cytoplasmic tail of M2 can directly interact with the LC3 protein, causing relocalization to the plasma membrane. HA proteins can undergo proteolytic cleavage which also increases autophagy induction through an unknown mechanism. Autophagy activation also increases indirectly from the help of viral NS1, which increases HA and M2 production. M2 can also interact with Beclin1, which stops the autophagosomes from maturing,

giving rise to apoptosis (Desai, et al., 2015). This is shown in Figure 1.9. During IAV infection, TLR7 can detect viral PAMPs (e.g. vRNA) within autophagosomes (Kawai and Akira, 2010). Thus, autophagy is vital for TLR activation, and the induction of the host immune response.
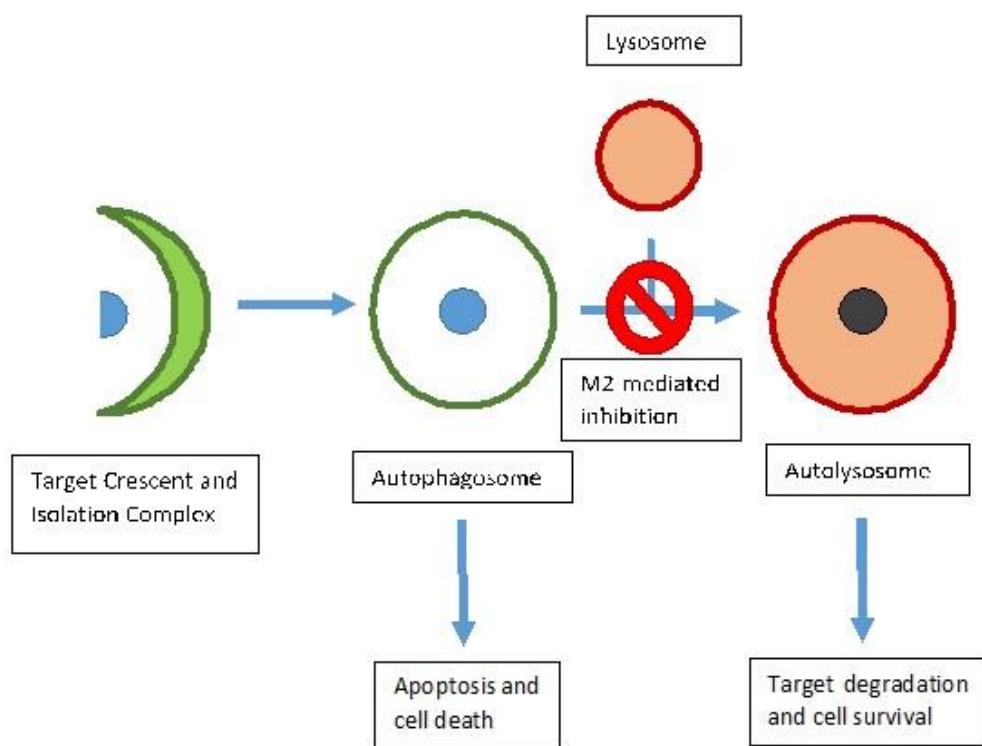
Figure 1.9 The IAV M2 protein blocks autophagosome-lysosome fusion. IAV causes the activation of autophagy, M2 blocks autophagy maturation and stops autophagy completion, which then induces apoptosis which enhances virus replication and budding (Figure modified from Rossman and Lamb, 2009).

1.8 Aim of the Project

The main aim of the project is to see what the functional differences are in the behaviour of IAV due to different viral morphologies. Although filamentous and spherical virions are favoured by different conditions, why one morphology is selected for is still not known. This thesis sought to see if morphology affected virus functions or host responses to the virus. Different factors, viral, physical and host, have been introduced to the cells to ascertain if the filamentous virions react differently from the spherical virions. The study will help us to better understand how the two morphologies function in different conditions, and to determine if filaments have any advantages over spheres during IAV infection.

CHAPTER 2

MATERIALS AND

METHODS

2.1 Materials

2.1.1 Cells, Media and Virus

A number of different cell lines were used for this study, and these are listed in table 2.1.

Cell Name	Abbreviation	Base media used for growth	Paper/ Source (Catalogue Number)
Madin-Darby Canine Kidney Cells	MDCK	DMEM	Rossman lab (used as previously described in Rossman, 2012)
Adenocarcinomic Human Alveolar Basal Epithelial Cells	A549	DMEM	Rossman lab (used as previously described in Rossman, 2012)
Human Embryonic Kidney Cells 293- with SV40 T antigen	HEK 293 T	DMEM	Rossman lab (used as previously described in Rossman, 2012)
U937 monocytic cells	U937	RPMI 1640	ATCC, Virginia, USA (CRL-1593.2)

RAW Blue murine macrophages expressing the NF-κB-SEAP Reporter	RAW Blue	RPMI 1640	InvivoGen, San Diego, California, USA (16123-MM)
Macrophage Cell Line Derived from Wild Type Mice	Wild Type Macrophage	RPMI 1640	BEI Resources, NIAID, NIH, Maryland, USA (NR-9456)
Macrophage Cell Line Derived from TRIF Knockout Mice	TRIF	RPMI 1640	BEI Resources, NIAID, NIH (NR-9566)
Macrophage Cell Line Derived from TRIF/TRAM Knockout Mice	TRIF/TRAM	RPMI 1640	BEI Resources, NIAID, NIH (NR-9568)
Macrophage Cell Line Derived from TRAM Knockout Mice	TRAM	RPMI 1640	BEI Resources, NIAID, NIH (NR-9567)
Macrophage Cell Line Derived from TLR1 Knockout Mice	TLR1	RPMI 1640	BEI Resources, NIAID, NIH (NR-19977)

Macrophage Cell Line Derived from TLR2 Knockout Mice	TLR2	RPMI 1640	BEI Resources, NIAID, NIH (NR-9457)
Macrophage Cell Line Derived from TLR2/4 double Knockout Mice	TLR2/4	RPMI 1640	BEI Resources, NIAID, NIH (NR-19975)
Macrophage Cell Line Derived from TLR3 Knockout Mice	TLR3	RPMI 1640	BEI Resources, NIAID, NIH (NR-19974)
Macrophage Cell Line Derived from TLR4 Knockout Mice	TLR4	RPMI 1640	BEI Resources, NIAID, NIH (NR-9458)
Macrophage Cell Line Derived from TLR6 Knockout Mice	TLR6	RPMI 1640	BEI Resources, NIAID, NIH (NR-19972)
Macrophage Cell Line Derived from TLR7 Knockout Mice	TLR7	RPMI 1640	BEI Resources, NIAID, NIH (NR-15634)

Macrophage Cell Line Derived from TLR9 Knockout Mice	TLR9	RPMI 1640	BEI Resources, NIAID, NIH (NR-9569)

Table 2.1 Table listing the cell lines used for this study

The cells were grown in either Dulbecco's Modified Eagle Medium (DMEM) (Gibco, Fisher Scientific, Loughborough, UK) for MDCK, A549, HEK-293T or in Roswell Park Memorial Institute (RPMI-1640) media (Gibco) for the macrophage cell lines in T75 flasks. To the media 10% Foetal Bovine Serum (FBS) (Gibco) and 1%Penicillin- Streptomycin (Sigma-Aldrich, St. Louis, Missouri, USA) were added. The cells are washed with Phosphate Buffered Saline (PBS), and removed from the flask using TrypLE Express (Gibco). Cells were passaged every 2-5 days at 50-90% confluency and were grown at 37ºC in 5% CO_2.

Virus Name	Subtype	Isolation Country	Collection Date
A/Udorn/301/1972	H3N2	Russia	1972
A/WSN/1933	H1N1	United Kingdom	1933
A/California/04/2009	H1N1	California, USA	2009
A/PR/8/1934	H1N1	Puerto Rico	1934

Table 2.2. List of the viruses used in the study

The virus strains used for the study were all provided by the Rossman lab and were used as previously described (Rossman, 2012). The viruses used are the filamentous A/Udorn/301/1972 (H3N2), its mutant spherical variant (M1-A41V), the spherical A/WSN/1933 (H1N1), the filamentous A/California/04/2009 (H1N1) and the spherical A/PR/8/1934 (H1N1). The virus was grown at 0.01 MOI (multiplicity of infection) on MDCK cells and stored at -80ºC.

2.1.2 Antibodies

A number of antibodies were used throughout the thesis. The polyclonal anti-Udorn goat monoclonal antibody mainly recognizes Udorn M1, NP and HA, with some recognition of NA and M2, was made in the lab as described in Rossman, 2010. The anti-LC3B mouse monoclonal antibody was obtained from Sigma Aldrich (ABC432). NF-kB P65 mouse monoclonal antibody was obtained from Santa Cruz Biotechnology (F-6 clone). 4′,6-Diamidine-2′-phenylindole dihydrochloride (DAPI) was bought from Sigma Aldrich. Donkey anti-mouse and donkey anti-goat Alexa Fluor 488 and 594 labelled secondary antibodies were attained from Thermo Scientific (Loughborough, UK). Cascade-blue labelled dextran (10Kda MW D1976) was obtained from Fisher Scientific. Alexa-594 labelled human transferrin (TI3343) and Fluosphere carboxylate-modified microspheres (F8803) were both obtained from Fisher Scientific.

2.2 Methodology

2.2.1 Cell Culture

The above mentioned cells were grown in T-75 cm2 vented cap flasks (Sarstedt, Nümbrecht, Germany) at 37ºC in 5% CO_2. They were either grown in DMEM (Gibco) (MDCK, A549, HEK-293T) or RPMI 1640 (Gibco) (all the macrophage cell lines). 10% FBS (Gibco) and 1% Penicillin-Streptomycin (Sigma Aldrich) were added to the media. During sub culturing, the media was first removed carefully from the flask, and then washed with 5ml PBS and discarded. Then 3ml TrypLE Express (Gibco) was added to detach the cells from the flask. This was then incubated for 10-20 minutes at 37ºC in 5% CO_2, until all the cells detached. 7ml of the media was then added to the flask, and the media containing the cells was transferred to a sterile 15ml falcon tube (Sarstedt) and centrifuged (Heraeus Megafuge 40R, Thermo Scientific) for 10 minutes at 1000 RPM. The supernatant was then discarded, and the cell pellet resuspended in 10ml of the desired media and transferred to a new flask at the required concentration. For example, MDCK cells were subcultured at 1 in 10 dilution to be 90-100% confluent in 4 days.

U937 monocytic cells are not naturally adherent and grow in suspension. The U937 cells were grown in DMEM media at 37ºC in 5% CO_2, and when required plated in 6 well plates. They were treated with PMA (Phorbol 12-myristate 13-acetate) (Sigma-Aldrich) at 60ng/ml for 24 hours to differentiate into macrophages.

2.2.2 Infection for viral stock production

MDCK Cells were grown in T-75 cm2 flasks and infected with either A/Udorn/72 or Udorn-A41V. The growth media was removed from the flask and replaced with the virus in 3ml DMEM at 0.01 multiplicity of infection (MOI). Cells were then incubated for 2 hours at 37ºC, 5% CO_2 with gentle rocking every 15 min to prevent them from drying. After the incubation, the media containing the virus was replaced with 12ml of serum-free media with 1% N-acetyl trypsin (NAT) (Sigma Aldrich). The cells were then incubated for 2-3 days, until cytopathic effects were observed- i.e. changed morphology and dead cells in media. The virus was then harvested by taking the media in a 15ml sterile conical tube and centrifuging for 20 min at 1000 RPM in a Heraeus Megafuge 40R centrifuge to pellet the cell debris. The supernatant containing the virus was then transferred to a new 15 ml sterile tube. This was aliquoted to cryovials at 1ml per tube and stored at -80ºC for further analysis.

For the different analysis, different MOIs of the virus are used, and they are mentioned in each of the experiments.

2.2.3 Plaque Assay

Plaque assays were used to check the viral titre after each infection passage. MDCK cells were grow in 6 well plates, with 90% confluency. A serial dilution of 10^{-2} to 10^{-7} was prepared with 1% BSA in DMEM. The media from the wells was aspirated, and the cells washed with PBS. 400µl

of the correct virus dilution was added to the wells and then incubated for 2 hours at 37ºC at 5% CO_2 with gentle rocking every 15 min to prevent them from drying. After the incubation, the media was removed from the wells and replaced with replacement media containing 50% Avicel (Sigma Aldrich) and 50% 2x DMEM (with 2µg/ml NAT). The Avicel works as an overlay media similar to agarose and restricts free virus spread, enabling localised plaque formation. The plates were incubated for 3 days at 37ºC and 5% CO_2, until the plaques could be observed. After the incubation, the wells are stained with crystal violet (0.1% naphthalene, 4% glacial acetic acid, 1.36% anhydrous acetic acid with 92.5% water) overnight and the plaques counted the next day. The plaque assays were done in duplicates, and the virus titre was calculated by the equation:

$$\text{Viral Titre} = \frac{\text{Number of plaques}}{\text{Dilution x volume of virus added to the well (ml)}}$$

The unit for the virus titre is Plaque Forming Units (PFU) per ml.

2.2.4 Purification

For purification, the virus (Udorn or A41V-Udorn) at 0.001 MOI was grown on MDCK cells as described above. The viral supernatant (12ml) was then harvested and placed in a centrifuge tube over a 1ml 60% Optiprep Density Gradient Medium (Sigma-Aldrich) cushion. This was ultracentrifuged (Optima LE-80K, Beckman Coulter, California, USA), at 24000 RPM for 1 hour at 4ºC, in a SW28 rotor. This formed a band at the bottom, containing

all the virus. The bottom 2 ml, including the band is taken and added to 10 ml of PBS. This was then placed over an Optiprep gradient, made by adding PBS, and making a series of concentrations from 60%-15% Optiprep. Again, the tubes were ultracentrifuged at 24000 RPM for 1 hour at 4ºC. This formed three separated bands in between the gradients. The different morphologies have different densities which causes them to form separate bands in between the different densities. These were obtained using a syringe and stored at -20ºC.

2.2.5 Immunoblotting

For immunoblotting, cells were plated in 6 well plates and grown overnight and infected with IAV at 1 MOI for the indicated timepoint. The cells were lysed post infection in a NuPAGE MES SDS Laemli Sample Buffer (1X) (Thermo Fisher) and were prepared according to the protocol of Bolt Bis-Tris Plus Mini Gel Electrophoresis System (Life Technologies). Lysates were first heated to 90ºC, and 20µl of each sample per well was loaded to the Mini-PROTEAN Any kDa precast gels (Bio-Rad, California, USA). One of the wells was loaded with 10µl SeeBlue Plus2 Pre-stained protein Standard (Novex, Life Technologies, California, USA). By using an EC570-90 Power supply (Thermo EC), the gel was run at 160V for 40 mins. The proteins were then transferred to a polyvinylidene difluoride (PVDF) membrane (iBlot Dry Blotting System, Life Technologies) using the iBlot Gel Transfer Device (Life Technologies). The membrane was first blocked by

incubating in blocking buffer (5% dry milk in PBS with 0.1% Tween-20) for 1hr. Viral proteins were then detecting using immunoblotting with the anti-Udorn primary antibody at a 1:200 dilution in blocking buffer for 1hr. They were then washed with PBS. Next, a donkey anti-goat secondary antibody conjugated with horseradish peroxidase (HRP) (Thermo Fisher Scientific) at a 1:1000 dilution in blocking buffer was added for 1hr. They were then washed 4x 5min PBS + 0.1% Tween-20. The blot was then treated with Western Breeze Chromogenic Immunodetection kit (Invitrogen, California, USA) before visualization on the SynGene G Box F3- Gel Imaging for Fluorescence and Visible Application.

2.2.6 Protein Quantification Assay

The three separated layers from the virus purification (spherical, filamentous and debris) were used to set up a Protein Quantification Assay, as described in the protocol of Pierce™ BCA Protein Assay Kit (Thermo Scientific). A series of standards were prepared by mixing albumin standard ampules with PBS. 25µl of the standards and samples were set up in a 96 well plate, in triplicates, and then 200µl of the working reagent (50:1 of BCA A with BCA B) was added to them. Then the plate was put on a shaker for 30 seconds, followed by 30 minute incubation at 37ºC. The plate was left to cool to room temperature, and then read on a CLARIOstar plate reader (BMG Labtech, Aylesbury, UK) at 562 nm. The protein concentration of the standards was plotted against absorbance using Microsoft Excel in order to

generate a standard curve. The results from the samples were then compared to the standard curve, to find the protein concentration in each band.

2.2.7 TEM

The separated bands form the virus purification utracentrifugation assay were negatively stained with 1% Phosphotungstic Acid (PTA) for 30 seconds before absorption to TEM grids and imaging. Freshly glow discharge treated 400 mesh copper grids were used and were provided by the Biomolecular Imaging Facility. Samples were imaged on a JEOL 1230 (Tokyo, Japan) electron microscope using a Gatan 831digital camera (Pleasanton, California, USA). The percentage of filamentous virions was calculated following TEM imaging of A/Udorn/72 supernatant. Virions termed filamentous possessed lengths greater than 250 nm. Image processing was limited to cropping and equal adjustment of image levels.

2.2.8 Immunofluorescence

Cells were grown on sterile coverslips in 6 well plates before being infected as described at different MOIs (0.1, 0.5, 1 or 3 MOI) for the indicated time. Cells were fixed in 10% formalin for 10 min at room temperature and permeabilised with 0.4% Triton X-100 (Bio-Rad) for 15 min. The coverslips were then blocked with PBS containing 1% BSA for 30 min before

incubation with the indicated primary antibodies at 1 in 200 dilution in PBS + 1% BSA for 1 hour at room temperature, followed by washing 4 times with PBS. Alexa-labelled secondary antibodies were then added at 1 in 1000 dilution in PBS + 1% BSA, and covered as they are light sensitive, and incubated for 1 hour at room temperature. Again, cells were washed 4 times with PBS, and blotted dry before mounting on glass slides using Prolong Gold (Invitrogen), and left overnight to dry before they were viewed with epifluorescence microscopy (LumaScope, Etaluma, California, USA) or confocal microscopy (Zeiss LSM 880 with Airyscan, Oberkochen, Germany).

For the entry pathway analysis, freshly split RAW Blue cells with 5×10^5 cells per sample, were resuspended in 1 ml DMEM and 10% FBS at 37°C. Cascade-blue dextran (1mg/ml), Alexa-594-Transferrin (50ug/ml) , and FluoSpheres (1×10^8) were added to the cells. To this 3 MOI of Alexa-488-A/Udorn/72 labelled with vibrant DiD in DMSO (1×10^6 PFU/ml) was added. The samples were gently shaken at 37°C in sealed tubes for 0-60 minute. Sample uptake was then stopped by the addition of ice-cold PBS. Samples were washed 3 times with cold PBS, fixed with 4% formaldehyde for 15 min, pelleted, and washed 3 times with PBS. Cells were then viewed on a Zeiss LSM 880 confocal microscope to detect virus entering cells by macropinocytosis, clathrin-mediated endocytosis and phagocytosis.

2.2.9 Confocal Microscopy

Confocal microscopy was performed using the Zeiss LSM 880 confocal microscope with a plan-apochromat 63x objective (Zeiss) using Zeiss Zen software and automatic image setting parameters. For NF-kB p65 imaging, single Z-sections through the cell mid-plane were used and Zen software was used to define the nucleus and then compare the intensity of p65 fluorescence in the nucleus and cytoplasm. For entry pathway analysis, Airyscan detection was used with Z-section 3D imaging.

2.2.10 QUANTI-Blue NF-kB Activation Assay

96 well plates were set up as described in the manual provided by the QUANTI-Blue (InvivoGen). QUANTI-Blue is designed to detect secreted embryonic alkaline phosphatase (SEAP) that is produced under control of a NF-kB responsive promoter. RAW Blue cells (InvivoGen) were grown as described and were treated with CPZ (20uM) and/or EIPA (80uM) (both from Sigma Aldrich) for 1 hour, and then infected with either Udorn or M1-A41V at 3 MOI for 1 hour. 200µl of QUANTI-Blue was added to the plate, and 20µl of the pre-treated RAW Blue cells were added to them. This was then incubated for 30 minutes at 37°C. After the incubation, the plates were read on a CLARIO-star (BMG Labtech) plate reader at 620 nm. The results were used to plot a graph in Excel showing the absorbance for each of the conditions and required calculations, including Student's T Test to look at the significant differences, were carried out.

2.2.11 IncuCyte Autophagy Activation Assay

IncuCyte live cell imaging plates were set up with A549 cells that stably express the autophagy sensor LC3-mCherry-eGFP as described by IncuCyte (Essen Biosciences, Ann Arbor, MI). Cells infected with either filamentous Udorn or spherical PR8 viruses at 1 or 5 MOI and live imaged on the IncuCyte Zoom imaging system 37°C with images taken at 10x every 1 min for 120 min. Live images were processed using IncuCyte software to calculate and display eGFP and mCherry fluorescence over time for each condition.

2.2.12 UV Inactivation of Virus

IAV was grown as previously described and taken in a sterile petri dish and were subjected to UV radiation at 254 nm for 30 minutes. This makes the virus lose its infectivity. The UV inactivated virus was used in plaque assays to confirm that they were unable to form plaques i.e. cannot infect cells anymore.

CHAPTER 3

RESULTS

3.1 Purification of Influenza Virus Morphologies

3.1.1 Introduction

Influenza virus can display various morphologies, ranging from spherical, ellipsoidal and filamentous, although some random shapes can also be sometimes observed (Noda, 2012) (Calder et al., 2011). However, the spherical and filamentous shapes are the most commonly seen. The spherical viruses, as named are spherical structures, and are usually 120 nm in diameter. The filamentous structure is more elongated, and they can be a few micrometres long, but normally they go up to 1μm. However, the diameter remains 100-120 nm. The spherical structure is more common in the laboratory grown strains, while the filamentous are observed more in samples from clinical isolates (Elton et al., 2013). Many different viral and host factors can influence the structure to be either spherical or filamentous. The virus undergoes mutations to adapt to the different environments and thus their phenotype changes accordingly (Elton et al., 2013).

The first part of the experiments was to determine that A/Udorn/72 strain is actually pleomorphic, and that it was indeed worth using Udorn and its mutant, M1-A41V, to determine the differences in spherical and filamentous virus. The Udorn strain can retain its filamentous morphology during passages. However, when there is a single point mutation of its M1 protein at position 41 from alanine to valine, the Udorn strain completely loses its ability to form filaments, and only forms spherical virions (Campbell et al., 2014).

3.1.2 Results: Purification of spherical and filamentous influenza viruses

To determine the morphology of Udorn, the viruses were grown in MDCK cells and harvested. They were then separated by ultricentrifugation to look at the difference in morphology and to separate the spheres from the filaments. This was done by setting up an iso-osmotic gradient of Optiprep, followed by ultracentrifugation at 24000 RPM for 1 hour at 4°C. This separates the filaments from the spheres, and they accumulate in separate bands within the media, due to their different densities.

Figure 3.1 shows the separated bands after ultracentrifugation. The spheres have the lowest density and settle at the top layer. Filaments have a higher density than spheres and accumulate in the second layer. The third layer only comprises of cell debris.
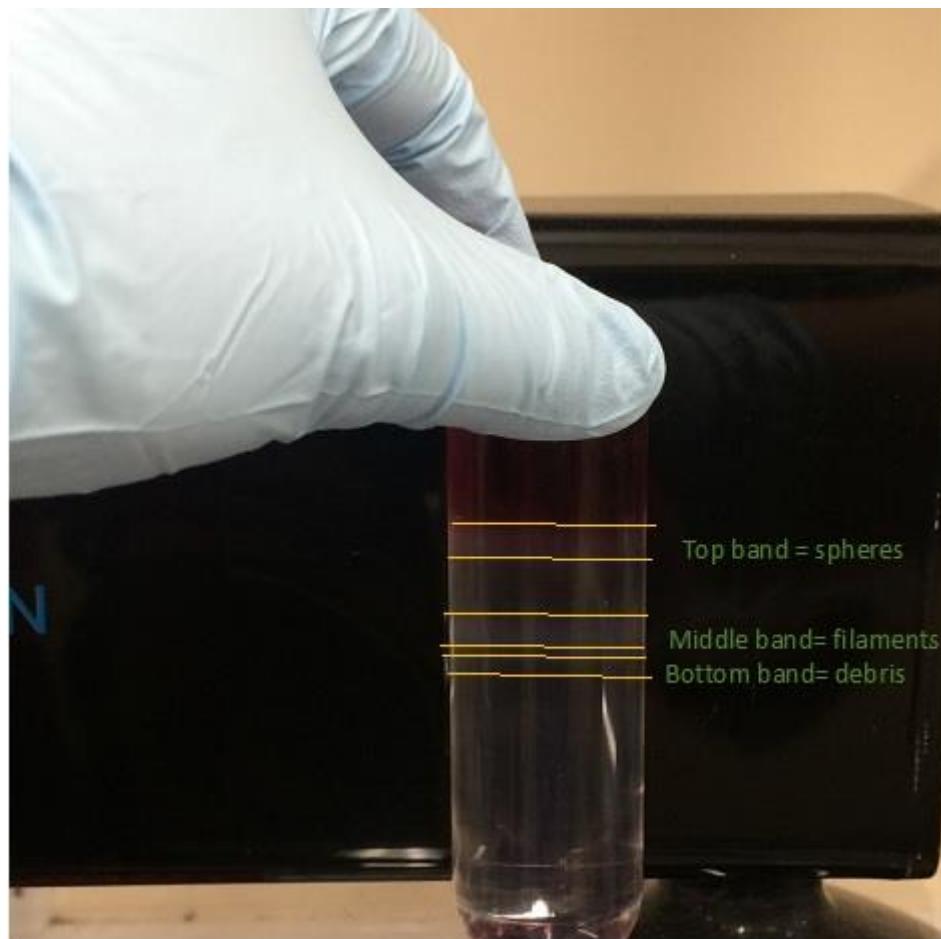
Figure 3.1 Separation of Influenza A virus (Udorn) morphologies. Udorn grows as a mixture of filamentous and spherical virions. MDCK cells were infected with the virus at 0.001 MOI and left for 48hours. The supernatant was then collected and ultracentrifuged at 24000 RPM for 1 hour on an Optiprep gradient, to separate the filaments from the spheres. The gradients were set up at a series of densities (from 60% to 7.5%). The different morphologies have different densities which causes them to settle in between the Opriprep gradient that can then be extracted.

3.1.3 Results: Analysis of purified fraction

IAV are pleomorphic and can express different morphologies. The assays above were used to show that the strain used, A/Udorn/72 does indeed consist of both spherical and filamentous virions and these can be separated using ultracentrifugation. The separation with ultracentrifugation depends on the density, and thus it forms three distinct layers, which can be separated and analysed. To confirm the separation of filaments and spherical virions, the layers were extracted from the gradient, separated and subjected to TEM (Figure 3.2 and 3.3), protein quantification (3.4) and immunoblot (Figure 3.5) analysis.

To determine virus morphology, purified fractions were subjected to negative staining and visualization by TEM. TEM analysis showed successful separation of filamentous and spherical virions (Fig. 3.2 and 3.3). The protein quantification assay was used to calculate the total amount of protein present in each of the virus fractions (Figure 3.4) whereas immunoblotting was used to show the presence of the specific viral proteins in the separated bands (Figure 3.5).

The protein concentration assay shows that all the three layers contain comparable amounts of protein, but it is not possible to determine what they are from this assay. Immunoblot analysis was done further on the bands, and these show that the top and middle band contains most of the viral proteins, thus confirming that these fractions contain the purified viruses.

Although the bottom band contains some viral protein, the amount is significantly less, suggesting that this fraction is mostly just debris.
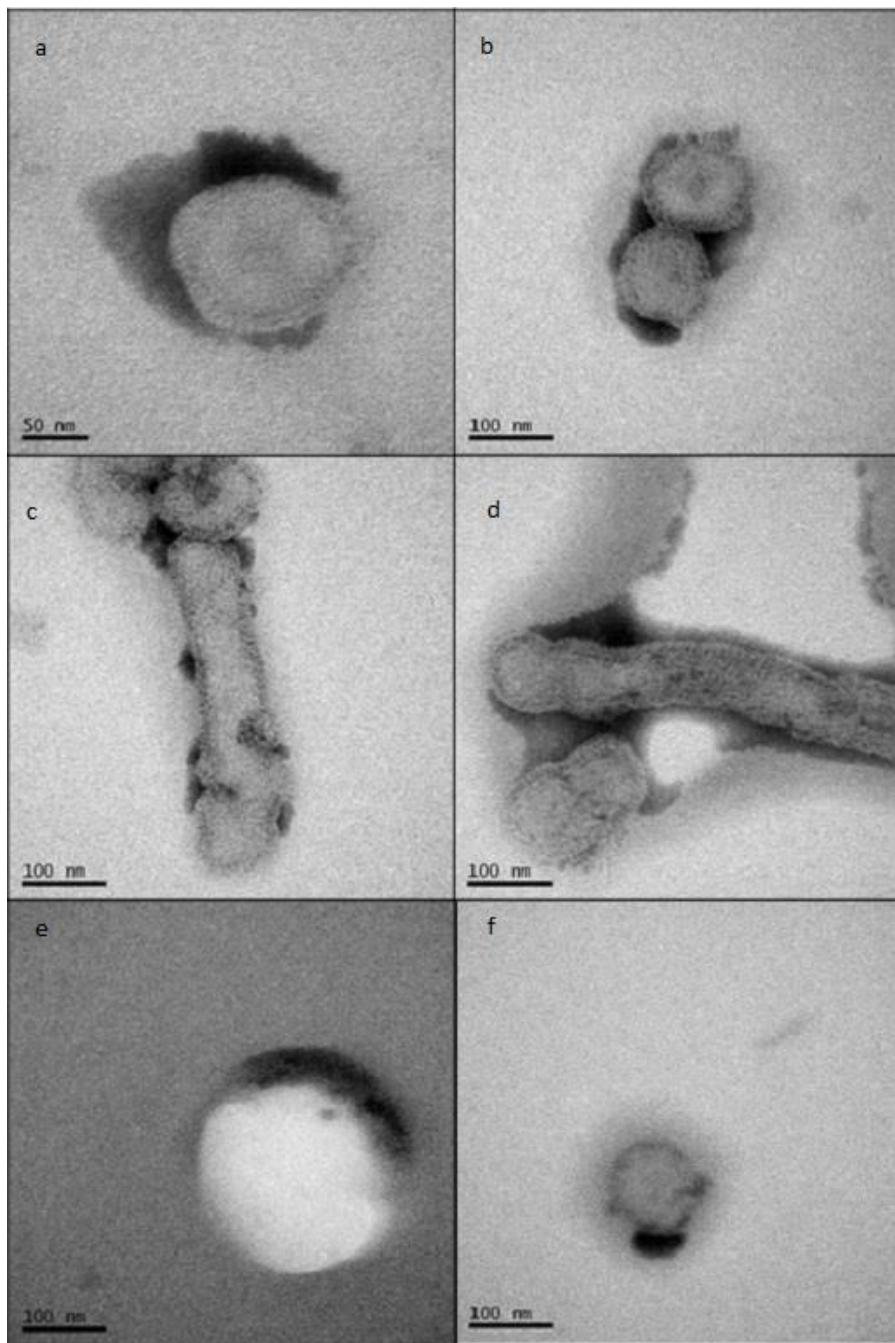

Figure 3.2 Pleiomorphic morphology of A/Udorn/72. The separated bands following ultracentrifugation purification were observed following negative staining and TEM imaging. Figure a and b shows the constituents of the top

band, and mostly spherical structures can be observed. Figure c and d are taken from the middle band, and mostly filamentous structures can be seen, although a few spheres are also observed. Due to the high forces present, some of the filaments can disintegrate or curl up as seen in the images. Figure 2e and 2f show the bottom band which is filled with debris that lacks the outer spiky layer of Haemagglutinin and is significantly larger or smaller than 100nm virions.

TEM was used to further confirm the results, that the bands actually show the separated morphologies. For A/Udorn/72 (Figure 3.2) it was seen that the top band consisted mostly of the spherical virions. The middle band consisted of filaments. These filaments however curl up and disintegrate because of the very powerful ultracentrifugation process, and thus cannot be further used to infect cells. The third band mostly shows debris. These assays helped to show that Udorn actually consists of both filamentous and spherical virions, and thus were used in the following experiments. In case of M1-A41V, it still formed 3 layers, but in the middle layer, unlike Udorn, the virions look similar to the spherical virions. They are slightly bigger in size, and some look like bacilliform, hence the difference in density.
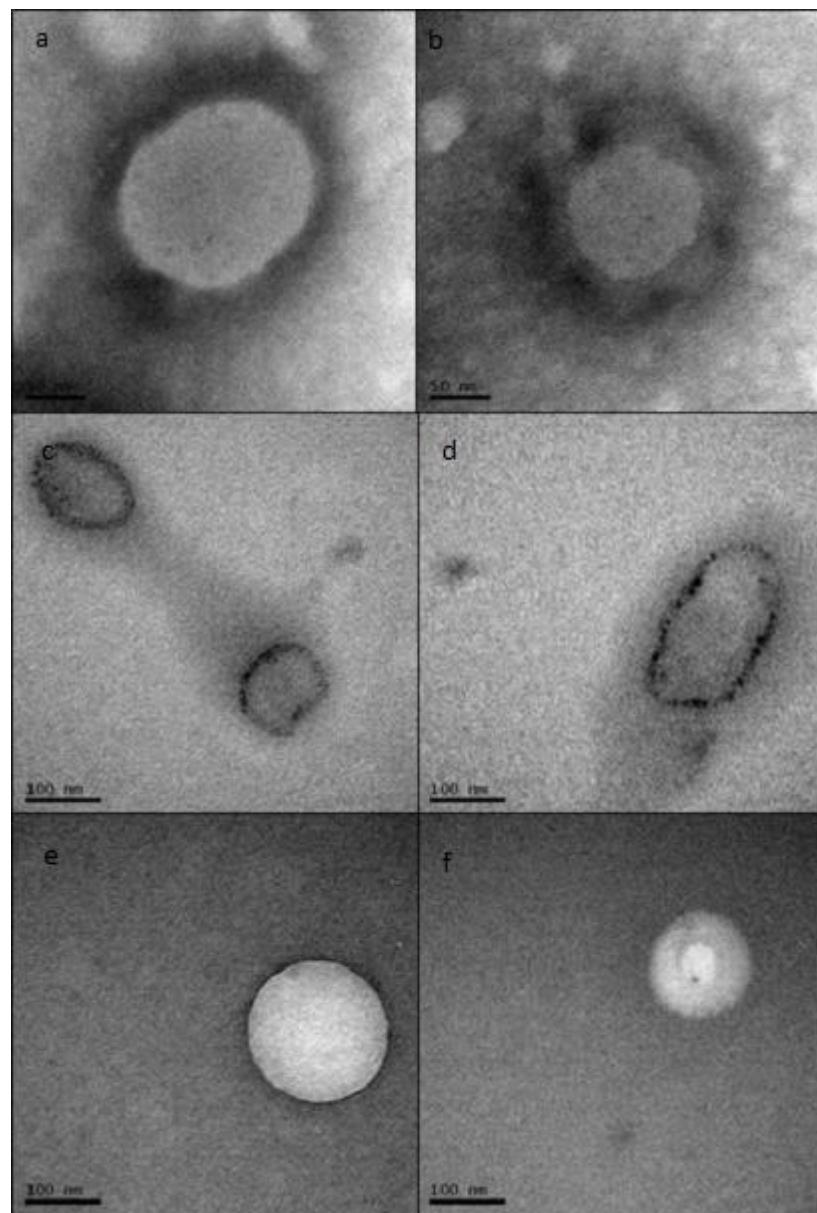
Figure 3.3 M1-A41V does not form filamentous virions. M1-A41V virus grown at 0.001 MOI on MDCK cells, were subjected to ultracentrifugation on an optiprep gradient. The virions separated to form 3 layers. The upper layer showed spherical virions (a and b). The middle layer showed slightly larger virions, which looks like bacilliform (c and d). The last layer consisted of debris (e and f). This shows that unlike, A/Udorn/72, filaments do not form in M1-A41V.
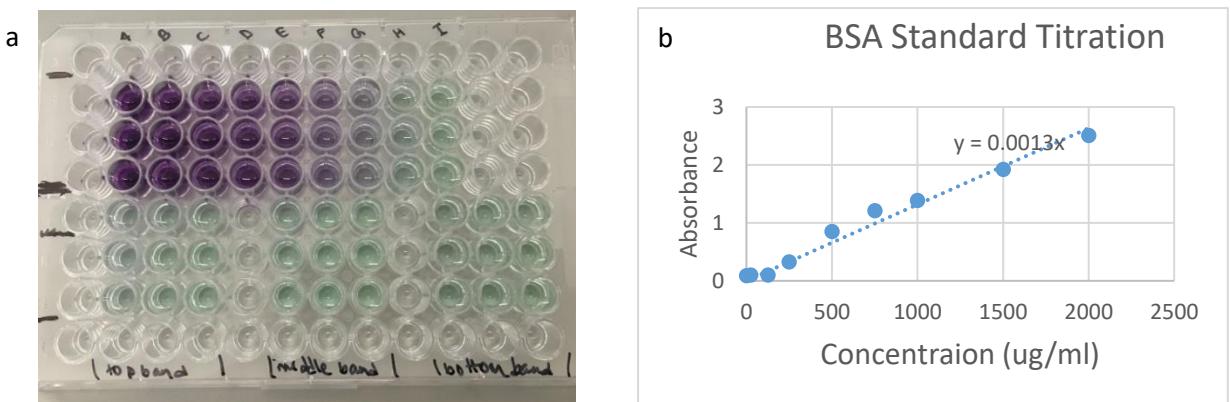
Udorn	Absorbance	Protein
Top band	1.077	828.4615
Middle Band	1.567	1205.385
Bottom Band	1.5005	1154.231

M1-A41V	Absorbance	Protein
Top band	0.1751717	134.74747
Middle Band	0.136697	105.15152
Bottom Band	0.1437879	110.60606

Figure 3.4 Protein concentration of the separated bands of A/Udorn/72 and M1-A41V. A BCA protein concentration assay was carried out on the samples from the three bands. This was done on a 96well plate with a Pierce BCA Protein Assay Kit, as shown in a. The results were read on a plate reader, and a BSA standard curve was plotted in Microsoft Excel. The gradient of the curve was calculated and used to calculate the concentrations for the separated bands as shown in the table.
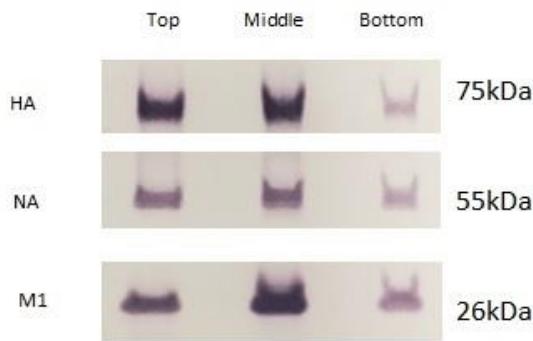
Figure 3.5 Protein contents of A/Udorn/72 fractions. Extracted fractions were subjected to SDS-PAGE and immunoblotted with the anti-Udorn antibody, showing the bands for HA (75kDa), NA (55kDa) and M1(26kDa) from each separated fraction.

3.1.4 Summary

From previous studies we know that A/Udorn/72 is pleomorphic in nature, and its mutant M1-A41V only forms spherical virions; however, we first sought to confirm this before using the strains for all the further experiments. The results from the immunoblot analysis and TEM confirm that Udorn does indeed form filamentous and spherical virions. The results also show that the morphologies can be separated, due to their difference in density. Although the harsh process of separating them breaks the filaments, hopefully fewer harming techniques will be discovered in the future to separate them, so that studying the difference between spheres and filaments become easier.

3.2 Priming of Host Cells by infecting with UV treated Virus

3.2.1 Introduction

It is essential for the IAV infection to spread for their growth and survival, and this is aided by their budding process. The infection can either spread from one cell to another or they can spread in between different hosts. It has been suggested that many filaments may not complete the budding process but may be there to aid in infection of other virions (Badham and Rossman, 2016). Budding IAV filaments are long enough that they can easily contact a neighbouring uninfected cell. Given that viral contact triggers the induction of macropinocytosis (Badham and Rossman, 2016) if a filament contacts a neighbouring cell, the upregulation of macropinocytosis may prime the cell to take up other free spherical or filamentous viruses that it next encounters (Badham and Rossman, 2016). So, these 'non-infectious', long and thin filaments may prime the cells beforehand for other infectious virions. For these reasons it was thought if cells were primed it would help IAV infection to work better and more efficiently, which may explain a function of the filamentous morphology, as shown in Figure 3.6 (Siezkarski and Whittaker, 2005).
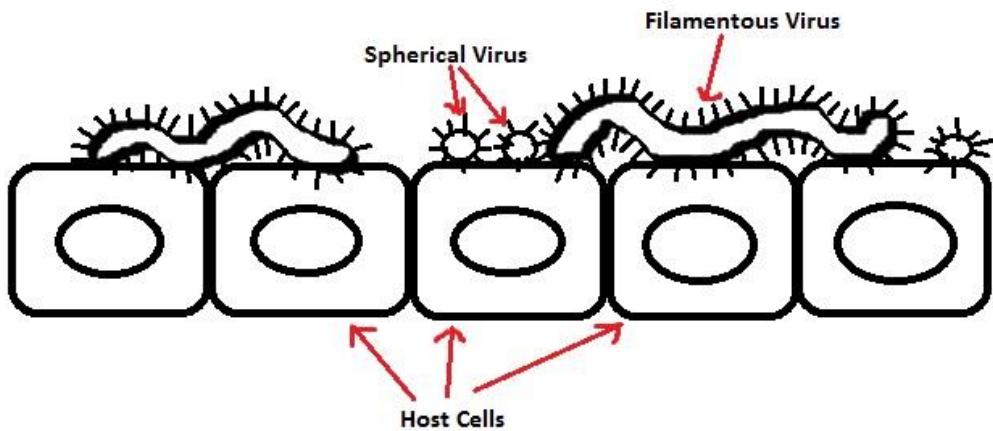
Figure 3.6 Priming of host cells may enhance IAV infection. Schematic diagram to show that the long, thin filamentous virions can come in contact with multiple cells at the same time. This binding increases the chance of macropinocytosis activation to occur. This may help more spherical and filamentous virions to enter the cells, and thus increasing the chance of infection. Spherical virions do not come into contact with multiple cells at the same time to induce macropinocytosis. For this reason, it was hypothesised that filaments can prime cells before infection, to make the overall infection process faster.

3.2.2 Results: Filamentous virion priming of infection

As it was hypothesised that non-infectious filamentous IAVs can prime cells, the virus was inactivated with UV treatment. Both Udorn and control spherical M1-A41V virions were subjected to UV radiation at 254 nm for 30 minutes. Subjecting to UV treatment damages the RNA genome, thus inactivating the virus; but in turn they can act as mimics of the non-infectious filamentous virions. To confirm UV inactivation, plaque assays were carried out. Plaque assays are the standard method to check infectious virus concentration by measuring the plaque forming units (pfu) of the sample virus. The results for both Udorn and M1-A41V are given in Figure 3.7. Figure 3.7a shows results from untreated M1-A41V virus where the titre was 1.1×10^6 pfu/ml. Figure 3.7b shows the result for UV treated M1-A41V. Even in the first well, there is no plaques, so the concentration is 0 pfu/ml. Figure 3.7c, shows the plaques for A/Udorn/72, with a titre of 5.0×10^5 pfu/ml In Figure 3.7d, when the same virus is inactivated with UV treatment, it again fails to form plaques and the titre is 0 pfu/ml. Although the untreated virus of the same source forms plaques as normal, when they were UV inactivated, they lose their ability to form plaques, i.e. the UV treatment did indeed inactivate both Udorn and M1-A41V successfully. This is shown in more details in the 'Appendix' section.

As it was confirmed that the treated viruses lose their ability to infect, they were next taken to check if non-infectious filamentous or spherical virus can indeed prime cells for better infection. To test this, MDCK cells were grown on 6 well plates, and first 'infected' with the UV inactivated virus for 1 hour

at 1 MOI. This was then followed by infection with untreated virus again at 1 MOI, for 4, 6, 8 and 18 hours. The infected cells were then lysed and immunoblotted to check the changes in IAV protein expression over time. The results are shown in Figure 3.8, which shows that over time, when the cells were infected with UV treated virus only, the viral proteins decreases. This happens because the virus enters the cells, but the cell degrades them over time and no viral proteins are being expressed. No subsequent viruses are being formed, as they fail to infect and replicate, the viral proteins are no longer seen at the longer infection timepoints. However, the results also do not show any differences between the viral protein expression levels, when the cells were primed first with inactivated virus, as compared to just infection with untreated virus. This suggests that previous IAV contact does not prime cells to better activate macropinocytosis and enhance virus infectivity.

To confirm these results further, Epifluorescence Microscopy was used (Figure 3.9) to check if any differences in viral protein distributions could be spotted between the different conditions. MDCK cells were again infected with UV inactivated virus for an hour at 1 MOI, followed by infection with untreated virus at 1 MOI for 6, 8 and 18 hours. The cells were then fixed and stained with an anti-Udorn antibody, followed by Alexa-488 secondary antibodies and epifluorescence imaging. The results confirm that UV treatment of virus eliminates its ability to productively infect cells, irrespective of the incubation time. The results also show that priming of

cells with UV treated virus, before infection, does not show any difference in infection.

Following this, Epifluorescence Microscopy was again used to check if there is any difference in priming ability due to the morphology of the priming and infecting virus, using A/Udorn/72 and M1-A41V (Figure 3.10). MDCK cells were once again infected with UV treated Udorn or M1-A41V at 1 MOI for 1hour. This was followed by infection with the untreated Udorn or M1-41V at 1 MOI for 8 hours. The cells were then prepared for immunofluorescence microscopy by staining with anti-Udorn antibody as before. The cells were then mounted in the presence of DAPI and viewed with an epifluorescence microscope. The results show that there was no difference between M1-A41V and A/Udorn/72 in terms of priming or infectivity. Priming with filamentous or spherical UV inactivated virus beforehand does not show any difference in subsequent infectivity of either filamentous or spherical virions. However, in both cases it was noticed instead of aiding infection, as was hypothesised, the expression of viral proteins decreases for both filaments and spheres. This means that priming with inactivated virus is not actually helping the virus to enter cells better but is actually inhibiting viral entry.
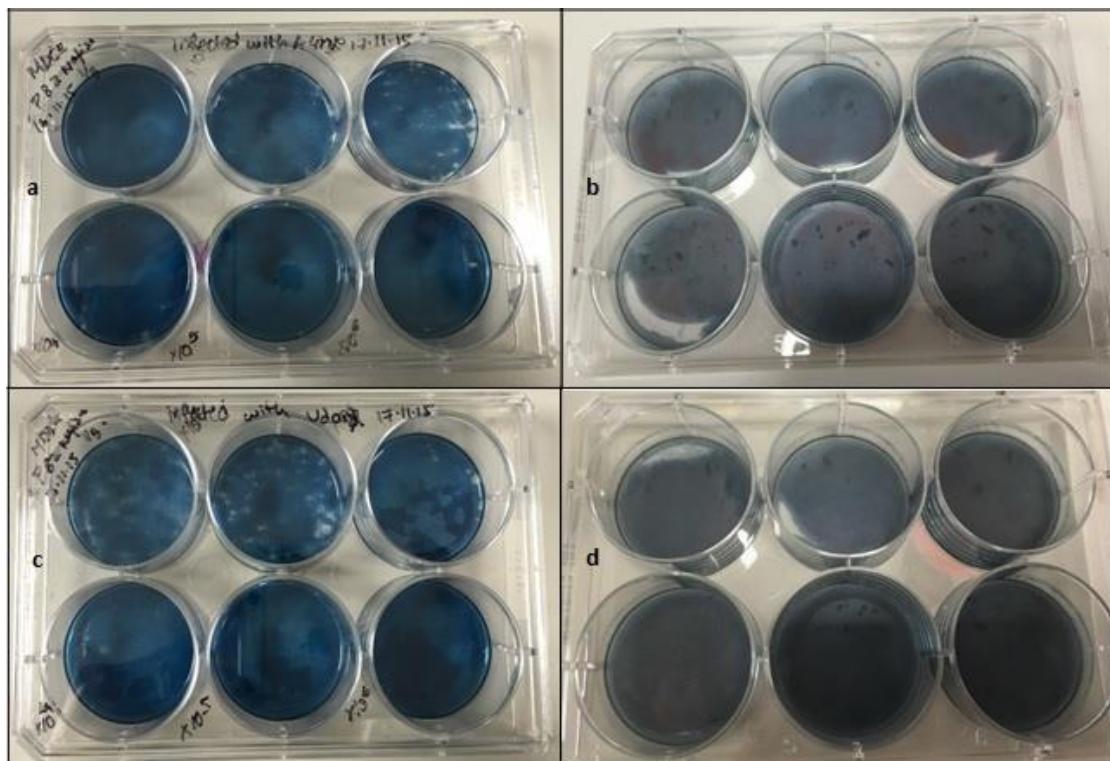
Figure 3.7 Plaque assay to confirm UV inactivation of Virus. To inactivate the virus, viral stocks were exposed to UV radiation for 1/2 hour at 294 nm. This inactivated virus was then used to infect MDCK cells in a 6 well plate, at 1 MOI for 48 hours. To compare the results, MDCK cells were also infected at the same conditions with untreated virus, from the same source. As shown in 'a', with wild type M1-A41V infection, plaques form as normal. However, when the same virus strain is UV treated, it loses its ability to form any plaques ('b'). This is also seen when infected with Udorn; when infected by wild type plaques form ('c') as usual but are unable to form then when it is UV treated ('d').
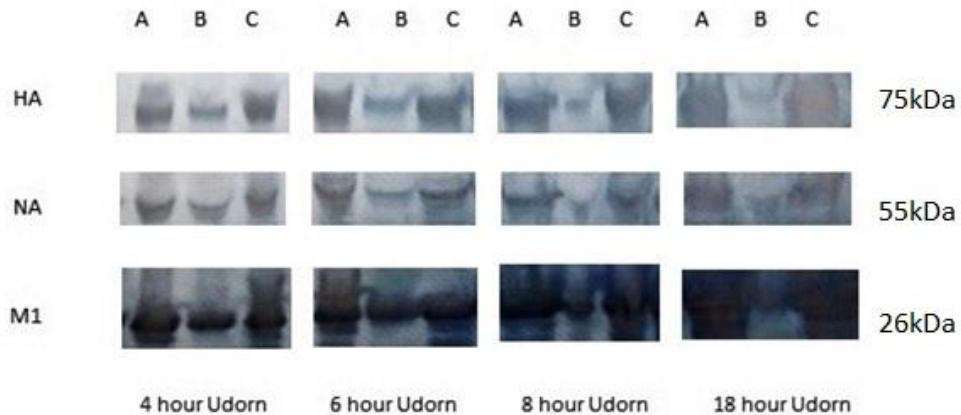
Figure 3.8 UV inactivation disrupts viral protein synthesis. Immunoblot results to show the effect of UV inactivation on viral protein expression after different hours of infection. For UV priming, MDCK cells were grown in 6 well plates, and first treated with UV inactivated virus for 1 hour. The cells were then washed with PBS and again infected with the normal untreated virus. They were infected for different time points, to look at differences in infection due to time. 'A' shows results for infection of cells with first UV inactivated virus followed by untreated virus, 'B' shows results for infection with only UV inactivated virus and 'C' shows results from infection with only untreated virus. The viral proteins can be seen in the early hours after infection, but at later hours protein synthesis is disrupted in UV inactivated virus. No difference can be spotted in viral proteins due to priming of cells, before infection.
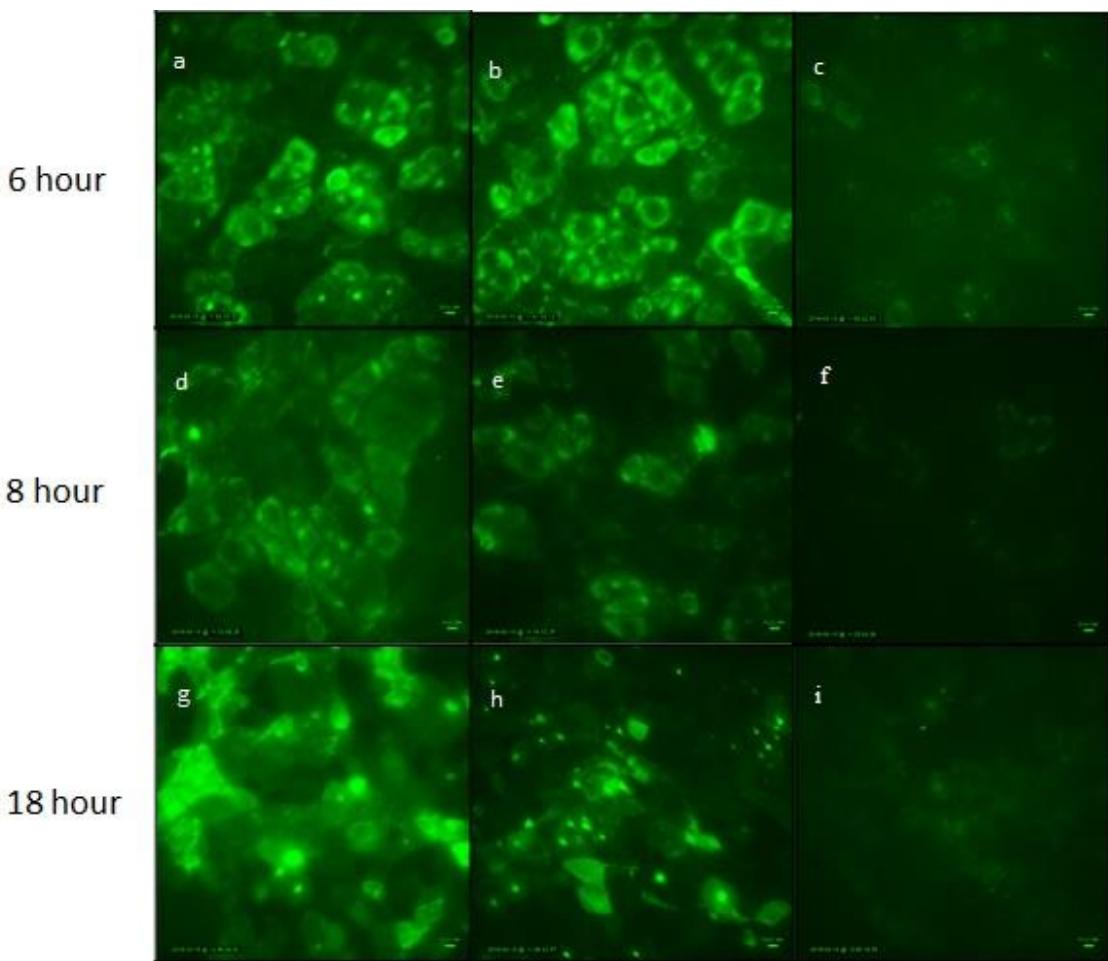
Figure 3.9 Infectivity differences following virus priming over time. Epifluorescence microscopy was used to check if there are any difference in infectivity due to priming of MDCK cells, at different time points. MDCK cells were first infected with UV treated virus for 1 hour at 1 MOI. This was followed by infection with untreated A/Udorn/72 at the same MOI for 6, 8 and 18 hours. Figures 'a', 'd', and 'g' are showing results for infection with untreated A/Udorn/72 only; 'b', 'e' and 'h' are showing results for infection with UV treated virus, followed by untreated virus; 'c', 'f' and 'i' are showing results for infection with UV treated virus only. The cells were stained with

anti-Udorn antibody and Alexa-488 labelled secondary antibodies before visualisation. The scale bar shows 10um.
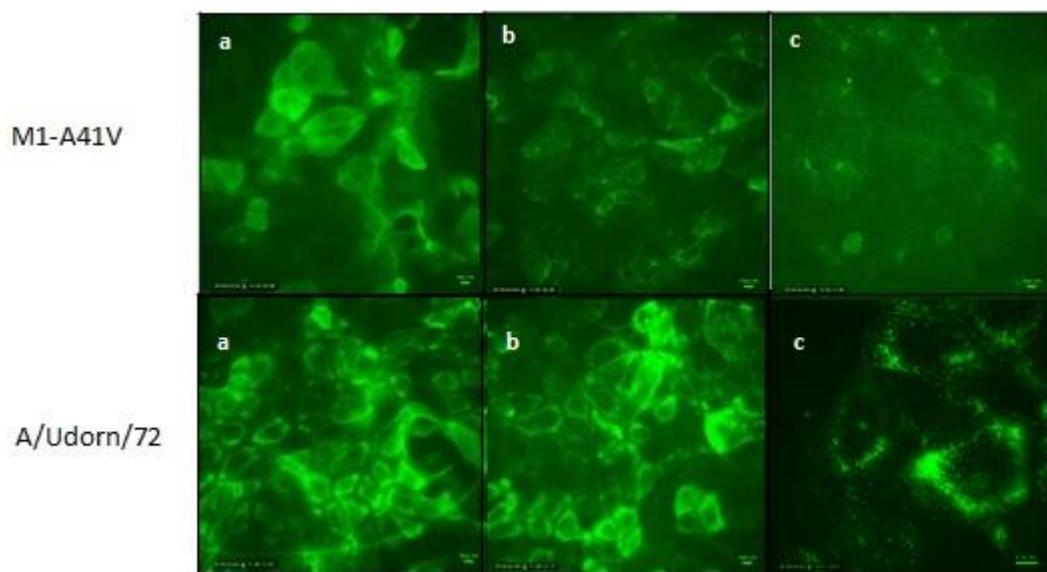
Figure 3.10 Morphology effect on MDCK cell priming with UV inactivated Virus. MDCK cells were infected with UV inactivated virus (either A/Udorn/72 or M1/A41V) at 1 MOI for 1 hour. This was then infected with untreated Udorn or A41V virus at 1 MOI for 8 hours. The cells were then prepared for immunofluorescence by staining with anti-Udorn antibody and viewed with epifluorescence microscopy. In 'a' the cells were infected with only M1-A41V or A/Udorn/72, in 'b' they were first infected with UV treated M1-A41V or A/Udorn/72 followed by infection with the same untreated virus, and finally in 'c' they were only infected with UV treated virus. The scale bar shows 10um.

3.2.3 Summary

Filaments are long and thin and can come in contact with multiple host cells at the same time, even during the course of virus budding. This can potentially induce macropinocytosis and thus the cells can engulf other IAV virions at a greater rate (Badham and Rossman, 2016). It was thought that some filamentous virions are never released from the infected cell, and their only purpose may be to induce macropinocytosis in neighbouring cells (Badham and Rossman, 2016), thus priming the cells for infection, and making the viral infectivity process much faster and more efficient.

To test this hypothesis, cells were infected with UV inactivated virus, before infecting with untreated virus. UV treatment of the virus damages their RNA genome; thus, they lose their ability to productively infect cells. The cells were first treated with UV inactivated virus, which acted like the 'un-infectious' filamentous virions, to prime the cells for latter infection. The cells were then treated with untreated virus, and the results were viewed with the help of immunoblotting and epifluorescence microscopy.

From both assays, the results concluded that priming of host cell prior to infection, with UV inactivated virus, does not aid and make infection quicker. The infection for both Udorn and A41V did not show any differences due to priming. This means the infectivity of both Udorn and A41V are the same, and priming does not assist the filaments in any way as it was hypothesised. However, it was noticed from the assays that in both filamentous Udorn and spherical A41V, if the host cells were primed beforehand, then infectivity

was reduced. This suggests that instead of making the whole process faster and more efficient, as it was thought, priming actually decreases virion infectivity through an unknown mechanism. This mechanism may be that priming causes the innate antiviral proteins to activate faster and more easily. It also may be due to the factor that macropinocytosis causes a peak, but then it declines, thus reducing infectivity.

Chapter 3.3 Differences in Host Factors can affect the activity of viral morphologies

3.3.1 Introduction

Host factors seem to play an important role in determining the morphology of the virus. The immune system of the host, both innate and adaptive, also plays an active role in viral infectivity and replication and thus may be affected by virus morphology (Fukuyama and Kawaoka, 2011). The innate immune system is the first line of defence against IAV, and the following experiments will be looking at differences in infectivity of IAV due to host cell factors, and how they can differ between the two morphologies.

3.3.1.1 Differences in NFkB expression due to IAV morphology

NF-kB is one of the most important regulators of the innate immune response of hosts and is sometimes termed as the central mediator of immune responses (Hiscott et al., 2016). It plays an important role against viral infection, and thus viruses have evolved to work around the NF-kB pathway for better infection progression. During influenza virus infection, viral proteins interact with the host proteins and use them for their own benefits, including the NF-κB signalling cascade. NF-κB signalling is essential for the host immune response, and the viral proteins manipulate the molecular function of the signalling molecules involved to assist in their pathogenesis (Nimmeriahn et al., 2004). Figure 3.11 shows the NF-kB

pathway, which gets activated when TLRs recognise PAMPs (TLR7 for IAV), which may be presented to them in endosomes or autophagosomes.

As TLRs respond to PAMPs in internal vesicles and filaments and spherical virions enter cells by different endocytic pathways, it is possible that morphology can affect TLR and subsequently NF-kB signalling at early stages of infection.
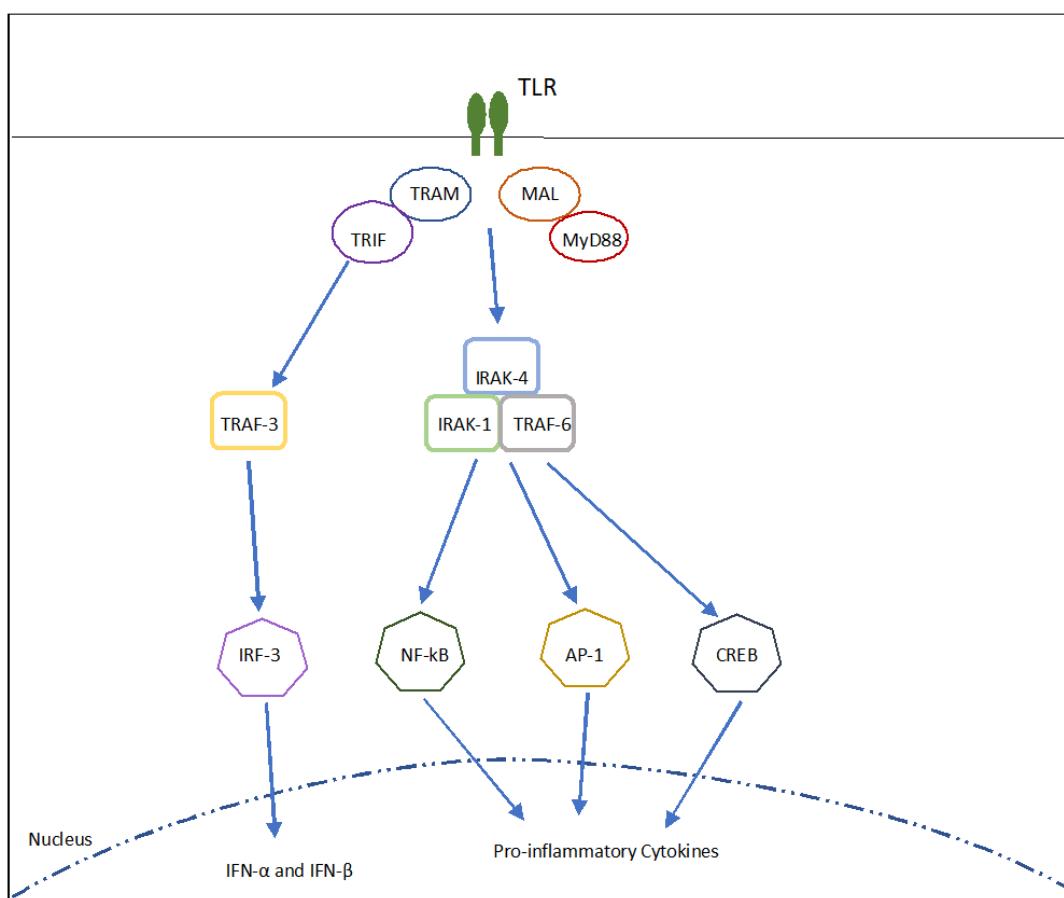

Figure 3.11: Diagrammatic representation of the innate immunity pathways of the host cell leading to pro-inflammatory cytokine production. The TLR comes across a pathogen, it triggers the NF-kB pathway which causes the NF-kB to get activated and produce pro-inflammatory cytokines (figure modified from O'Neill, Gollenback and Bowie, 2013).

3.3.1.2 Results: NF-kB activation

To check if there is a difference in NF-kB activity due to the difference in morphology, during early infection, epifluorescence and confocal microscopy were used. MDCK cells were grown in 6 well plates and were infected with A/Udorn/72 or A41V cells for 1 hour at 3 MOI. The infected cells were then stained with anti NF-кB (p65) and anti- Udorn antibodies, before being mounted with DAPI and observed by immunofluorescence microscopy.

In figure 3.12, NF-kB is shown in green, the virus (A/Udorn/72 or M1-A41V) is shown in red and the MDCK cell nucleus is shown in blue (DAPI). It can be seen that when infected with M1-A41V, NF-kB traffics to the nucleus of the cells. However, this cannot be seen when the MDCK cells were infected with Udorn. When infected with Udorn, the NF-kB does not enter the nucleus but remains at its periphery. This suggests that when infected with A/Udorn/72, NF-kB fails to get activated. However, NF-kB does get activated when infected with the spherical virus M1-A41V. This means that filaments are somehow preventing NF-kB activation, and thus it does not enter the nucleus.

To confirm these results, the experiments were repeated on different cell lines, including immune cells that exhibit robust innate antiviral immunity and starting with U937 cells. U937 cells are human monocytes from lymphoblasts, and when treated with PMA they differentiate to form macrophages. They were infected and stained in the same method as

before and observed by epifluorescence microscopy. The results are shown in Figure 3.12, which again confirms that filaments somehow block the activation of NF-kB. Again, it can be seen that in A/Udorn/72 NF-kB remains in the cytoplasm, while when infected by M1-A41V, NF-kB enters the nucleus. This again shows that spheres facilitate NF-kB activation, but filaments somehow prevent this.

To test if this happens on multiple cell lines, the experiments were again repeated on different cell lines. Human epithelial 293T and A549 cells were infected at 1 MOI with either Udorn or M1-A41V for 1 hour, and again stained with the same antibodies, and were compared with MDCK results. This time confocal microscopy was used to look at the cells. As seen in Figure 3.13, the difference between M1-A41V and Udorn is hard to see in both 293T and A549 cells. Although, some NF-kB nuclear localization can be seen in A549 cells infected with M1-A41V, but it cannot be seen in 293T cells. This means that NF-kB nuclear localization during spherical virus entry is not universal for all cells, and that IAV activation of NF-kB varies in different cell lines.
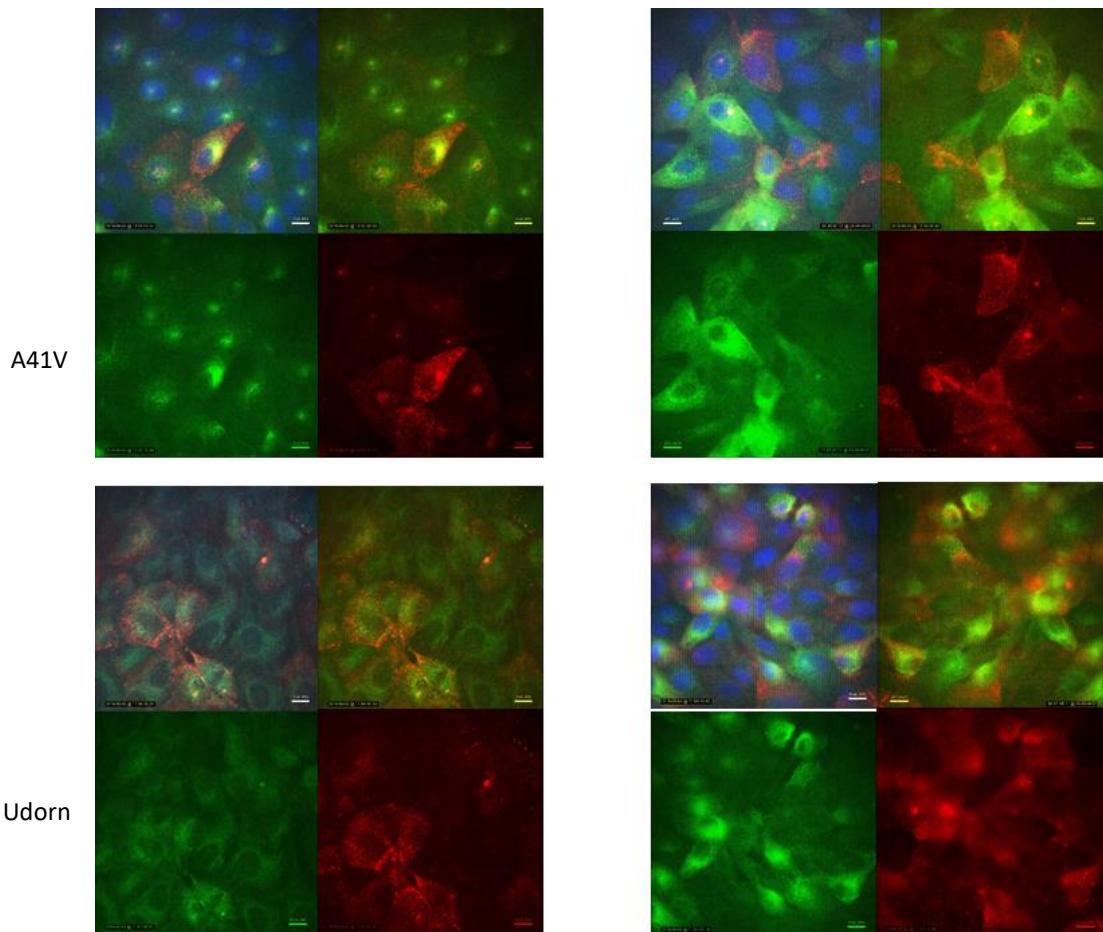
Figure 3.12: Nuclear Localization of NF-kB in MDCK cells. MDCK Cells were either infected with A/Udorn/72 or M1-A41V at 1 MOI for an hour. Anti-NF-kB (p65) (green) and anti-Udorn antibodies (red) were added to the cells and imaged by epifluorescence. MDCK cell nuclei are show in blue (DAPI). As it can be seen from the staining, NFkB is localized in the nucleus of the cells infected with A41V, but not infected with Udorn. Scale bar shows 10um.
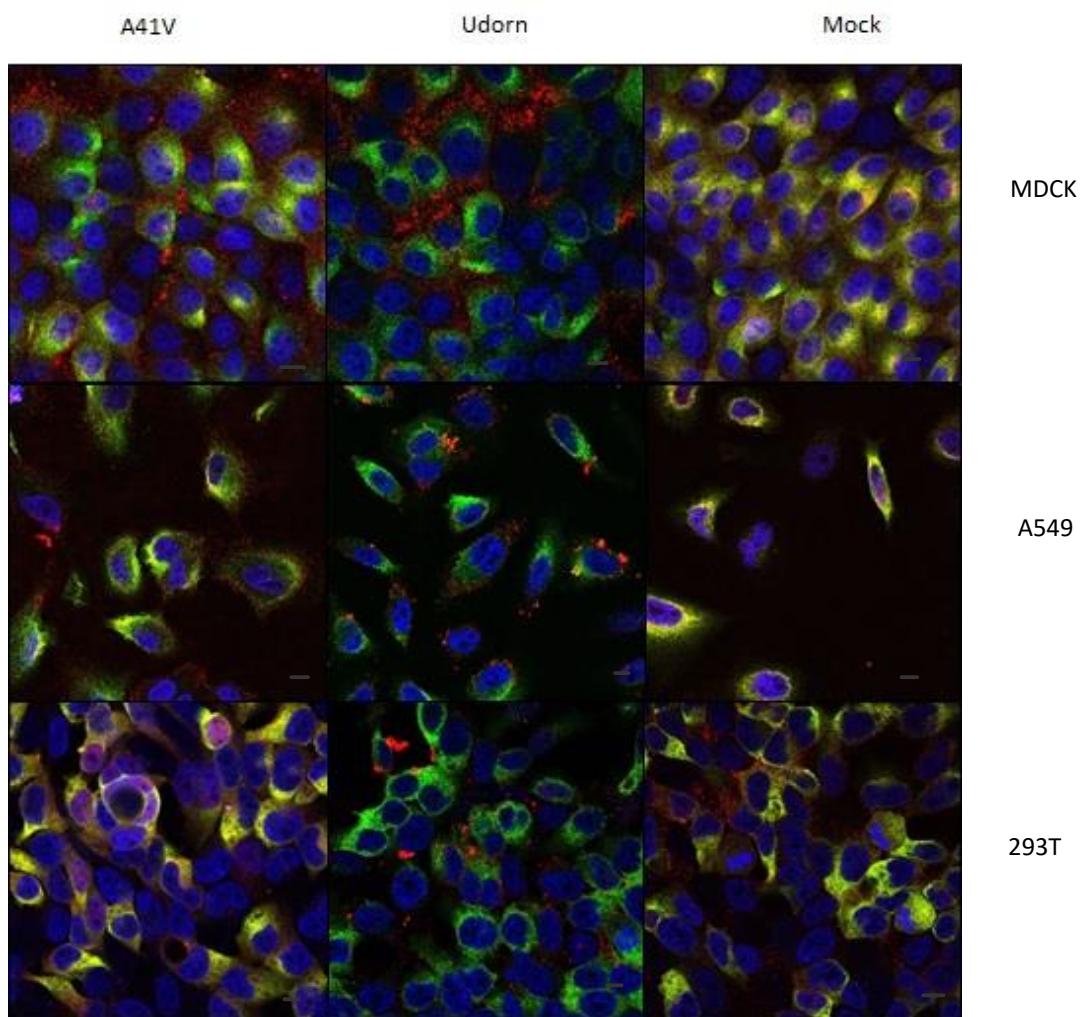
Figure 3.13 Confocal images showing the difference in nuclear localization of NFkB in different cell lines. The cells were infected with either A/Udorn/72 or M1-A41V at 1 MOI for 1 hour. They were then stained with anti-Udorn antibody (red) and anti-P65 for NF-kB (green). The cell nuclei are shown in blue (DAPI). As can be seen in image 3.15a (293T cells) and 3.15b (A549 cells), the difference between the spheres and filaments are not really noticeable, but in case of MDCK cells, as shown in Figure 3.15c, the difference is more dramatic. In MDCK cells, when infected with A/Udorn/72, NF-kB fails to enter the nucleus, but when infected with M1-A41V it enters the nucleus. This difference is not noticeable in A549 or 293T cells. The scale bars in the figures show 10um.
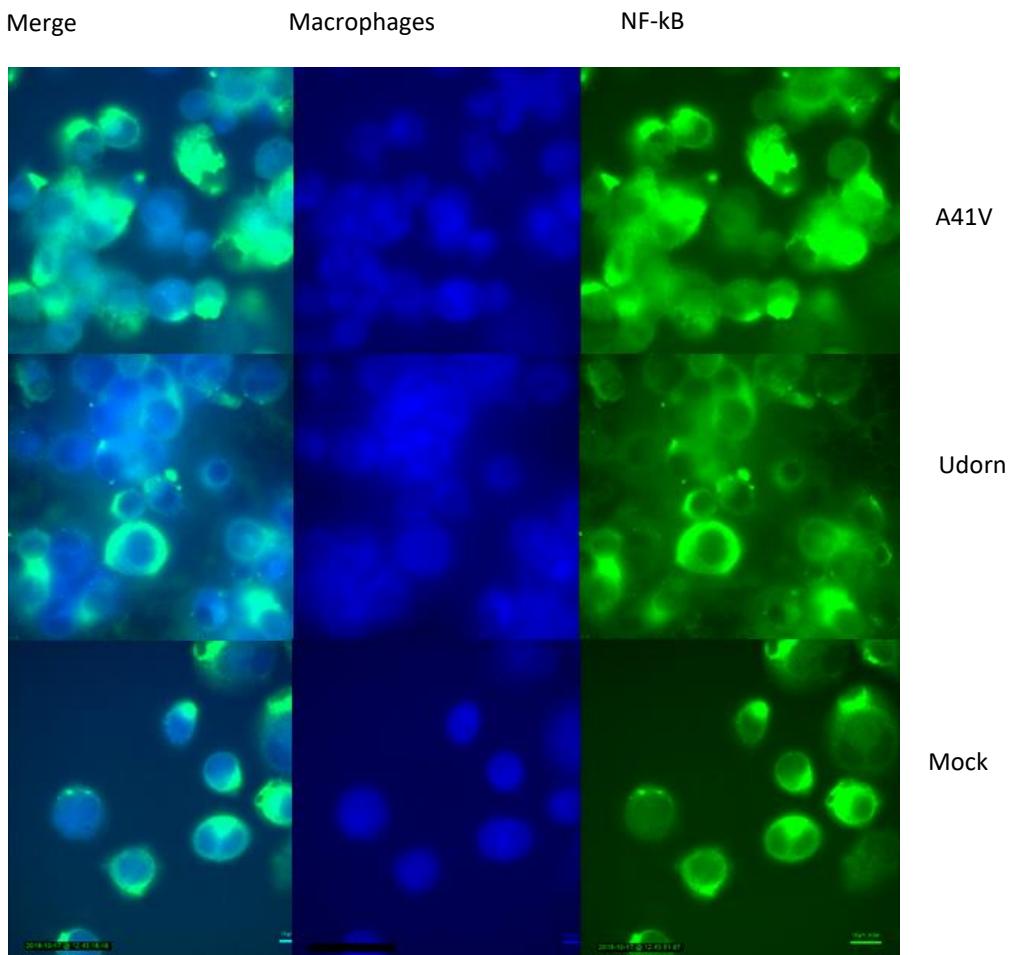
Figure 3.14 Epifluorescence Images of NF-kB nuclear localization in U937 cells. U937 cells were differentiated with PMA and grown on 6 well plates and infected with either A/Udorn/72 or M1-A41V at 1 MOI for 1 hour. They were then stained with anti-P65 (NF-kB) antibodies (green). The cells were mounted with DAPI (blue) and imaged. It can be seen that when infected with M1-A41V, NF-kB enters the nucleus, but fails to do so when infected with the filamentous A/Udorn/72. The scale bars show 10 um.

3.3.1.3 Results: quantification of NF-kB nuclear localization

Zen Blue software was used to quantify the results from confocal microscopy by measuring fluorescent intensity in different regions of the cell. This was done as shown in Figure 3.15. For the different cell lines and viral infections, the ratio of intensity of Nf-kB (in green) was calculated in the cytoplasm and the nucleus. This was done by drawing outlines around the cytoplasm and the nucleus of specific cells, and using the software to calculate the ratio of fluorescence intensities, which can then be plotted. Figure 3.16 shows the difference in NF-kB localization in MDCK and A549 cells, after infecting with either Udorn or A41V. Unfortunately, due to equipment failure, the U937 results were only looked at with epifluorescence microscopy, thus similar calculations could not be done. As can be seen from the graph, there is a definite difference in the NF-kB localization between A41V and Udorn infection in MDCK cells, but this is not noticeable in A549 cells. This is further confirmed by doing a student's unpaired T test, which shows that the difference in MDCK cells between Udorn and M1-A41V is less than 0.05, thus there is a significant difference. However, in A549 cells there is no significant difference between the two.
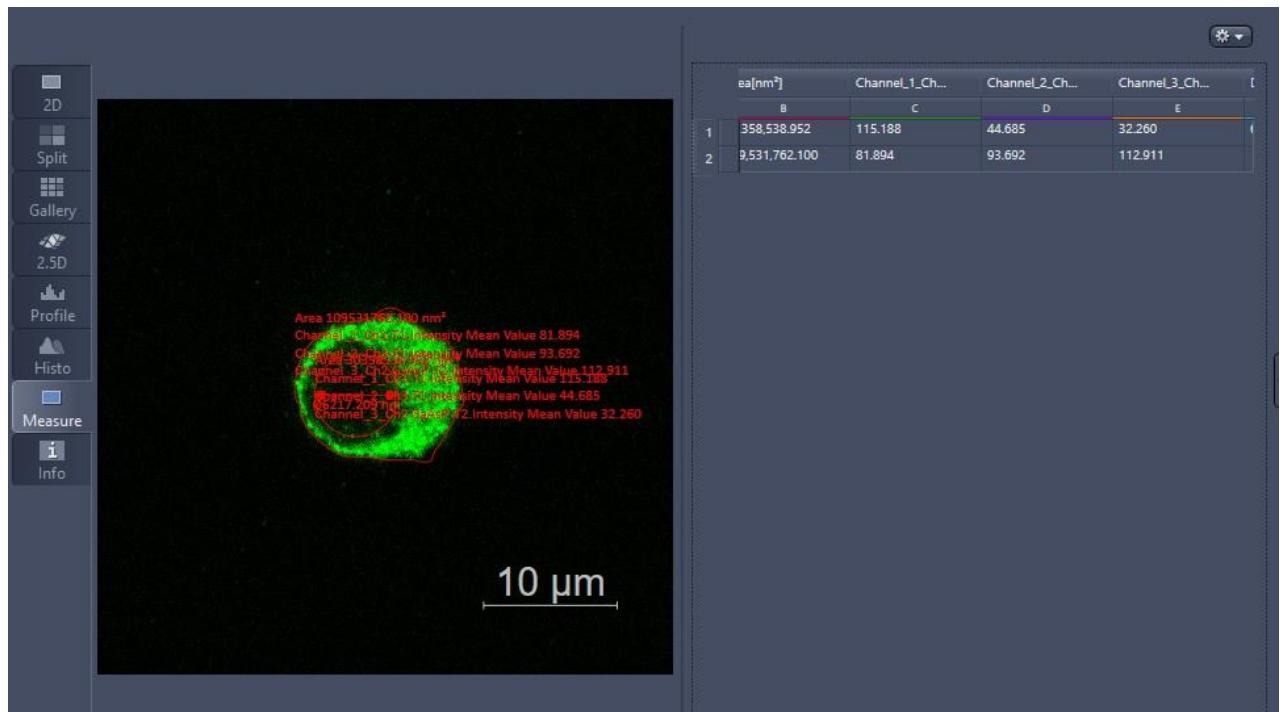
Figure 3.15 Quantifying NFkB localization from the confocal images. First a circle is drawn around the nucleus, and then another is drawn around the cytoplasm. The program gives the intensity in that area automatically, and from that the ratio can be found, for each of the cells. An average was calculated from the total number of cells of each condition and the average calculated, and data graphed and analysed by a Student's T-test.
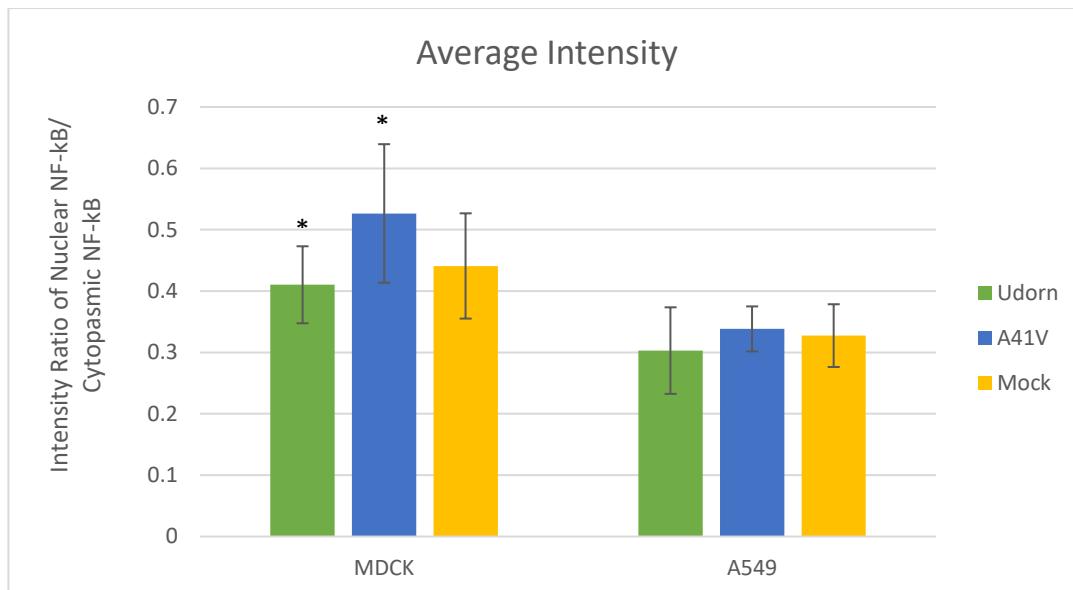
Student's unpaired T Test (Udorn vs M1-A41V)

MDCK	A549
0.001299478	0.208360619

Figure 3.16 Graph showing that NFkB nuclear localization due to different IAV morphologies varies in different cells lines. The results from Figure 9 can be further confirmed from the results of the quantification. As shown in MDCK cells the difference in NF-kB nuclear localization between spheres and filaments is much greater than in A549 cells. A Student's unpaired T Test was carried out, which confirms that in MDCK cells, the difference between A/Udorn/72 and M1-A41V is significant, but not in A549 cells. For each cell type 42 cells were considered. The error bars are showing the standard deviation, while the asterisks indicate a p<0.05 for the Student's unpairedT test.

To confirm the difference in NF-kB activity in the different cell lines, the experiments were repeated in RAW Blue cells. These are a mouse macrophage reporter cell line, which express a secreted embryonic alkaline phosphatase (SEAP) which is induced by NF-kB activity. Macrophages are one of the first responders of IAV infection, and the virus is capable of directly infecting these cells (Cline, Beck and Bianchini, 2017). NF-kB is one of the key responders of macrophage, and thus macrophages may give one of the highest levels for NF-kB activation when infected with IAV. It was noticed before that the NF-kB nuclear localization is best seen in macrophages (U937 and mouse macrophages), and thus this cell line was used to further confirm the results. Quanti Blue analysis was used to compare the results, shown in Figure 3.17. Quanti Blue is a colourimetric assay to detect Alkaline Phosphatase activity. The RAW Blue cells infected with either Udorn or M1-A41V were added to a 96 well plate, and Quanti Blue was added to them. The change in colour was read by a plate reader, and the results exported to Excel for graphing. LPS was used as a control, as it is a known robust activator of TLR4 and NF-kB in macrophages. It was noticed that at high (3) MOI infections, the difference in NF-kB nuclear localization is not very noticeable between Udorn and A41V. However, at low (0.5) MOI infectious, the difference is significant between Udorn and A41V. A Student's unpaired T Test was used to confirm the results, and it shows that in low MOI, there is a significant difference in Udorn vs M1-A41V. Although the p value is <0.05 for high MOI, but from the results it can be seen that NF-kB nuclear localization is higher in Udorn when compared

to A41V, so this is not considered. When the values were again scrutinised for high MOI, it did not show much difference between A41V and Udorn, suggesting that at high MOI, there is no significant difference in the two conditions. The calculations of the T test are shown in the 'Appendix'. This further confirms our theory that filaments somehow block NF-kB activation and nuclear localisation.
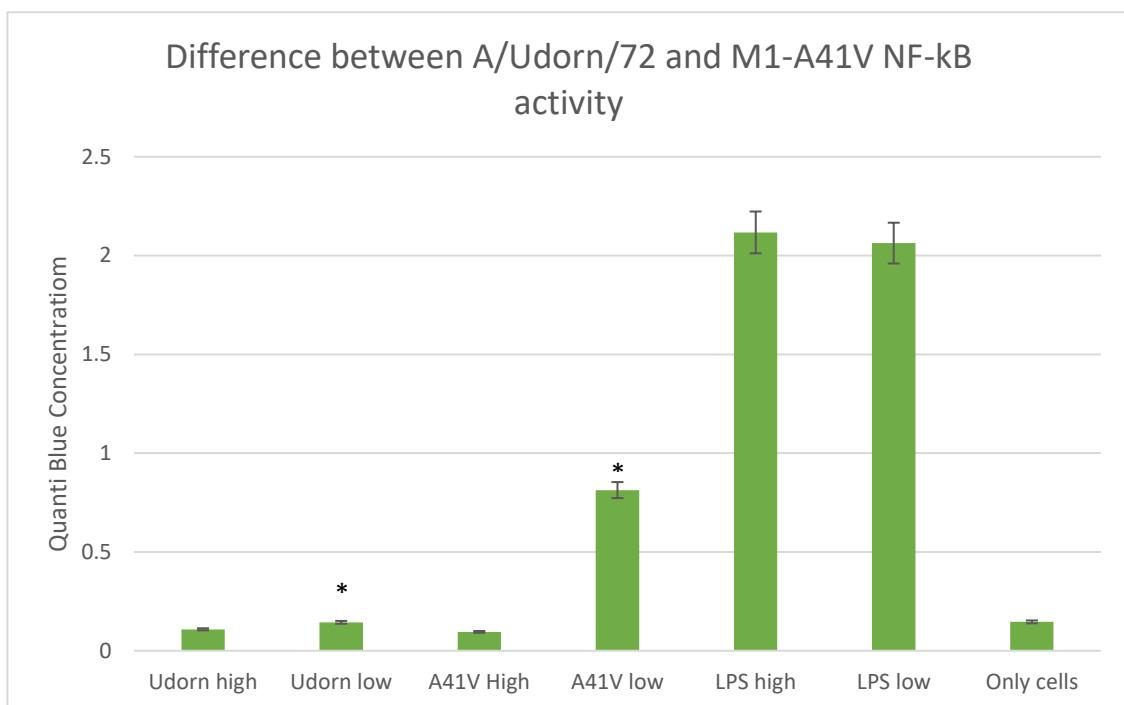
Student's unpaired T Test

Udorn Vs M1-A41V (High)	Udorn Vs M1-A41V (Low)
0.002320643	5.49501x10^-06

Figure 3.17: Quanti Blue results to show the difference in NF-kB activation between Udorn and A41V in RAW Blue Cells. In the RAW blue cells, the differences in NF-kB activation are greater with a lower MOI infection (0.5 MOI). As can be seen from the graph, there is a large difference between

NF-kB activation Udorn low-MOI and A41V low-MOI, which again shows that NF-kB gets activated and traffics to the nucleus during sphere infections, but not with filaments. This was confirmed by a Student's unpaired T Test, which confirms that in low MOI there is a statistically significant difference between Udorn and M1-A41V NF-kB activation, shown by the asterisks which indicate a $p<0.0005$. For each condition tested 60 cells were considered. The error bars are showing the standard error.

So far, all the assays were performed using Udorn and M1-A41V viruses. This does not let us know if the difference in nuclear localization of NF-kB is exclusive to Udorn and its mutant strain or is a general property of virus morphology. To test this, the experiments were repeated with different IAV strains- A/WSN/33, A/PR/8/34 and A/Cal/09. A/WSN/33 and A/PR/8/34 are spherical strains while A/Cal/09 is a filamentous strain. Figure 3.18 shows the results for the assay. The experiment was carried out in A549 cells, which show moderate difference in NF-kB activation between filaments and spheres. A549 cells were used as this assay was carried out before the RAW Blue cells became available. The A549 cells were grown in 6 well plates, and infected with one of the viruses at 3 MOI for 1 hour. The viruses were stained with anti-Udorn and anti-P65 antibodies. From the results it can be seen, that in all the spherical strains, NF-kB is activated, which is

noticeably different in Udorn. However, NF-kB nuclear localization can also be seen in the filamentous A/Cal/09 strain, though the proportion of filaments to spheres produced by this A/Cal/09 strain is lower than that produced by A/Udon/72. Again, due to equipment failure, calculations could not be done.

It was also important to show that Udorn suppresses NF-kB activation because of the filaments, and not due to any other effects of M1-A41V mutation. To test this, the Udorn virus was first vortexed. Vortexing Udorn causes the long filaments to break into spherical-like viruses (Rossman, 2010), with no loss of infectivity. However, this does not affect the spherical viruses. Wild type Udorn and Vortexed Udorn was then used to infect MDCK cells for 1 hour at 3 MOI, and the results are shown in figure 3.19. The results show that the vortexed virus loses its ability to block NF-kB nuclear localization. This helps us to conclude that the reduction of nuclear localization was occurring due to the presence of filamentous virions.
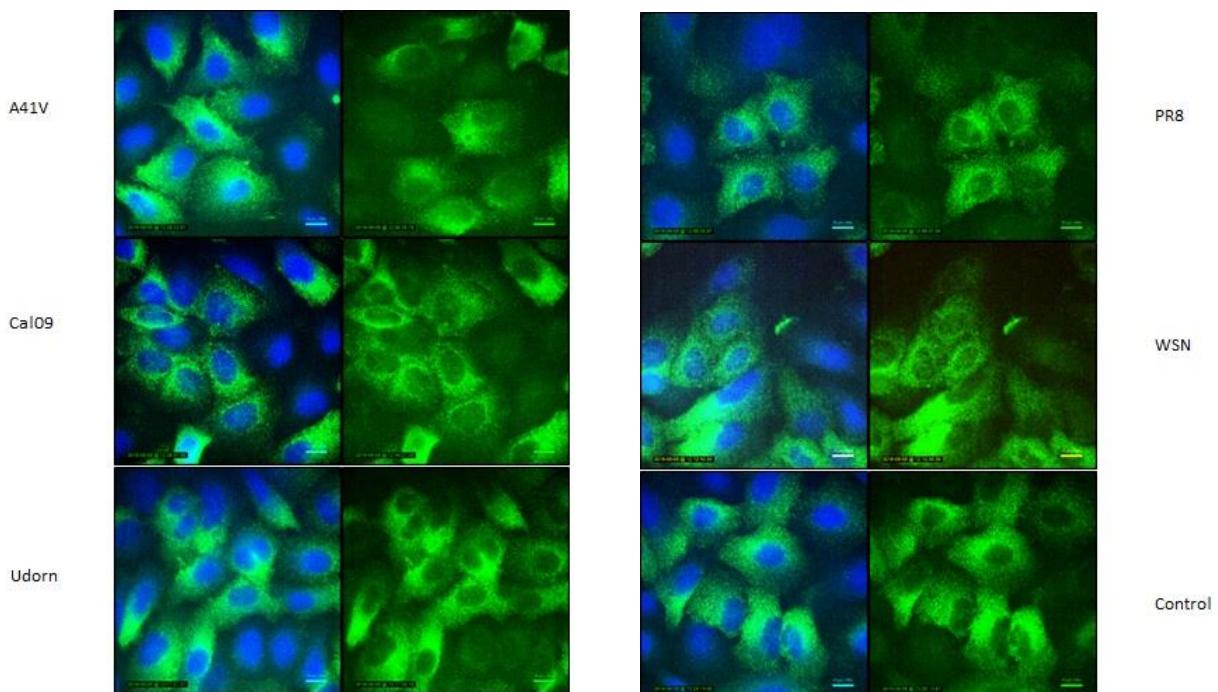
Figure 3.18: NF-kB nuclear localization following infection of different strains of IAV in A549 cells. A549 cells were infected with the different virus strains at 3 MOI for 1 hour before immunostaining, fixation and mounting with DAPI (blue). The They were viewed with Epifluorescence Microscopy to look at NF-kB activity (green). The scale bar shows 10um.

Wild Type Udorn

Vortexed Udorn

Control
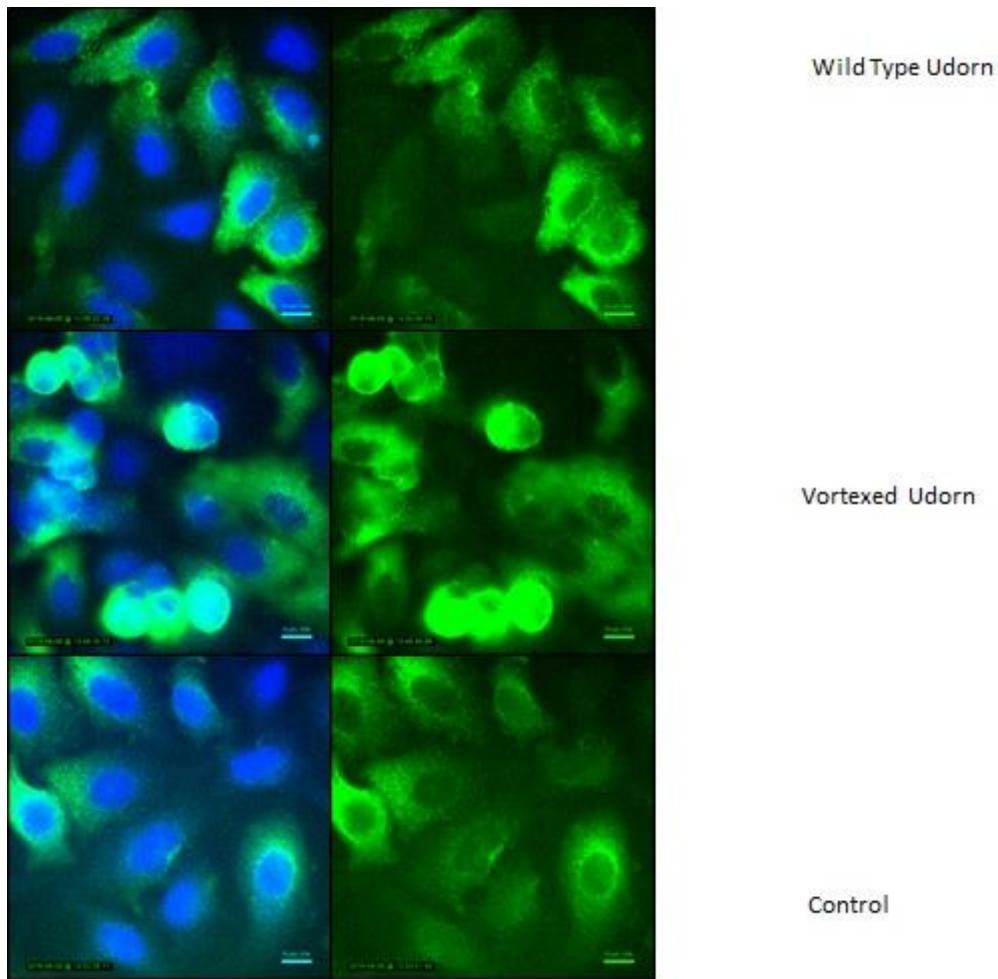
Figure 3.19 NF-kB nuclear localization in vortexed Udorn infected cells. Udorn was vortexed to break their filamentous structure, and the vortexed virus or M1-A41V was used to infect MDCK cells at 3 MOI for 1 hour before immunostaining, fixation and mounting with DAPI (blue). It was noticed again that with spherical viruses NF-kB is activated (green), which does not occur with normal filamentous wild type Udorn virus. The scale bar shows 10um.

3.3.1.4 Summary

A/Udorn/72 is a mixture of filamentous and spherical virions. However, only 15% of the virions are filamentous (Badham and Rossman, 2016), so even a small difference between A/Udorn/72 and M1-A41V represents a larger actual difference between filaments and spheres. Although filaments and spheres can be separated using ultracentrifugation as shown earlier, the filaments deform, and the purified filaments can thus not be used further for infection. As a result, we have to rely on these mixed morphology strains to test the hypothesis.

From the above results it can be seen that filaments are somehow reducing NF-kB activation, compared to spherical virion infections. Although we are still not sure what causes the differential activation, some of the ways will be looked at the following sections, but there is enough evidence to show that filaments are somehow blocking the innate immune activation of the host cells. When infected with spherical virions, the IKKB pathway gets triggered and NF-kB gets activated and enters the nucleus of the cell, activating the inflammatory response. However, somehow filaments are stopping this activation from happening, and thus NF-kB is unable to enter the nucleus of the cells.

The data also show that this phenomenon is not exclusive to Udorn and A41V, but all the other spherical strains also activate NF-kB. It was also shown that when Udorn filaments are fragmented into spherical-like viruses, they can no longer block NF-kB activation. This suggests that the

virus is causing NF-kB activation due to some property of filamentous virions (i.e. filaments enter cells by macropinocytosis while spheres enter by clathrin-mediated endocytosis) which is absent in the spherical virions.

3.3.2 Why is there a difference in NFkB activation with different virus morphologies?

Although we saw a difference in NFkB activation between filamentous and spherical virions, we still do not know why there was a difference. So firstly, we looked to see if TLRs or their adapters have any role in IAV-dependent NF-kB nuclear localization. Toll like receptors are transmembrane proteins of cells of the innate immune system. They recognize foreign microbes and activate different signalling pathways, including NF-kB. So, do the filamentous and spherical virions differentially affect TLR activity, thus in turn, changing NF-kB activity? Next, it was determined if the viral entry pathway has any role in the NF-kB activation. Spheres enter mostly by clathrin mediated endocytosis which can be blocked with chloropromazine (CPZ), while filaments enter by macropinocytosis, which can be blocked by Na^+/H^+ pump inhibitor 5-(N-ethyl-N-isopropyl) amiloride (EIPA). The aspect that was investigates was if any viral-induced changes in autophagy activity can in turn causes the changes in NF-kB activation. When virions enter cells by macropinocytosis, the autophagy pathway gets activated. NF-kB is one of the first responders of innate immunity, and both the effects of NF-kB and autophagy are very rapid. So, is it can be possible that the morphology-dependent activation of NF-kB is driven by the autophagic pathway, and changes in autophagosome production due to morphological changes can cause the variation in NF-kB activation.

3.3.2.1 Results: Are TLRs responsible for the changes in NFkB activity?

Toll like receptors (TLRs) are a group of proteins which are important for activation of the innate immune system. TLRs can recognise structural proteins (PAMPs) of microbes and trigger the innate immunity pathways to defend the host against them. They activate intracellular signalling pathways that lead to changes in gene expression, and thus eventually stop the bacteria or virus from replicating and spreading further (Xagori and Chlichlia, 2008, Mahla, 2003).

One of the pathways that gets activated when the TLRs respond to the PAMPs is the IKKB pathway to activate NF-kB. It was thus essential to look at if any TLR activations are affected by the change in morphology of IAV. Thus, macrophages from different TLR and TLR-adapter K/O mice were grown in the lab, and the NF-kB activity was assessed by imaging nuclear localization after infecting with A/Udorn/72 filaments or spheres. These modified macrophages each have a specific knock out (K/O), and these are shown in Figure 3.20.
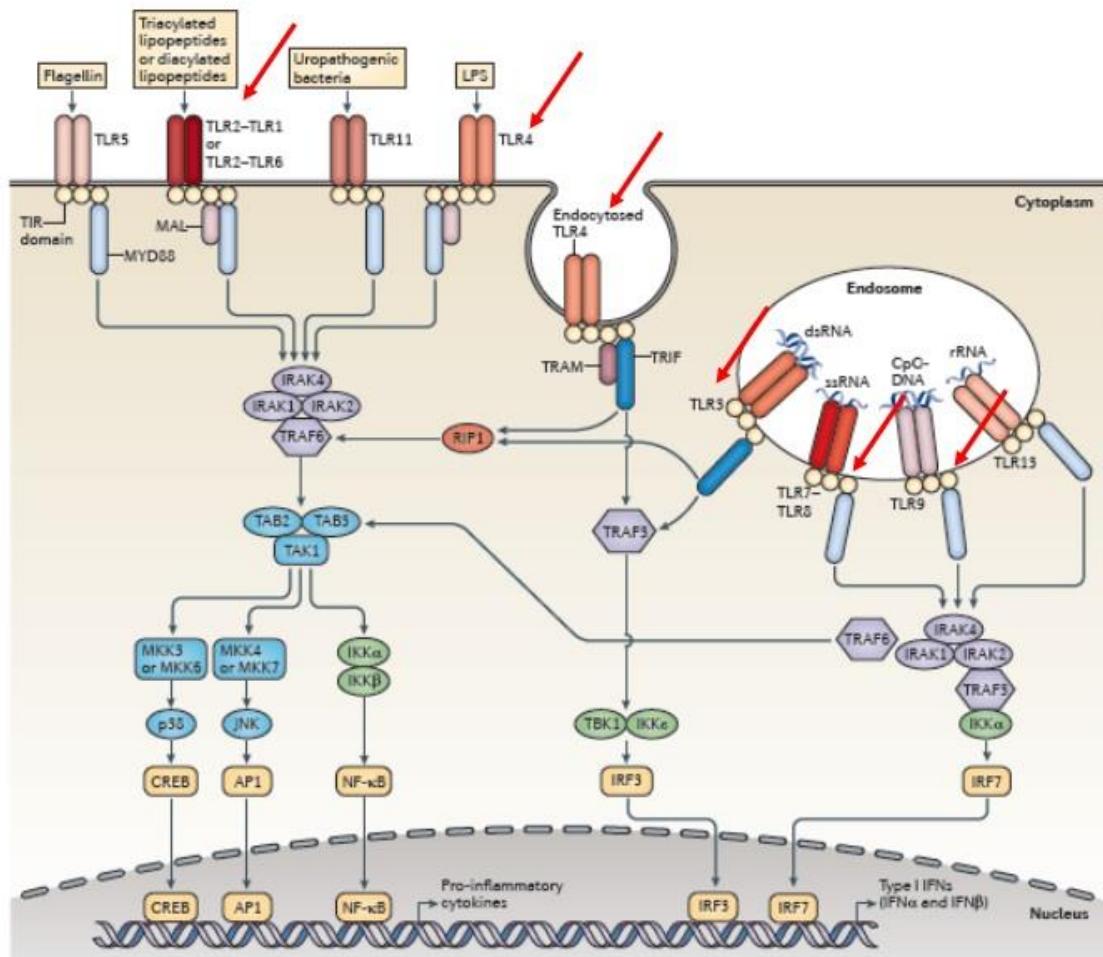
Figure 3.20 The toll like receptor pathway from O'Neill et al., 2013, modified to summarise the mouse macrophage K/O cells (in red) which were used to check if TLRs play a role in the morphological immunity of IAV.
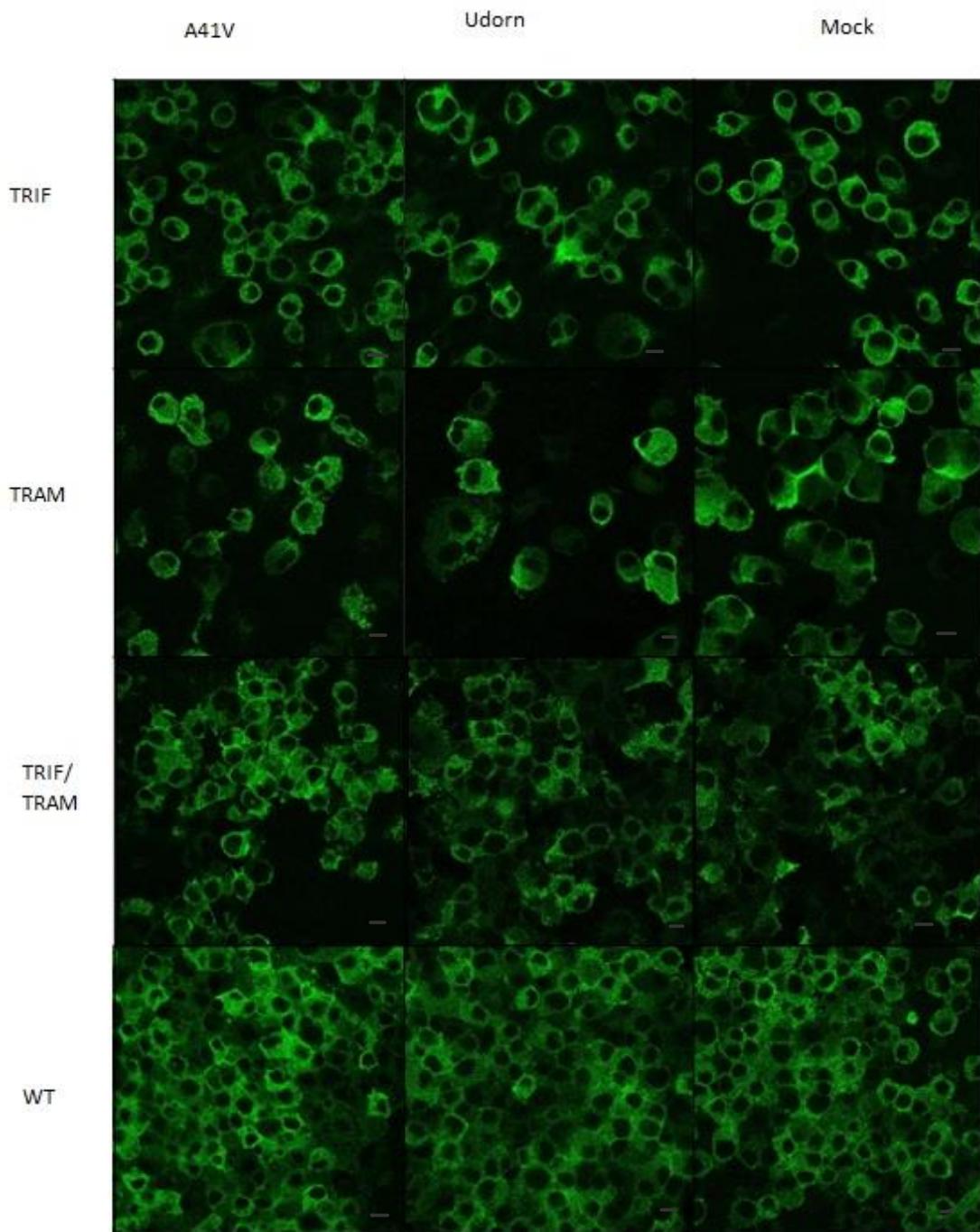
Figure 3.21 Confocal images of NF-kB nuclear localization in mouse macrophages, with specific K/Os, infected with either A/Udorn/72 or M1-A41V at 3MOI for 1hour. The results show that with TRIF and TRAM K/Os there are no difference between NF-kB localization when infected with spheres or filaments. The green shows the immunostaining with p65 to show NF-kB activity. The scale bar shows 10um.

Graph Showing NF-kB Nuclear localization in Different TLR Adaper Protein K/Os
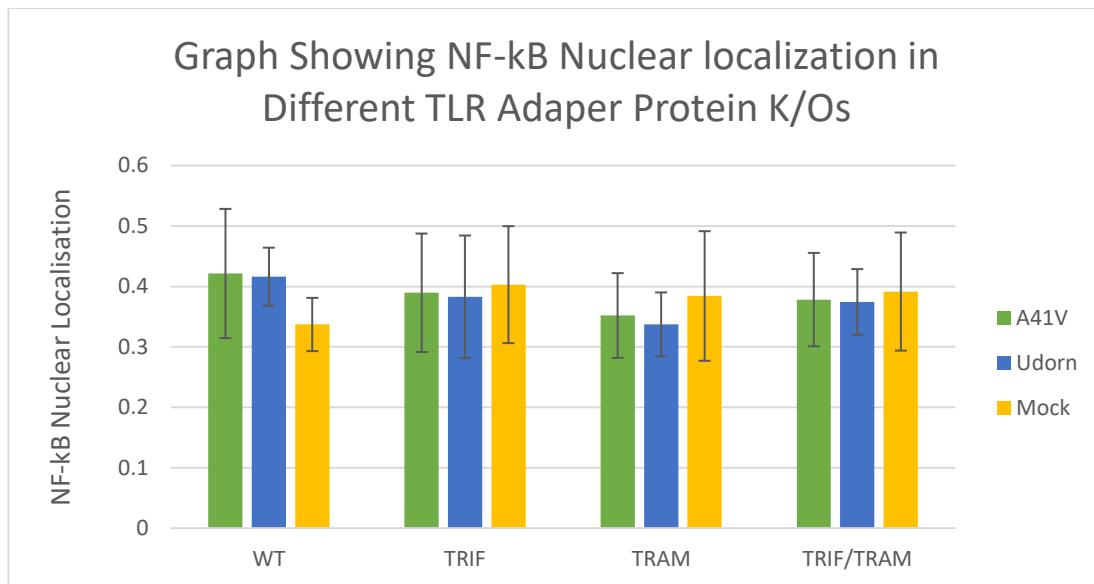
Student's unpaired T test p-value (Udorn vs A41V)

Wild Type	TRIF	TRAM	TRIF/TRAM
0.827498	0.81923482	0.422243	0.818757

Figure 3.22 Graph showing the difference in NF-kB nuclear localization when infected with either Udorn or A41V. From the results it can be concluded that the TLR adapter proteins do not play any role in NF-kB activation due to morphological changes in the virus. The standard deviation is shown by the bars.

3.3.2.2 Results: role of specific TLRs in IAV NF-kB activation

To test if any of the specific TLRs or their adaptor proteins play any role in NF-kB activation during infection with Udorn or A41V, mouse macrophages with specific K/Os were used. At first the macrophages that were used had K/Os of either TRIF or TRAM or a double K/O of TRIF and TRAM. The cell lines were infected with either Udorn or A41V, and then they were imaged with confocal, to look at NF-kB nuclear localization in the cells. This is shown if Figure 3.21. These were then used to calculate the ratio of NF-kB localization in the nucleus and cytoplasm of the cells, and the results are plotted in Figure 3.22. A student's unpaired T Test (refer to 'Appendix' for calculations) was carried out, from the results it can be seen that there are no significant differences between Udorn and A41V infection. This means that the adaptor proteins TRIF and TRAM do not mediate the difference in NF-kB activation when infected with spheres or filaments.

Next, specific TLR K/O mouse macrophages were used to check if they play any role in this NF-kB activation. The TLR K/Os used were TLR1, TLR2, TLR3, TLR4, TLR2/4 double K/O, TLR 6, TLR 7 and TLR 9. The cells were grown on 6 well plates and were infected with either Udorn or A41V at 3 MOI for 1 hour. They were fixed and stained with anti-Udorn, anti-P65 (NF-kB) antibody and mounted with DAPI. The confocal images for the results are shown in Figure 3.23. The results for wild type mouse macrophages, without any TLR K/Os is also shown. The NF-kB nuclear localization of the different K/Os were then calculated, and the results are shown in Figure3.24. From the results it can be seen that when infected

with Udorn, NF-kB activity rises in TLR 2, TLR3 and TLR2/4 K/Os. This suggests that either the filaments can somehow utilise TLR 2 and 3 to help reduce NF-kB activation or that these TLR K/Os alter other signalling pathways in the cell. It can also be noticed that with TLR 9 K/O, the NF-kB activity rises in A41V, this is unexpected as TLR K/O was expected to reduce NF-kB activation, so it can be suggested that spheres may exploit TLR 9 to somehow decrease NF-kB activation. However, it was also noticed that NF-kB activity is high in almost all the K/Os cells when compared to the wild type, suggesting there might be upregulation of other signalling pathways that could affect either IAV entry of NF-kB activation.
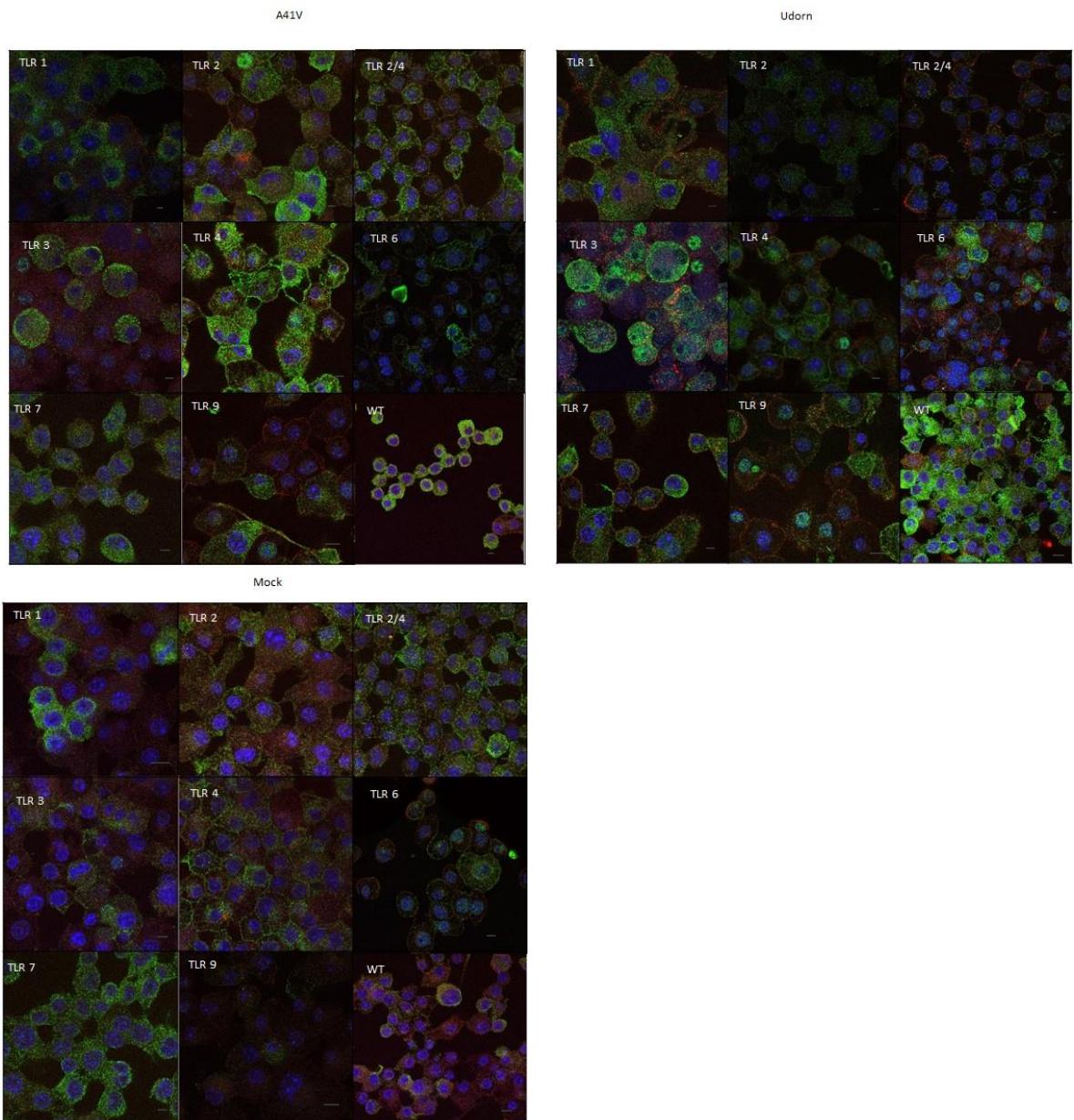
Figure 3.23 Confocal results to show the co-localization of NF-kB when infected with either Udorn or A41V, with different TLR K/Os. The different K/O mouse macrophages were infected with either M1-A41V or A/Udorn/72 at 3 MOI for 1 hour. They were stained with α-Udorn (red), α-P65 (green) and DAPI (blue) and viewed with confocal microscopy.
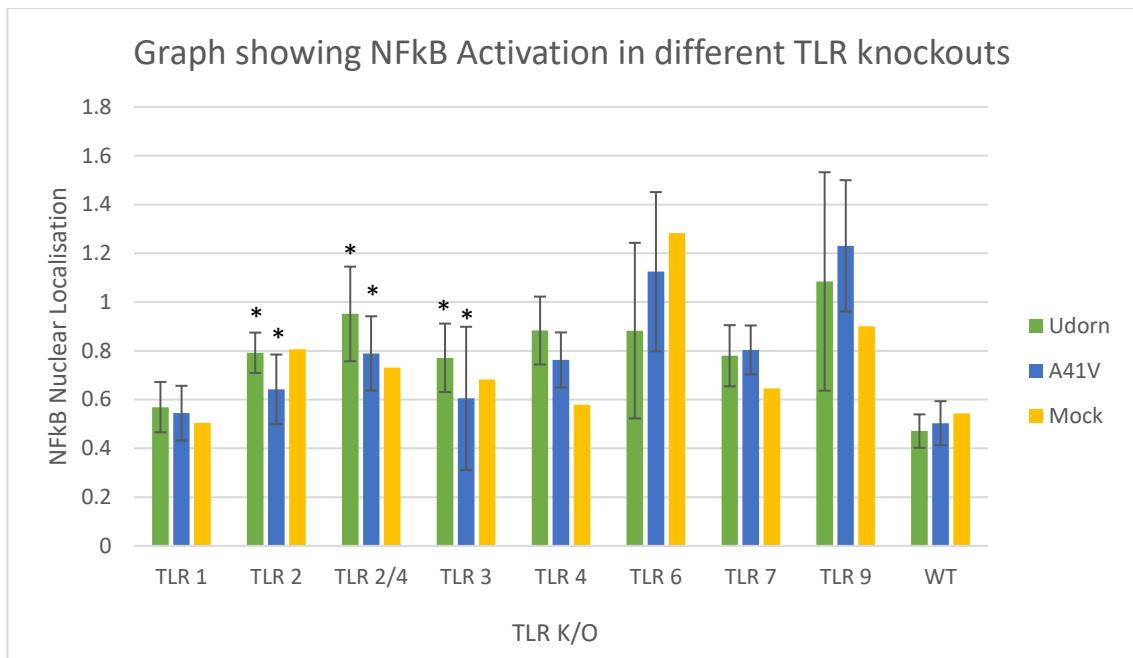
Student's unpaired T Test p-values (Udorn vs A41V)

TLR1	TLR2	TLR2/4	TLR3	TLR4	TLR6	TLR7	TLR9	Wild Type
0.582	0.0046	0.0048	0.0291	0.2133	0.0987	0.6147	0.3428	0.32575

Figure 3.24 Graph showing the confocal results from the NF-kB nuclear localization in different TLR K/O macrophages when infected with either Udorn or A41V and stained for P65. From this it can be seen that when there is a TLR 2, TLR 3 or TLR2/4 knockout, NF-kB activation when infected with filaments increases significantly. This means that filaments may uses these two TLRs to somehow block NF-kB activation. The Standard deviation is shown by the bars. The asterisk shows the p<0.05 when calculated using Student's T test.

3.3.2.3 Summary

It was suggested that the difference in NF-kB activity due to the change in morphology of IAV is due to the activity of TLRs or their adaptor proteins. This was looked into with specific K/O mouse macrophages. From the results it can be seen that the TLR adaptor proteins TRIF and TRAM do not have any effect on NF-kB activity. Specific K/Os of TLR were also looked into. It can be seen that TLR2 and TLR3 have a definite difference between NF-kB activation in M1-A41V and A-Udorn/72. This suggests that these two TLR receptors can be utilised by filament in reducing NF-kB activity.

3.3.3.1 Results: Does the specific IAV entry pathway play a role in NF-kB activation?

As explained previously, spherical virus enters the host cells mainly via clathrin mediated endocytosis. Filaments are too large to use this pathway, and they thus instead use macropinocytosis to enter the host cells (Rossman, Lesser and Lamb, 2012). Spherical virions can also enter cells by macropinocytosis.

From the previous section we concluded that filaments somehow can reduce NF-kB activation compared to spheres. However, we do not know how this happens. One of the possibilities is that the different IAV entry pathways might play a role in setting up this activation.

To test this, RAW blue cells were grown in 6 well plates and they were treated with either CPZ, EIPA or both. Clathrin mediated endocytosis was blocked by using CPZ while macropinocytosis was blocked by EIPA. They were treated with one of the drugs or both for 1 hour. This was followed by infection with Udorn or M1-A41V at 3 MOI for 1 hour in the presence of the drug. The cells were prepared for immunofluorescence microscopy by staining for P65 (NF-kB) and were imaged by confocal microscopy. Figure 3.25 shows the confocal results, with RAW cells treated with CPZ or EIPA or both, and infected with A41V or Udorn. The results do not show difference in NF-kB activation between Udorn and A41V, and when the entry pathways are blocked the results look similar. However, when both the pathways are blocked the NF-kB localization in the nucleus increases

considerably, when infected with M1-A41V. The images were used to calculate the ratio of NF-kB in the nucleus and the cytoplasm of the cells (Figure 3.26). The results were used to do a Student's unpaired T Test, which confirms that there is a significant difference between Udorn and M1-A41V infection, when treated with both CPZ and EIPA. The control results also show a significant difference, with a p value 0f 0.007 between Udorn and A41V. Although the number of cells for the control was only 12, due to unforeseen reasons (instead of 30 like other conditions), but even then we can notice from the control that Udorn is significantly reducing NF-kB activation when compared to A41V infection. This is shown in more details in 'Appendix' section.
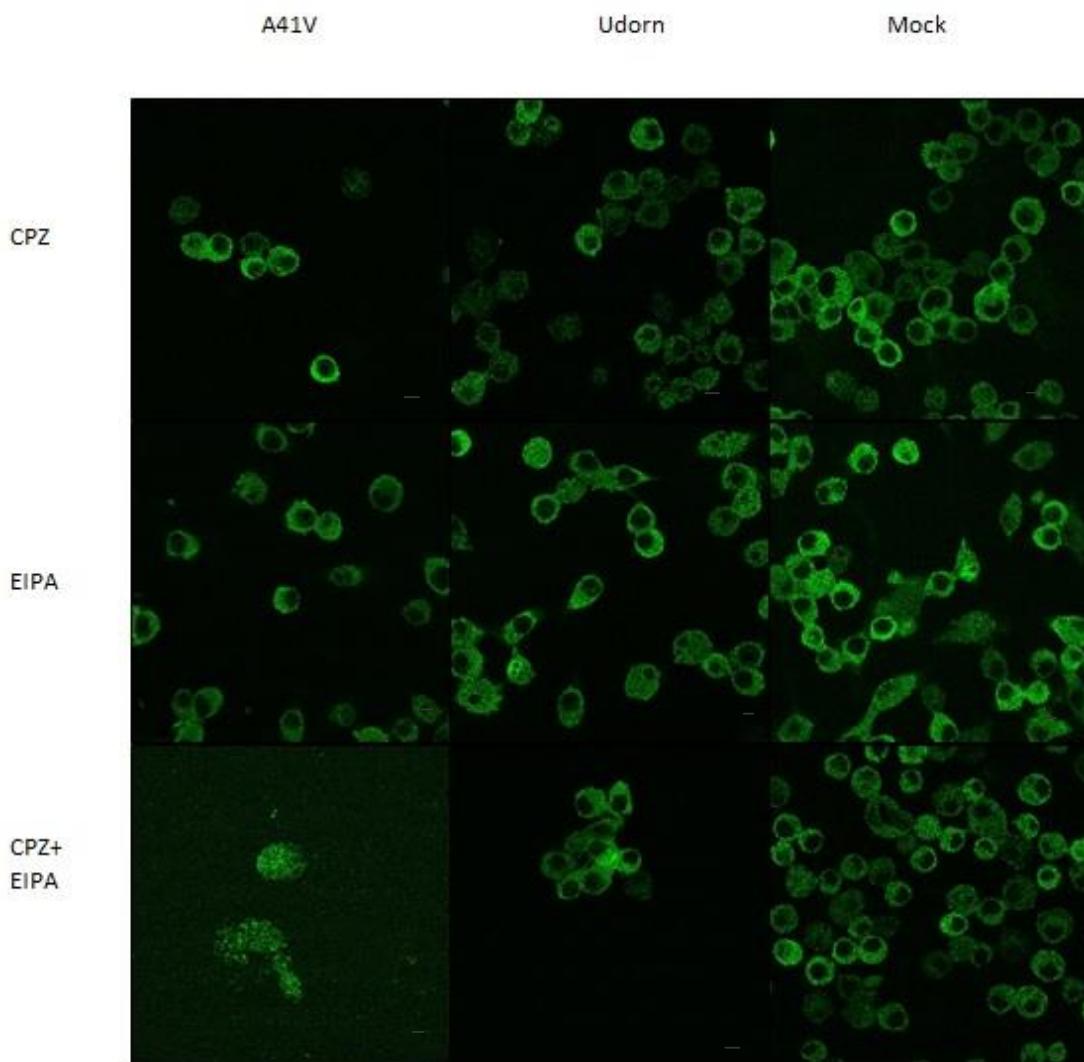
Figure 3.25 To look at the effects of blocking entry pathways during IAV infection, either clathrin mediated endocytosis was blocked using Chloropromazene (CPZ) or macropinocytosis was blocked using 5-(N-Ethyl-N-isopropyl) amiloride (EIPA). When these pathways are individually blocked, no significant difference is noticed in NF-kB activation due to infection by either Udorn or A41V. However, when both the pathways are blocked, suddenly NF-kB activation increases drastically, mainly when infected with A41V. The images show results from RAW Blue cells, infected with Udorn or M1-A41V at 3 MOI for 1 hour. They were stained with p65 to show the NF-kB activation (in green). The scale bar shows 10um.
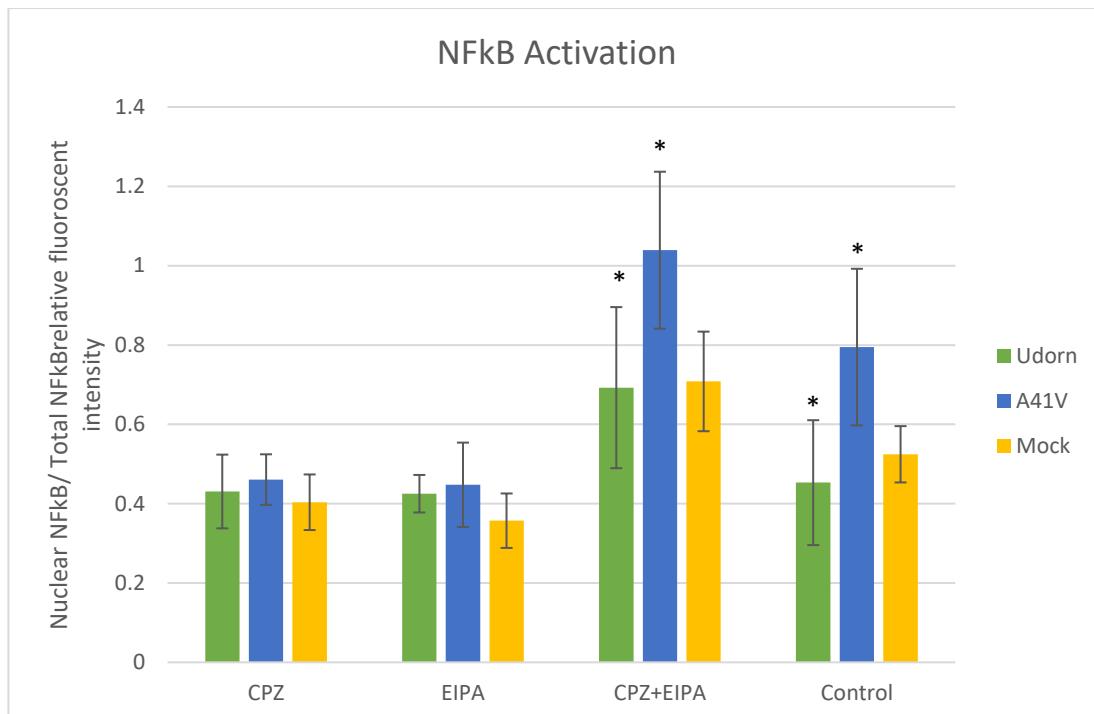
Student's T Test p-values (Udorn vs A41V)

CPZ	EIPA	CPZ and EIPA	Control
0.36637014	0.510448	0.00034	0.007475

Figure 3.26 The nuclear and cytoplasmic intensities of NF-kB from the confocal image results were used to plot a graph. The Graph further confirms that, when CPZ blocks clathrin mediated endocytosis, and EIPA blocks macropinocytosis separately, there is no significant difference seen in NF-kB activation. However, when both the pathways are blocked, the difference changes considerably. NF-kB activity in A41V infection increases significantly, as seen by the Student's unpaired T test, indicated by the asterisks to show a p<0.05. A significant difference is also seen in Control

Udorn and A41V infection, as Udorn can more successfully reduce NF-kB activation during infection. The error bars show the standard deviation.

This suggests that when IAV cannot enter cells by clathrin mediated endocytosis or macropinocytosis, the virus uses a third pathway to enter the cells, possibly in all cells or just in macrophages. To test if the third pathway is phagocytosis (one of the dominant immune stimulatory uptake pathways in macrophages), RAW Blue cells, grown in 6 well plates with media containing FBS or no FBS, were infected with fluorescently-labelled A41V virus (purple) at 3 MOI for 1 hour. During the infection, the cells were treated with fluorospheres (green), fluorescent-dextran (blue) and fluorescent-transferrin (red). Dextran is taken up by cells via macropinocytosis, while transferrin is taken up via clathrin mediated endocytosis. The fluorosphere beads enter cells by phagocytosis. The 4 reagents were added directly to the cells and left for 2 hours. They were then fixed, and the slides were mounted and viewed by confocal microscopy. In Figure 3.27 it can be seen that in both conditions- cells grown in media with FBS, or cells grown in media without FBS, there was no co-localization between the virus and the fluorospheres, suggesting that IAV does not enter macrophages by phagocytosis, even in the presence of serum which enhances macropinocytosis.
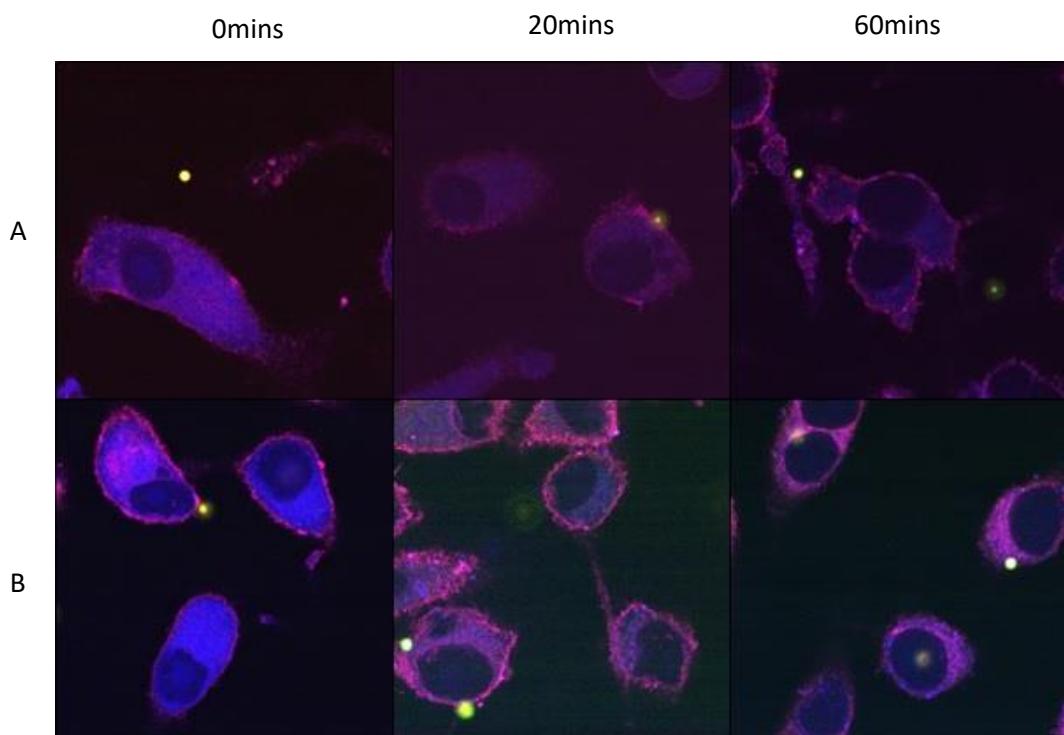
Figure 3.27 Activation of Phagocytosis after IAV infection. RAW Blue cells grown in media with (B) or without (A) FBS were infected at 3 MOI for 1 hour with fluorescent M1-A41V (purple) and treated with fluorescent-dextran (blue), fluorescent-transferrin (red) and fluorospheres (green) for 2 hours. The cells were fixed and mounted and viewed with confocal microscopy.

3.3.3.2 Summary

Although we know that NF-kB activation can be altered by viral morphology, we thought the entry pathways of IAV could have a role to play. However, we found that when blocking different entry pathways, the NF-kB activation does not change. Blocking clathrin mediated endocytosis by CPZ or macropinocytosis by EIPA does not have any effect on NF-kB activation, and the nuclear localization looks similar in both. However, when both the pathways are blocked, NF-kB activation suddenly increases, especially with spherical virus. This suggests that when both clathrin mediated endocytosis and macropinocytosis gets blocked, a third pathway gets activated that enhances NF-kB activation.

It was assumed that the third pathway was phagocytosis, and this was looked into by treating RAW Blue cells with fluorospheres. However, the results showed that the virions did not enter by phagocytosis during infection. This mean that although a third pathway may get activated, it is not phagocytosis.

3.3.4.1 Role of Autophagy During Early Infection of IAV

Autophagy, which means "self-eating", is a controlled process of removing unwanted cellular components from the body. It can aid in removal of proteins, maintaining homeostasis and assist in both innate and adaptive immunity. It happens in all nucleated cells (Ryter et al., 2013, Kroemer et al., 2010, Perot et al., 2018).

Viruses can use autophagy to their advantage, to prevent inhibition by autophagosomes. RNA viruses can stop autophagosomes from maturing and replicate themselves inside the immature autophagosomes (Deretic and Levine, 2009). This helps them in staying undetected by the host's innate immune system, and also increases their productivity by increasing their concentration (Perot et al., 2018).

Influenza virus can also use autophagy during replication for their advantage, and it has been seen that when autophagy is blocked, IAV replication decreases (Zhou et al., 2009). When virions enter the cells by macropinocytosis, it can trigger autophagosomes to form, and thus activate autophagy. This can induce the innate immune system, by triggering the NF-kB pathway. Both the effects of autophagy and NF-kB occur rapidly after infection, so it can be suggested that autophagy may play a role in the changes in NF-kB activity due to changes in morphology.

3.3.4.2 Results: Autophagy

We know from previous data that IAV can efficiently utilize the process of autophagy for their advantage, to increase replication (Zhou et al., 2009, Perot et al., 2018). However, the question arises, if filamentous and spherical virions can cause any differences in autophagosome production during early infection that activates innate immunity, affecting NF-kB activity.

To test this, MDCK cells were grown on 6 well plates and infected with either Udorn or M1-A41V virions at 3 MOI for 1 hour. The infected cells were prepared for immunofluorescence microscopy by staining with anti-Udorn and anti-LC3 antibodies and mounting with DAPI. The slides were viewed by epifluorescence microscopy.

Figure 3.28 shows the epifluorescence microscopy results of LC3 localization. In both the conditions, when infected with A41V or with Udorn, LC3 forms foci in the cells, indicating autophagy activation. However, similar number of foci seem to be produced, suggesting that morphology does not drive autophagosome activation. As this was not done with confocal microscopy, it could not be confirmed statistically. This means that the morphological changes of IAV do not appear to affect autophagy during entry of the virus.
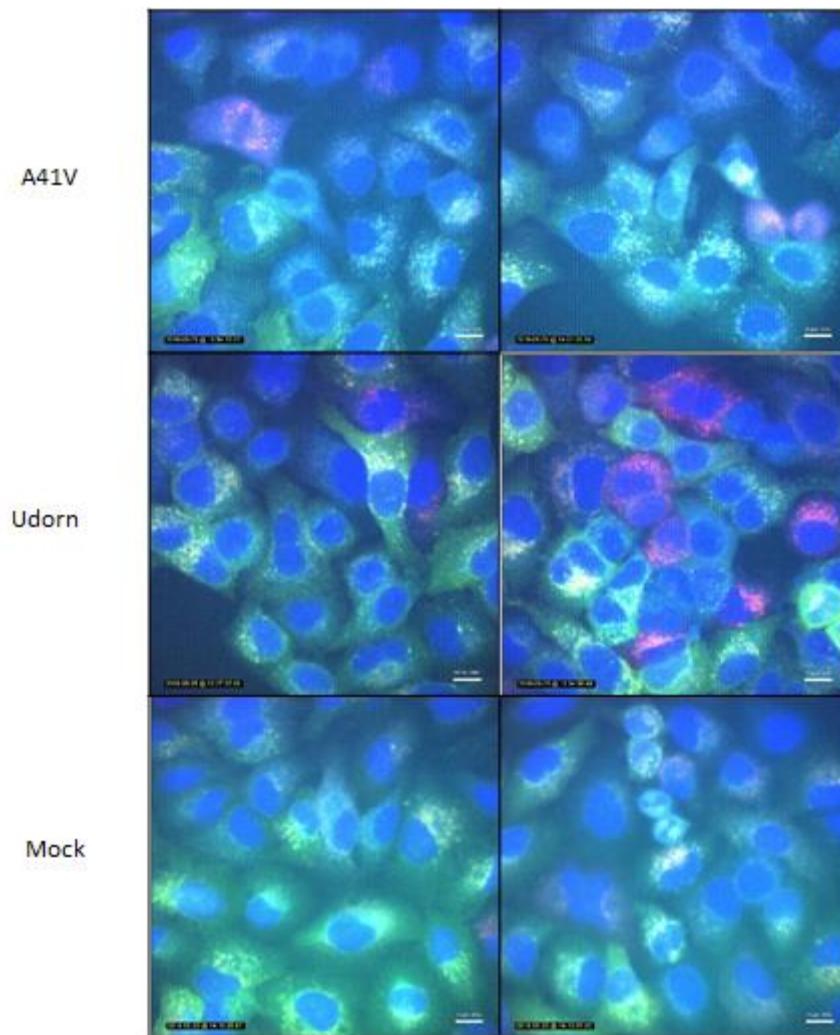
Figure 3.28 LC3 localisation in MDCK cells. Cells, grown in 6 well plates were infected with either A/Udorn/72 or M1-A41V at 3 MOI for 1 hour. They were stained with anti-LC3 (green), anti-Udorn (red) antibodies and DAPI (blue- MDCK cells) before epifluorescence imaging. The scale bar is showing 10um.

As the epifluorescence data could not be quantified, we used the IncuCyte quantitative live cell imaging system to assess autophagy activation with the different morphologies. A549 cells stably expressing the autophagy reporter LC3-mCherry-eGFP were infected with A/Udorn/72 (at 1 MOI) or A/PR/8/34 (at 1 and 5 MOI) and imaged every 1 min for 120 min on the IncuCyte Zoom system. The mCherry of the autophagy sensor shows the total level of autophagy induction and the eGFP shows autophagy maturation, as GFP signal goes down when autophagosomes mature and are acidified but the mCherry signal remains the same. The first graph shows the total number of autophagosomes formed. It indicates that for all the 3 virus conditions, the number remains similar, indicating that morphology does not affect autophagy induction. The second graph shows the number of autophagosomes that mature. The levels start low, indicating mature autophagosomes, but with time the GFP intensity increases, meaning that they stop maturing. This is irrespective of virus morphology (spheres or filaments), confirming that during early infection autophagosome production does not vary due to morphological changes.
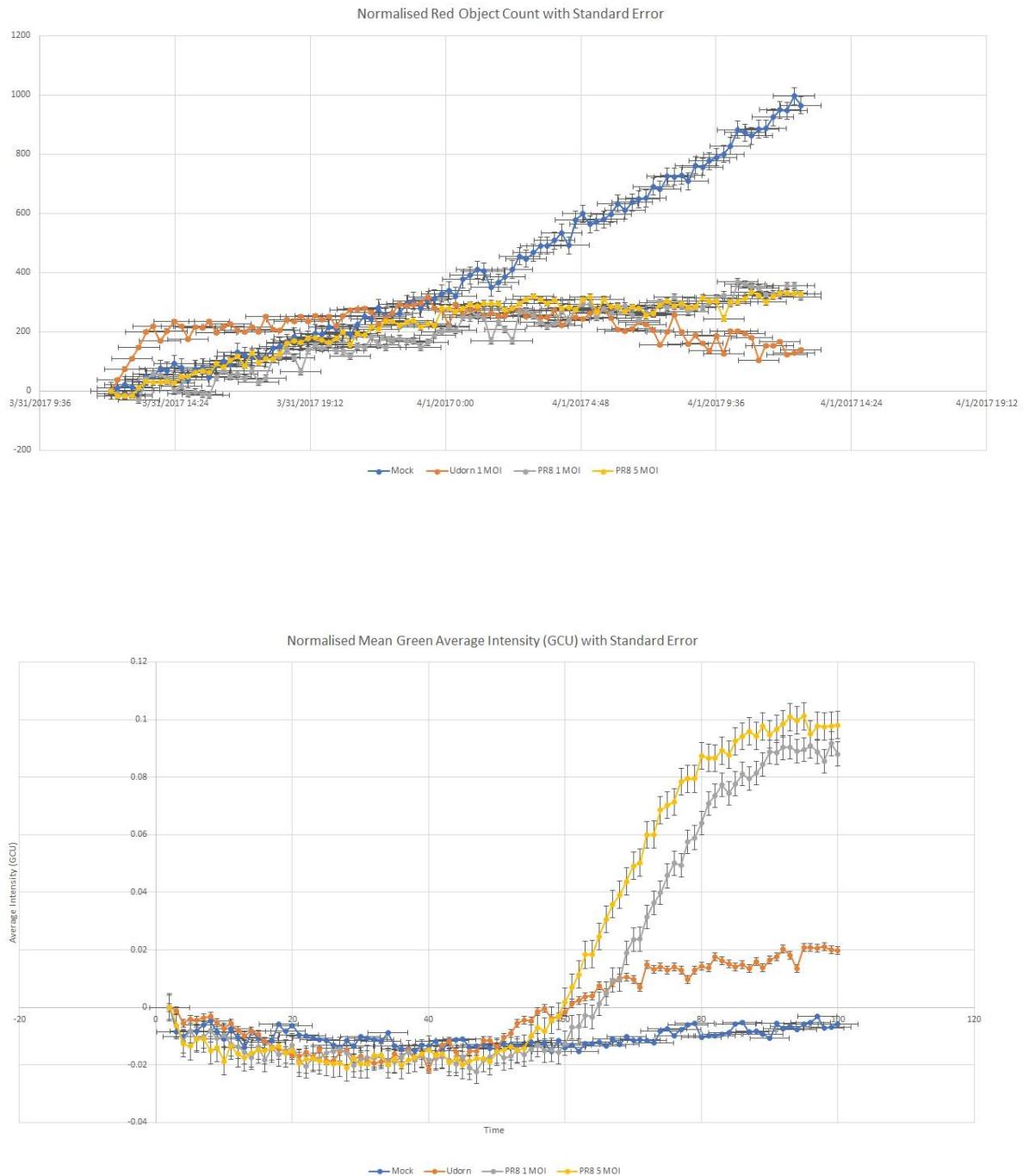
Figure 3.29 IncuCyte data for autophagy formation and maturation. A549 cells stably expressing LC3-mCherry-eGFP were infected with A/Udorn/72 or A/PR/8/34 at 1 and 5 MOI and images were collected at 10x every 1 min.

In both the graphs, Udorn is shown in red, PR8 1 MOI in grey and PR8 5 MOI in yellow. The mock infected sample is shown in blue. Graph A shows mCherry fluorescence and indicates the total number of autophagosomes being produced, and it remains constant for all three conditions throughout. Graph B shows eGFP fluorescence and indicates the number of autophagosomes that mature. Lower levels indicate that autophagosomes are more mature. At first a drop is seen in the curve suggesting that autophagosomes form, but then the curve rises, indicating that they fail to mature during longer time durations.

The ability of the virus to inhibit autophagy maturation was also confirmed by infecting A549 autophagy sensor cells with 3 MOI of filamentous A/Udorn/72, filamentous A/Cal/09 or the spherical mutant of Udorn M2-Helix for 18 hours followed by staining with anti-M2 and imaging by confocal microscopy. The cells show green and red autophagy foci when infected with either virus, indicating that all can block autophagy maturation (Figure 3.30).

LC3 M2 Variants
Eng/09

LC3 M2 Variants
Udorn

LC3 M2 Variants-
M2 Helix Udorn)
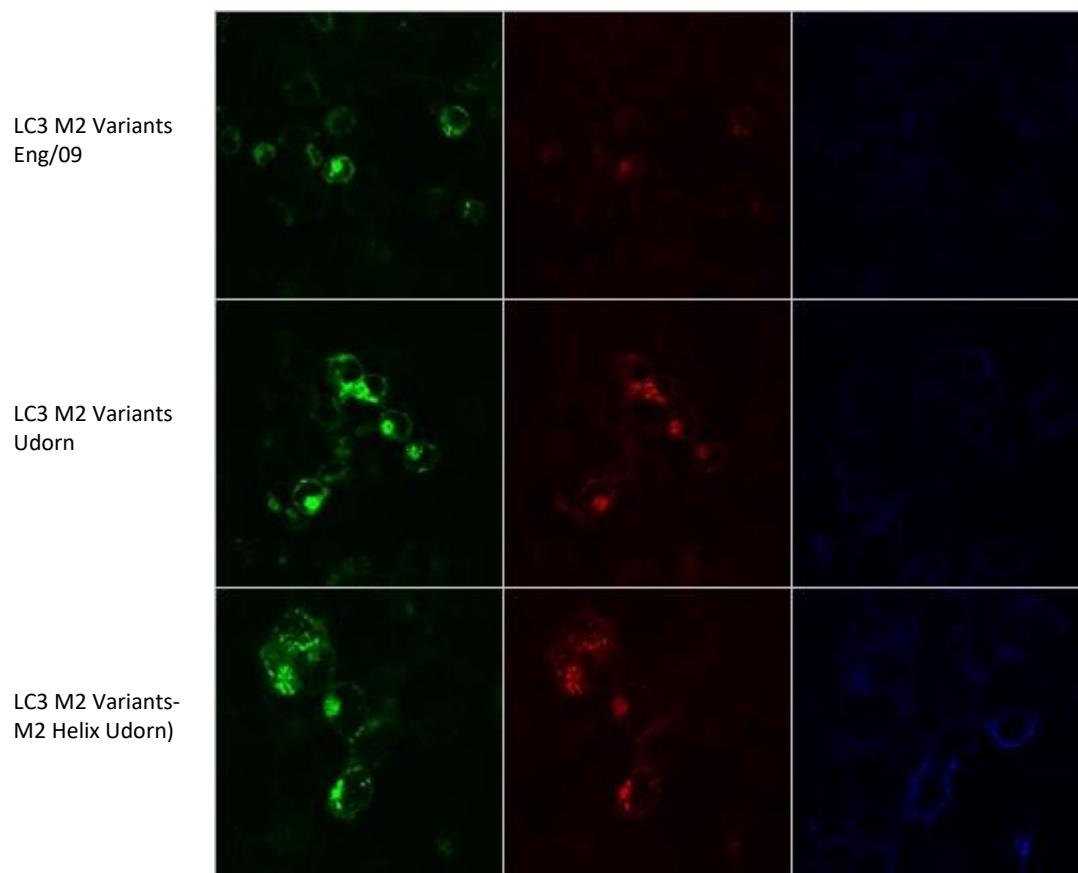
Figure 3.30 Autophagy mutation with diffident virus strains. A549 cells stably expressing LC3-mCherry-eGFP were infected with A/Udorn/72, A/Eng/09 or Udorn M2-Helix at 3MOI for 18hr before staining with anti-M2 (blue) and viewing by confocal microscopy. Red foci indicate autophagosomes and green foci indicate immature autophagosomes. All strains activate the autophagy pathway and inhibit its maturation, regardless of virus morphology.

3.3.4.3 Summary

Autophagy is activated due to stress responses caused by IAV entering cells. Entry by macropinocytosis causes induction of the autophagic pathway. It was assumed that the activation of the autophagic pathway can induce NF-kB activation, as it is one of the first responders of the innate immune system, and both the pathways start working rapidly after infection.

The activity of LC3 was looked into when A/Udorn/72 or M1-A41V infects hosts cells. It was hypothesised that the filamentous virions will somehow block the autophagic pathway. However, it was seen that both the morphologies work in the same way, activating autophagy during early stages of infection. During early stages of infection both spheres and filaments forms similar numbers of autophagosomes. Due to enhanced expression of the M2 protein at later stages of infection, IAV can withhold the autophagosomes from maturing. However, since the response remains similar in early stages, it can be said that early IAV NF-kB activation is not driven by autophagy.

CHAPTER 4

DISCUSSION

4.1 Purification of A/Udorn/72

IAV is a pleomorphic virus and consists of both filamentous and spherical virions. Some strains can only form spherical virions, while other strains can form a mixture of both filaments and spheres. When IAV is passaged in the lab, they are found to be spherical. However, filaments are continuously found in clinical samples, suggesting they are required to form for IAV to survive (Siezkarski and Whittaker, 2005).

A/Udorn/72 is of pleomorphic nature and can form both filamentous and spherical virions. After continuous passaging, Udorn seems to retain its ability to form filaments, unlike other filamentous strains. A single mutation of Udorn at position 41 of M1 protein, causes the virus to stop forming filaments, and only forms spherical virions. For our experiments A/Udorn/72 and its mutant M1-A41V were used. However, to confirm that they were indeed a mixture of spheres and filaments, the virions were purified by ultracentrifugation.

The purification process successfully separated the spherical virions from the filamentous, confirming that the strain is indeed pleomorphic (figure 3.2 and 3.3. However, the long and thin filamentous virions lose their shape because of the harsh ultracentrifugation process. This means that the virions cannot infect host cells as filaments anymore. If they would still remain infective and filamentous, then this could have been used to study the differences between filaments and spheres. Since, a pure filamentous strain does not exist, and the purification process is not amenable to

subsequent infections, A/Udorn/72 and its mutant M1-A41V was the best strain to use for further experiments.

4.2 Priming of host cells by UV treated Virus

It has been suggested that some filamentous virions do not infect host cells at all, but are there to aid the infection of other spherical and filamentous virions (Badham and Rossman, 2016). These filamentous viruses may lack the ability to infect host cells or never be released from cells during budding. As filaments are long, they can come in contact with multiple host cells at the same time. This can induce macropinocytosis, thus other infective viruses may be able to enter the cells along with it. This priming mechanism could help the infective virions to be more successful and spread faster.

To test this hypothesis, A/Udorn/72 and M1-A41V virions were inactivated with UV treatment. The UV treated virus was first introduced to the cells, to prime them, followed by infection with untreated virus. The results showed that there was no difference in the infectivity due to changes in morphology, i.e. both the spherical and filamentous virions showed similar levels of infection. However, it was noticed that priming of host cells beforehand did not aid infection. It actually reduced the level of infection.

This suggests that priming of cells for infection with un-infectious virus does not aid in consecutive infection. The infection slows down, and the infectivity is reduced. This means that instead of aiding infection, it is actually reducing its efficiency. This may be due to the fact that once the cells are primed, the

host's immune system is already prepared for the infection, and it activates the host's immune pathways to react to the infection immediately. Even during the first hour of infection the host's innate immune system can produce NF-kB and IRF-7, which induces the production of proinflammatory cytokines and type I IFNs which can aid in reduction of infection (Iwasaki and Pillai, 2014). Alternatively, the duration of micropinocytosis induction could be very brief and end before the other virions reach the primed cell.

4.3 Differences in NF-kB activation due to IAV morphology

NF-kB is one of the first responders of the host's immune cell, and the effects are rapid. To overcome this, IAV has schemed to manipulate the IKKB pathway, to use it to its own advantage (Nimmeriahn et al., 2004). Thus, it was worth looking at if viral morphology affects the early ability of the virus to activate NF-κB.

To test this, A/Udorn/72 and M1-A41V were used to infect host cells and the activity of NF-kB was assessed. The results suggest that, during early infection, when infected with spherical virions the NF-kB pathway gets activated, as NF-kB enters the nucleus. However, when infected with filaments, this effect is much reduced. NF-kB localization in the nucleus is decreased, showing that it fails to get activated. This means somehow the filamentous virions are reducing the activation of NF-kB. This suggests that the filamentous virions have found a way to work around the NF-kB pathway, which may make them more effective when infecting hosts, during

early stages of infection. However, we are not sure why and how this change in NF-kB activation occurs.

4.4 TLRs can drive the changes of NF-kB activation

TLRs are essential for many aspects of the innate immune system to work, as they recognise PAMPs from microbes, which triggers the innate immune pathways to respond to them. One of the pathways that gets activated is the NF-kB pathway. To test if TLRs or any of its associated proteins can cause the change in NF-kB activity, macrophages from specific K/O mice were obtained.

The results showed that the associated proteins (TRIF and TRAM) did not have any effect on NF-kB activity when infected with spheres and filaments. They both produced the same level of activated NF-kB. Again, this was repeated on specific TLR K/Os and this showed that TLR2, TLR3 and TLR2/4 K/Os showed a significant difference in NF-kB activation, when infected with filaments versus spheres. This suggests that these TLRs can be responsible for the difference in NF-kB activation in filaments and spheres.

It was also noticed that in almost all the TLR K/Os, the level of NF-kB activity was higher than in the wild type. This suggests, some other pathways may

be upregulated due to the inhibition of the TLR and that this change in cellular signalling may have affected the TLR K/O results above.

4.5 Entry Pathways do not play a role in NF-kB activation

Spherical virions enter cells by clathrin mediated endocytosis, while filaments enter by macropinocytosis (Badham and Rossman, 2016). As the different morphologies enter by different pathways, this might have an effect on the NF-kB activity. When IAV enters the cells by macropinocytosis, the innate immune system gets activated, triggering the activation of NF-kB. Thus, it was assumed that the difference in entry pathway might bring about the change in NF-kB activation.

To test this hypothesis, the entry pathways were blocked to see if it has any effect on NF-kB activation. Clathrin mediated endocytosis was blocked with CPZ and macropinocytosis was blocked by EIPA. When the pathways are blocked it was noticed that there is no difference in NF-kB activity when infected with Udorn or A41V. However, when both the pathways are blocked, NF-kB activation increases significantly with the spherical virions. This suggests a third pathway gets activated, when the normal pathways are blocked. It was thought that the third pathway might be phagocytosis, and this was looked into. The results show that the third pathway is not phagocytosis. However, this pathway might be another process of endocytosis and may result in stronger activation of NF-kB, when the usual pathways are blocked. It will be interesting to look at this further. This can be done by using a broader panel of chemical inhibitors to block additional

variant endocytosis pathways and looking at NF-kB activation. It will also be worthwhile to look at if any other functional proteins are affected. Type I IFNs can be activated as a response to the production of IRF 7, during the early stages of influenza infection. Cytokines including interleukin-1B (IL-1B) and IL-18 can also be released from phagosomes during the early stages of infection (Iwasaki and Pillai, 2014). These functional proteins can have an affect on the entry pathways of influenza, and it will be worthwhile to have a look at them.

4.6 Autophagy in activating NF-kB pathway

Autophagy is a controlled process of removing unwanted cellular components from the body. Autophagy can be induced by stress responses, which can be caused by microbes. When IAV enters cells by macropinocytosis, the cells can be triggered to produce autophagosomes. They can also be produced in response to TLRs recognising PAMPs. This can indirectly induce the activation of NF-kB activity. It was suggested that the production of autophagosomes can cause the change in NF-kB activity, and this can be controlled by the morphology of IAV.

To test this, the activity of autophagosome production was looked into during early infection. From the result it can be seen that there was no difference in autophagy activation during early infection, due to changes in morphology. It was also shown due to infection, at later stages IAV infection can reduce the autophagosomes from maturing, but there is no difference

between spheres and filamentous virions in this process. This means that autophagosomes are not driving the change in NF-kB activation due to morphological changes and morphology does not affect IAV-induced autophagy, during early stages of infection. However, if autophagy differs due to the difference in morphology at later stages was not looked into, and this may give different results, and will be worth looking into further.

4.7 Conclusion and Future Work

IAV is pleomorphic in nature and both the spherical and filamentous virions survive side by side. This suggests that they both play important roles in the survival and infection of virus. However, it is still unclear why the changes in morphology occur. We know that both viral and host factors play important roles in determining the morphology of the virus. Yet, it is still not known if that can cause a change in infectivity of the morphologies, nor what the function is of the different morphologies.

Here, it was shown that priming of host cells does not affect infectivity of virus as was previously suggested. It was proposed that filamentous virions can prime the host cells beforehand, so that the spherical and filamentous virions can work effectively during infection. However, as shown in the results this is not true, and priming somehow slows the infection process. Only A/Udorn/72 and its mutant M1-A41V was used to show this. The experiments can be repeated with other filamentous and spherical strains to determine if this effect is applicable to all filamentous strains or is unique

to Udorn and A41V. As epifluorescence microscopy was used to look at the results, they could not be as precisely quantified. So, it will be good to repeat the experiments with high resolution confocal microscopy and quantification.

It was shown that filaments can decrease the activation of NF-kB, during early infection as compared to spherical virions. As NF-kB is one of the first responders of the innate immune system of the host, this is very important. It means that filaments can slow down the activation process of the innate immune system. Spherical virions cannot do this. It was also important to see why this change in NF-kB activation occurs.

Firstly, it was important to see if this was driven by TLR activity. It was seen that TLR 2, TLR3 and TLR2/4 K/Os affect the difference in NF-kB activation, when infected with spheres or filaments. These TLRs also fail to activate the NF-kB pathway when infected by filamentous virions. It will be worth looking into how this happens and find the pathway by which filaments work and how NF-kB signalling differs in TLR K/O cells. For example, during a measles infection HA induces the activation of TLR 2 (Biebeck et al., 2002). This might also be occurring during influenza infection, and since the density and arrangement of the HA and NA differs in the different morphologies, this can cause the filamentous and spherical virions activate the TLR 2 differently. The glycoproteins on the surface of Ebola virus can help in activation of TLRs (Okumura et al., 2009), and it will be interesting to see if anything similar happens during influenza infection as well. MyD88

is also an important TLR associated protein, and was not investigated in this study, but it should be looked into for future work.

It was also suggested that since the two morphologies enter the host cell by different pathways, entry pathway might have an effect on NF-kB activation. Macropinocytosis can activate the NF-kB pathway. However, the results showed that there was no difference in NF-kB activity of the different morphologies due to the entry pathways. During the experiments it was found that when both the pathways of cell entry is blocked, IAV finds a third pathway to enter the cells. It was tested if the third pathway is phagocytosis, but the results show it is not. It will be good to find what the third pathway is, how it gets activated and if it works only in macrophages or in all cell types. It is possible that the third pathway is a variant of macropinocytosis or a different form of endocytosis, including caveolae endocytosis or CLIC/ GEEC pathway. Caveolae Endocytosis is an alternative clathrin independent endocytosis and is reported to be seen during influenza infection (Nunes-Correia et al., 2004).

Autophagy can indirectly affect NF-kB activity via macropinocytosis, and this was also looked into. However, the results showed that autophagosome production remains similar between filaments and spheres, thus it does not affect the NF-kB activation difference. However, it was also shown that at later stages of infection, IAV can reduce autophagosome maturation.

This study helped us to understand better how filamentous and spherical virions react differently to host and viral factors and how this may affect IAVs survival in nature. NF-kB is an important pathway which is one of the essential driving forces of innate immunity. If the path that filamentous virion take in blocking NF-kB activation can be found, it can be an important target for drug discovery.

CHAPTER 5

REFERENCES

Badham, M.D. and Rossman, J.S. (2016). Filamentous Influenza Virus. *Current Clinical Microbiology Reports.* 3(3), pp. 155-161.

Bieback K, Lien E, Klagge IM, et al. Hemagglutinin protein of wild-type measles virus activates toll-like receptor 2 signaling. *J Virol.* 2002;76(17):8729–8736.

Bron, R., A. P. Kendal, H.-D. Klenk, and J. Wilschut. 1993. Role of the M2 protein in influenza virus membrane fusion: effects of amantadine and monensin on fusion kinetics. *Virology.* 195, pp. 808-811.

Bruce, E.A., Digard, P. and Stuart, A.D. (2010) The Rab11 pathway is required for influenza A virus budding and filament formation. *J. Virol.* 84, pp. 5848-5859.

Bruce, E.A., Medcalf, L., Crump, C.M., Noton, S.L., Stuart, A.D., Wise, H.M., Elton, D., Bowers, K. and Digard, P. (2009). Budding of filamentous and non-filamentous influenza A virus occurs via a VPS4 and VPS28-independent pathway. *Virology.* 390, pp. 268-278.

Burry,R.W. (1998). PKC activators (phorbol ester or bryostatin) stimulate outgrowth of NGF-dependent neurites in a subline of PC 12 cells. *J.Neurosci.Res.* 53, pp. 214-222.

Calder, L.J., Wasilewski, S., Berriman, J.A. and Rosenthal, P.B. (2010). Structural organization of a filamentous influenza A virus. *Proc Natl Acad Sci USA*.107, pp. 10685–10690.

Centre for Disease Control and Prevention. (2015). Inactivated Influenza VIS. [online]. Available at: https://www.cdc.gov/vaccines/hcp/vis/vis-statements/flu.html (Accesses: 10 Sep 2018).

Chen B. J., Leser G. P., Morita E. and Lamb R. A. (2007). Influenza virus hemagglutinin and neuraminidase, but not the matrix protein, are required for assembly and budding of plasmid-derived virus-like particles. *J Virol.* 81, pp. 7111–7123.

Chen, C. and Zhuang, X. (2008). Epsin 1 is a cargo-specific adaptor for the clathrin-mediated endocytosis of the influenza virus. *PNAS.* 105 (33), pp.11790-11795.

Chen, Y., Lian, W., Yang, S., Wu, N., Gao, H., Sheng, J., Yao, H., Wo, J., Fang, Q., Cui, D., Li, Y., Yao, X., Zhang, Y., Wu, H., Zheng, S., Diao, H., Xia, S., Zhang, Y. and Yuen, K.Y. (2013). 381(9881), pp. 1916-1925.

Choppin, P.W., Murphy, J.S., Tamm, I. (1960) Studies of two kinds of virus particles which comprise influenza A2 virus strains. III. Morphological characteristics: independence to morphological and functional traits. *J Exp Med*. 112(18), pp. 945–52

Chu, C.M., Dawson, I.M., Elford, W.J. (1949) Filamentous forms associated with newly isolated influenza virus. Lancet. 1(6554), pp. 602

Chu, V.C. and Whittaker, G.R. (2004). Influenza virus entry and infection require host cell N-linked glycoprotein. *Proc Natl Acad Sci USA.* 101(52), pp.18153-18158.

Coates, B.M., Staricha, K.L., Wiese, K.M. and Ridge, K.M. (2015). Influenza A Virus Infection, Innate Immunity, and Childhood. *JAMA Pediatr.* 169(10), pp- 956-963.

Cox, N.J. and Subbarao, K. (2000). Global epidemiology of influenza: past and present. *Annu Rev Med.* 51, pp. 407-421.

Choi, Hyo-Jick & Montemagno, Carlo. (2014). Assessment of Osmotic Characteristics of Influenza Viruses. *Epidemiology- Theory, Research and Practice.* pp 19.

Deretic, V. and Levine, B. (2009). Autophagy, immunity, and microbial adaptations. *Cell Host Microbe.* 5(6), pp. 527-549.

Desai, M., Fang, R., & Sun, J. (2015). The role of autophagy in microbial infection and immunity. *Immunotargets and Therapy*, *4*, pp. 13–26.

Elleman, C.J. and Barclay, W.S. (2004). The M1 matrix protein controls the filamentous phenotype of influenza A virus. *Virol.* 321(1), pp. 144-153.

Elton, D., Bruce, E.A., Bryant, N., Wise, H.M., MacRae, S., Rash, A., Smith, N., Turnbull, M.L., Medcalf, L. and Daly, J.M. (2013) The genetics of virus particle shape in equine influenza A virus. *Influenza and other respiratory viruses.* 7, pp. 81–89.

Enami, M. and Enami, K. (1996). Influenza virus hemagglutinin and neuraminidase glycoproteins stimulate the membrane association of the matrix protein. *J Virol.* 70(10), pp. 6653-6657.

Falcone, S., Cocucci, E., Podini, P., Kirchhausen. T., Clementi E. and Meldolesi, J. (2006). Macropinocytosis: regulated coordination of endocytic and exocytic membrane traffic events. *J Cell Sci.* 119(22), pp. 4758-4769.

Fukuyama, S., and Kawaoka, Y. (2011). The pathogenesis of influenza virus infections: the contributions of virus and host factors. *Curr opin immunol.* 23(4), pp. 481-486.

Gaur, P., Munjal, A. and Lal, S.K. (2011). Influenza virus and cell signaling pathways. *Med Sci Monit.* 17(6).

Hales, C.M., Griner, R., Hobdy-Henderson, K.C., Dorn, M.C., Hardy, D., Kumar, R., Navarre, J., Chan, E.K., Lapierre, L.A. and Goldenring, J.R. (2001). Identification and characterization of a family of Rab11-interacting proteins. *J Biol Chem.* 276(42), pp. 39067-39075

Hayase, S., Uno, Y., Nii, F. (1995) Ultrahigh-resolution scanning electron microscopy of MDCK cells infected with influenza viruses. *J Electron Microsc (Tokyo)*. 44, pp. 281–288.

Hiscott, J., Kwon, H. and Génin, P. (2001*).* Hostile takeovers: viral appropriation of the NF-kB pathway. *JCI.* 107(2):143-151

Hiscott, J., Nguyen, T.L., Arguello, M., et al. (2006). Manipulation of the nuclear factor-kappaB pathway and the innate immune response by viruses. *Oncogene.* 25, pp. 6844–6867.

Horimoto, T. and Kawaoka, Y. (2001). Pandemic threat posed by avian influenza A viruses. *Clin Microbiol Rev.* 14(1), pp. 129-149.

Itoh Y, Shinya K, Kiso M, Watanabe T, Sakoda Y, Hatta M, et al. In vitro and in vivo characterization of new swine-origin H1N1 influenza viruses. Nature. 2009;460(7258):1021–1025.

Iwasaki A, Pillai PS. Innate immunity to influenza virus infection. *Nat Rev Immunol.* 2014;14(5):315–328.

Jill Seladi-Schulman, J., Campbell, P.J., Suppiah, S., Steel, J. and Lowen, A.C. (2014). Filament-Producing Mutants of Influenza A/Puerto Rico/8/1934 (H1N1) Virus Have Higher Neuraminidase Activities than the Spherical Wild-Type. *PLOS.* 9(11).

Job, E.R., Deng, Y., Barfod, K.K., Tate, M.D., Caldwell, N., Reddiex, S., Maurer-Stroh, S., Brooks, A.G. and Reading, P.C. (2013). Addition of Glycosylation to Influenza A Virus Hemagglutinin Modulates Antibody-Mediated Recognition of H1N1 2009 Pandemic Viruses. *J Immunol.* 201(7).

Johnson, N.P. and Mueller, J. (2002) Updating the accounts: global mortality of the 1918-1920 "Spanish" influenza pandemic. *Bulletin of the History of Medicine.* 76 (1), pp. 105-115.

Karin, M. and Ben-Neriah, Y. (2000). Phosphorylation meets ubiquitination: the control of NF-[kappa]B activity. *Annu Rev Immunol.* 18, pp. 621-623

Kawai, T. and Akira, S. (2010). The role of pattern-recognition receptors in innate immunity: update on Toll-like receptors. Nat Immunol. 11(5), pp. 373-384.

Keynan, Y., Fowke, K.R., Ball, T.B. and Meyers, A.F.A. (2011). Toll-Like Receptors Dysregulation after Influenza Virus Infection: Insights into Pathogenesis of Subsequent Bacterial Pneumonia. ISRN Pulmonology. 2011.

Kilbourne, E.D. (1959). Studies on influenza in the pandemic of 1957-1958. III. Isolation of influenza A (Asian strain) viruses from influenza patients with pulmonary complications; details of virus isolation and characterization of isolates, with quantitative comparison of isol. *J Clin Invest.* 38, pp. 266-274.

Kilbourne, E.D. (2006). Influenza Pandemics of the 20th Century. *Emerging Infectious Diseases.* 12 (1).

Kilbourne, E.D., Murphy, J.S. (1960) Genetic studies of Influenza Virus. I. Viral morphology and growth capacity as exchangable genetic traits. Rapid in ovo adaptation of early passage Asian strain isolates by combination with PR8. *J Exp Med.* 111, pp. 387–406

Koyama, S., Ishii, K. J., Kumar, H. et al., (2007). Differential role of TLR- and RLR-signaling in the immune responses to influenza A virus

infection and vaccination. Journal of Immunology. 179 (7) pp. 4711–4720.

Kroemer, G., Marino, G. and Levine, B. (2010) Autophagy and the integrated stress response. *Mol Cell*. 40, pp. 280–293.

Lakdawala, S.S., Lamirande, E.W., Suguitan, A.L.Jr., Wang, W., Santos, C.P., Vogel, L., Matsuoka, Y., Lindsley, W.G., Jin, H. and Subbarao, K. (2011). Eurasian-origin gene segments contribute to the transmissibility, aerosol release, and morphology of the 2009 pandemic H1N1 influenza virus. *PLoS pathogens*. 7.

Lamb, A.R. & Krug, R. (2001). Orthomyxoviridae: The Viruses and Their Replication. *Fields Virology*. Volume 1. 1.

Lee, B. L., Moon, J. E., Shu, J. H., Yuan, L., Newman, Z. R., Schekman, R., and Barton, G. M. (2013). UNC93B1 mediates differential trafficking of endosomal TLRs. *eLife*, *2.*

Leser, G. P., and R. A. Lamb. (2005). Influenza virus assembly and budding in raft-derived microdomains: a quantitative analysis of the surface distribution of HA, NA and M2 proteins. *Virology.* 342, pp. 215-227.

Levine, B., Mizushima, N., & Virgin, H. W. (2011). Autophagy in immunity and inflammation. *Nature*, *469*(7330), 323–335.

Lim, J.P. and Gleeson, P.A. (2011). Macropinocytosis: an endocytic pathway for internalising large gulps. Immunol Cell Biol. 89(8), pp. 836-843.

Lingwood, D. and Simons, K. (2010). Lipid rafts as a membrane-organizing principle. *Science.* 327(5961), pp. 46-50.

Lowen, A.C., Mubareka, S., Steel, J. and Palese, P. (2007) Influenza Virus Transmission Is Dependent on Relative Humidity and Temperature. *PLoS Pathog* 3(10).

Mahla, R.S., Reddy, M.C., Raghava Prasad, D.V. and Kumar, H. (2013). Sweeten PAMPs: role of sugar complexed PAMPs in innate immunity and vaccine biology. *Front Immunol.* 4(248).

Martin, K. and Helenius, A. (1991). Nuclear transport of influenza virus ribonucleoproteins: the viral matrix protein (M1) promotes export and inhibits import. *Cell.* 67, pp. 117–30.

Meffert, M.K., Chang, J.M., Wiltgen, B.J., Fanselow, M.S. and Baltimore, D. (2003). NF-kappa B functions in synaptic signaling and behavior. *Nat Neurosci.* 6, pp. 1072–1078

Molinari, N.A., Ortega-Sanchez, I.R., Messonnier, M.L., Thompson, W.W., Wortley, P.M., Weintraub, E. and Bridges, C.B. (2007). The annual impact of seasonal influenza in the US: measuring disease burden and costs. *Vaccine.* 25 (27), pp. 5086-5096.

Nayak DP, Hui EKW, Barman S. (2004). Assembly and budding of influenza virus. *Virus Res.*106(2):147–65.

Nimmerjahn, F., Dudziak, D., Dirmeier, U., et al. (2004). Active NF-kappaB signalling is a prerequisite for influenza virus infection. *J Gen Virol.* 85, pp. 2347–2356.

Noda, T., Sugita, Y., Aoyama, K., Hirase, A., Kawakami, E., Miyazawa, A., Sagara, H. & Kawaoka, Y. (2012). Three-dimensional analysis of ribonucleoprotein complexes in influenza A virus. *Nat Commun.* 3 (639).

Nunes-Correia, I., Eulálio, A., Nir, S. and Pedroso de Lima, M.C. (2004). Caveolae as an additional route for influenza virus endocytosis in MDCK cells. *Cell Mol Biol Lett.* 9(1): 47–60.

O'Neill,L.A.J., Golenbock, D. and Bowie, A.G. (2013). The history of Toll-like receptors — redefining innate immunity. *Nature Reviews Immunology.* 3, pp. 453–460

Okumura, A., Pitha, P.M., Yoshimura, A. and Harty, R.N. (2009). Interaction between Ebola Virus Glycoprotein and Host Toll-Like Receptor 4 Leads to Induction of Proinflammatory Cytokines and SOCS1*Journal of Virology.* 84 (1) 27-33.

Pahl, H.L. and Baeuerle, P.A. (1995). Expression of influenza virus hemagglutinin activates transcription factor NF-kappa B. *J Virol.* 69, pp. 1480–1484.

Palese, P. and Shaw, M.L.(2007). Orthomyxoviridae: The Viruses and Their Replication. *Virology*. 5, pp. 1647-1689.

Perot, B.P., Ingersoll, M.A. and Albert, M.L. The impact of macroautophagy on CD8(+) T-cell-mediated antiviral immunity*. Immunol Rev*. 255, pp. 40–56.

Richardson, J.C. & Akkina, R.K. (1991). NS2 protein of influenza virus is found in purified virus and phosphorylated in infected cells. *Archives of virology*. 116, pp. 69-80.

Roberts, P.C., Lamb, R.A. and Compans, R.W. (1998). The M1 and M2 proteins of influenza A virus are important fuk in filamentous particle formation. *Virology*, 240, pp. 127-137.

Rossman J.S. and Lamb R.A. (2011). Influenza virus assembly and budding. J *Virol.* 411(2), pp. 229-236.

Rossman, J.S., Jing, X., Leser, G.P. and Lamb, R.A. (2010). Influenza Virus M2 protein mediates ESCRT-independent membrane scission. *Cell.* 142(6), pp. 902-13.

Rossman, J.S. and Lamb, R.A. (2009). Autophagy, apoptosis, and the influenza virus M2 protein. *Cell Host Microbe*. 6(4), pp. 299-300.

Rossman, J.S., Leser, G.P. and Lamb, R.A. (2012). Filamentous Influenza Virus Enters Cells Via Macropinocytosis. *J Virol.* DOI: 10.1128/JVI.05992-11.

Ryter, S. W., Cloonan, S.M. and Choi, A.M.K. (2013). Autophagy: A critical regulator of cellular metabolism and homeostasis. *Molecules and Cells*. 36(1), pp. 7-16.

Scheiffele, P., Rietveld, A., Wilk, T. & Simons, K. (1999). Influenza viruses select ordered lipid domains during budding from the plasma membrane. *J Biol Chem*. 274, pp. 2038–2044.

Schmitt AP, Lamb RA. (2005) Influenza virus assembly and budding at the viral budozone. *Adv Virus Res.,* 64, pp. 383-416.

Seladi-Schulman, J., Steel, J., Lowen, A.C. (2013). Spherical influenza viruses have a fitness advantage in embryonated eggs, while filament-producing strains are selected in vivo. *J Virol*. 87(24), pp. 13343–13353.

Shinya, K., Ebina, M., Yamada, S., Ono, M., Kasai, N., and Kawaoka, Y. (2006). Avian flu: influenza virus receptors in the human airway. *Nature*. 440(7083), pp. 435-436.

Sieczkarski, S.B. and Whittaker, G.R. (2005). Characterization of the host cell entry of filamentous influenza virus. *Arch Virol*. 150(9), pp. 1783–1796.

Strauss, J. H. and E. G. Strauss (2008). Viruses and human disease San Diego, Academic Press**:** 147- 155

Takeda S., Yamashita A., Maeda K. and Maeda Y. (2003). Structure of the core domain of human cardiac troponin in the Ca(2+)-saturated form. *Nature*. 424, pp. 35–41.

Wang, X., Hinson, E.R. and Cresswell, P. (2007). The interferon-inducible protein viperin inhibits influenza virus release by perturbing lipid rafts. *Cell Host Microbe*. 2. pp. 96-105.

Wing-Yee Mok, B., Song, W., Wang, P., Tai, H., Chen, Y., Zheng, M., Wen, X., Lau, S., Wu, W.L., Matsumoto, K., Yuen, K. and Chen, H. (2012). The NS1 Protein of Influenza A Virus Interacts with Cellular Processing Bodies and Stress Granules through RNA-Associated Protein 55 (RAP55) during Virus Infection. *Journal of Virology.* 86(23).

Watanabe, K., Handa, H., Mizumoto, K. and Nagata, K. (1996). Mechanism for Inhibition of Influenza Virus RNA Polymerase Activity by Matrix Protein. *J Virol.* 70(1), 241-247.

World health organization. (2016). WHO manual for estimating the economic burden of seasonal influenza. [online]. Available at: http://apps.who.int/iris/bitstream/handle/10665/250085/WHO-IVB-16.04-eng.pdf;jsessionid=ED5F9993E79AE62B6C20B61EBA95C2D5?sequence=1 (Accessed: 10 Sep 2018).

Wang, J.P., Liu, P., Latz, F., Golenbock, D.T., Finberg, R.W. and Libraty, D.H. (2006). Flavivirus Activation of Plasmacytoid Dendritic Cells Delineates Key Elements of TLR7 Signaling beyond Endosomal Recognition. *The Journal of Immunology.* 177 (10) 7114-7121

Wu, C.F., Bi, X.L., Yang, J.Y., Zhan, J.Y., Dong, Y.X., Wang, J.H., Wang, J.M., Zhang, R. and Li, X. (2007). Differential effects of

ginsenosides on NO and TNF-alpha production by LPS-activated N9 microglia. *Int Immunopharmacol.* 7, pp. 313–320.

Xagorari, A. and Chlichlia, K. (2008). Toll-like receptors and viruses: induction of innate antiviral immune responses. *Open Microbiol J.* 2, pp. 49-59.

Yan, S., Weycker, D. and Sokolowski, S. (2017). US healthcare cost attributable to type A and type B influenza. *Hum Vaccin Immunother.* 13(9), pp. 2041-2047.

Ying, C.Y., Heaton, N.S., Gao, Q., Palese, P., Singer, R. and Lionnet, T. (2013). Colocalization of different influenza viral RNA segments in the cytoplasm before viral budding as shown by single-molecule sensitivity FISH analysis*. PLoS Pathog.* 9(5).

Yoshimura, A. and Ohnishi, S. (1984). Uncoating of influenza virus in endosomes. *J Virol.* 51(2), pp. 497-504.

Yuan, B., Campbell, S., Bacharach, E., Rein, A. and Goff, S.P. (2000). Infectivity of Moloney murine leukemia virus defective in late assembly events is restored by late assembly domains of other retroviruses. *J Virol.* 74, pp. 7250–7260.

Zhou, Z., Jiang, X., Liu, D., Fan, Z., Hu, X., Yan, J. , Wang, M. and Gao, G.F. (2009). Autophagy is involved in influenza A virus replication. *Autophagy*, 5, pp. 321-328.

Chapter 6

Appendix

MDCK		
Udorn	**A41V**	
0.436708	0.521316	
0.427391	0.50859	
0.42307	0.545773	
0.354085	0.530388	
	t test	0.001299478
A549		
Udorn	**A41V**	
0.352236	0.353413	
0.28248	0.327469	
0.331698	0.347606	
0.245844	0.32511	
	t test	0.208360619

T Test results for difference in NF-kB ratio between nucleus and cell in A549 and MDCK cells.

CPZ		EIPA		CPZ EIPA	
Udorn	A41V	Udorn	A41V	Udorn	A41V
0.32150176	0.37883873	0.479858	0.42457373	0.399281	0.914877
0.41171814	0.39407483	0.486192	0.500463769	0.681186	1.174807
0.46439245	0.5080407	0.409628	0.678625303	0.887329	1.101977
0.42781517	0.42811727	0.444202	0.596977166	1.128102	0.996824
0.42567396	0.60740546	0.390151	0.326089978	0.62764	0.864621
0.65613591	0.47464409	0.322694	0.362998543	0.552074	0.857501
0.40539661	0.48113627	0.389876	0.48820354	0.473577	0.859263
0.48085766	0.42062738	0.409966	0.468976013	0.610933	0.83304
0.48830768	0.52298296	0.481653	0.376902405	0.57449	1.204812
0.28990635	0.46320435	0.420897	0.391032783	0.685986	1.198933
0.43288173	0.41988981	0.414029	0.420200319	0.868347	1.482074
0.36416226	0.42983329	0.452544	0.336344554	0.821067	0.980411
ttest					
0.36637014			0.510447735		0.00034

T Test results for measure of NFkB in cell nucleus vs entire cell for Wild Type Mouse Macrophages blocked with CPZ or EIPA, infected with A/Udorn/72 or M1-A41V

WT		TRIF		TRAM		TRIF TRAM	
A41V	Udorn	A41V	Udorn	A41V	Udorn	A41V	Udorn
0.42055	0.410553867	0.2019817	0.298438	0.255997	0.336122	0.361319	0.300001
0.517186	0.369204527	0.38681223	0.308299	0.295457	0.336719	0.353017	0.300178
0.320225	0.4323025	0.44198326	0.283926	0.297723	0.385079	0.341069	0.370171
0.602008	0.41330711	0.30066581	0.368472	0.508291	0.316932	0.39047	0.355848
0.4549	0.36393062	0.332889	0.247532	0.332073	0.37403	0.591698	0.375466
0.352192	0.396891104	0.31935975	0.381593	0.345765	0.361675	0.532664	0.421323
0.267941	0.424084825	0.33893891	0.334542	0.363995	0.395853	0.446278	0.481765
0.288619	0.456007993	0.57928192	0.337551	0.411827	0.33611	0.3492	0.393859
0.318769	0.346942138	0.50905398	0.667775	0.438549	0.300655	0.324956	0.3748
0.581269	0.432141475	0.30554628	0.351101	0.306917	0.310902	0.307354	0.363755
0.456618	0.346412601	0.43754388	0.494161	0.259277	0.283868	0.273139	0.331241
0.469879	0.486591248	0.54572445	0.324373	0.443114	0.334168	0.457036	0.39806
0.281543	0.34362382	0.2562814	0.459021	0.346065	0.271635	0.330207	0.315325
0.515848	0.410216962	0.40468411	0.44439	0.326551	0.280932	0.305903	0.443253
0.320582	0.445000588	0.43709509	0.360951	0.338291	0.317223	0.363377	0.359118
0.454495	0.523051667	0.41739631	0.598333	0.327911	0.448311	0.407759	0.449228
0.354756	0.381747732	0.32994517	0.404764	0.381529	0.268881	0.317554	0.275823
0.641933	0.487241594	0.41216345	0.449418	0.296032	0.315294	0.347013	0.307869
0.547674	0.389765444	0.28478757	0.312577	0.327158	0.318744	0.377594	0.399742
0.427696	0.420490075	0.43363146	0.353355	0.515537	0.356059	0.263441	0.360838
0.398577	0.374187836	0.5119439	0.281855	0.32617	0.293793	0.421171	0.468246
0.311777	0.417994677	0.51308614	0.474352	0.280858	0.284489	0.377587	0.39143
0.371099	0.480467999	0.28071288	0.304049	0.405314	0.408218	0.458299	0.404451
0.439235	0.437372448	0.36748722	0.349337	0.316149	0.4624	0.39131	0.340891
T Test							
0.827498		0.81923482		0.422243		0.818757	

T Test calculations for TRIF TRAM when infected with A/Udorn/72 or M1-A41V

TLR1		TLR2		TLR3	
Udorn	A41V	Udorn	A41V	Udorn	A41V
0.465274	0.519522	0.875172854	0.550919	0.529430593	0.593852
0.457615	0.581871	0.882170418	0.60993	0.992680049	0.499885
0.536257	0.645363	0.822319083	0.573706	0.90353167	0.764693
0.606139	0.765312	0.829910349	0.566653	0.865557618	0.469122
0.596266	0.516222	0.862674489	0.477661	0.781201248	0.553929
0.562465	0.580976	0.860760264	0.402398	0.985067814	0.642715
0.720938	0.559718	0.615223499	0.693806	0.563778828	0.541032
0.436219	0.572908	0.73123988	0.762382	0.990039371	0.53664
0.435382	0.545496	0.716807227	0.596752	0.914037922	0.421074
0.672886	0.323341	0.707441834	0.857039	0.502321866	0.645939
0.695572	0.38434	0.807352704	0.791526	0.585848138	0.59419
0.641273	0.53648	0.792555813	0.821006	0.64156259	0.995136
T Test					
0.582486		0.004635414		0.029058506	

TLR4		TLR2/4		TLR6	
Udorn	A41V	Udorn	A41V	Udorn	A41V
0.86867058	0.578785	0.987952932	0.933667898	0.856247	1.394469525
0.942383772	0.723412	0.904057371	0.730991827	1.619498	1.666750568
1.095727046	0.656812	0.857149538	0.650057001	0.955566	1.250243819
0.915284627	0.964679	1.124015566	0.965372516	0.992277	1.018490444
0.816331994	0.511683	1.136425336	0.699952193	0.912994	0.909500629
0.883017383	0.470193	0.973994608	0.75184129	0.889053	1.730194268
1.107317659	0.514748	0.971435059	0.924792954	1.255344	0.996604303
0.885718743	0.645755	1.120680788	0.718719231	0.669315	1.017497165
0.749370958	1.446173	0.72593945	0.699952193	0.472422	1.072102529
0.614826906	0.597072	0.78066393	0.75184129	0.370252	0.641591232
0.756824757	1.093134	1.027118999	0.924792954	0.456637	0.89421272
0.963306419	0.950293	0.805616508	0.718719231	1.144235	0.905174014
T Test					
0.213325158		0.004839706		0.098729	

TLR7		TLR9		WT	
Udorn	A41V	Udorn	A41V	Udorn	A41V
0.790055581	0.72965748	0.849619	0.73355749	0.371938	0.364833
0.730113877	0.868324277	0.823988	1.010020467	0.53342	0.357966
1.027969648	0.662961946	0.69363	0.904983189	0.438075	0.56348
0.784693974	0.828915429	1.617419	1.442313693	0.374877	0.576796
0.520724028	1.025704951	2.007786	1.481557632	0.40399	0.408367
0.797300828	0.757795573	0.98248	1.01998781	0.497913	0.497864
0.684405635	0.85359204	0.686814	1.139564316	0.477254	0.53601
0.697858567	0.837141056	0.915628	1.242997799	0.586948	0.565265
0.766840211	0.739281628	1.061226	1.53729251	0.523702	0.442533
0.795146165	0.691396109	0.797038	1.458310254	0.452528	0.621478
0.929578335	0.888348159	0.826061	1.273765118	0.54272	0.59076
0.833515068	0.759413128	1.75309	1.525413868	0.4451	0.516508
T Test					
0.614651055		0.342804		0.325752	

T Test results for difference in NF-kB ratio between nucleus and cell in different TLR K/Os of mouse macrophages.

				Average
Udorn high	0.111	0.106	0.108	0.108333333
Udorn low	0.145	0.147	0.139	0.143666667
A41V High	0.096	0.097	0.093	0.095333333
A41V low	0.782	0.852	0.805	0.813
		T Test	Udorn Vs A41V high	0.002320643
			Udorn Vs A41V low	5.49501E-06

T Test results for Quanti blue Assay to look at difference of MOI of A/Udorn/72 Vs M1-A41V in activating NF-kB.

Counting plaques from plaque assay for UV inactivated virus